Head-Disk System and Integration for Extremely High Density Magnetic Data Recording

Ng Ka Wei

(B. Eng(Hons.)., University Technology of Malaysia, Malaysia)
(M.S., Singapore-MIT Alliance)

A THESIS SUBMITTED

FOR THE DEGREE OF DOCTOR OF PHILOSOPHY

DEPARTMENT OF ELECTRICAL & COMPUTER ENGINEERING

NATIONAL UNIVERSITY OF SINGAPORE

2008

Acknowledgements

Many thanks to my supervisors at Data Storage Institute (DSI): Associate Professor Liu Bo, for offering valuable advice and guidance throughout my Ph.D. study; and to Professor Chong Tow Chong, for the kind support of helping me completing my study.

Many thanks are given to my colleague on the valuable comments: Dr. Yuan Zhimin who has taken the time and troubles to alert me to errors in the research; special thanks to Dr. Leong Siang Huei, who subjected my text to rigorous scrutiny and much improved its quality.

I would also like to express my sincere thanks to my friends in DSI, for their friendship and companionship through good and bad times in DSI.

And finally never enough thanks to my wife and my parents for their relentless support throughout these years.

Table of Contents

Summary

This thesis investigates the key issues for ultra-low magnetic head-disk interface and configuration/integration technology of magnetic head-disk systems for extremely high density magnetic recording. The investigations include sub-nanometer resolution measurement of the stability of the head disk interface, the nanometer or sub-nanometer variation of the flying height caused by disk assembly and spindle motor, air-flow and thermal flying-height control, effects of the electrical potential on interface and exploration of new energy assisted magnetic recording for future magnetic recording.

One of the major challenges in increasing the areal density of magnetic disk drives is on reducing the head and media spacing, which commonly known as flying height. Current flying height for 150~200 Gb/in^2 areal densities is 6~7 nm. It is expected that a flying height of 3~3.5nm or below is required for the areal density of 1 Tb/in^2 and beyond. Under such an ultra-low flying height, the flying dynamics of the slider is a critical parameter for maintaining the reliability of the read/write function. The small flying height change caused by the disk distortion and spindle motor vibration must be considered, though such change is assumed to be negligible up to now. Such flying height change is investigated using in-situ flying height measurement method and self-developed hardware setup. The results show that the flying height stability is a function of the disk distortion and spindle motor vibration. Theoretical analysis with numerical modeling is carried out. Results indicate the dependence of such a flying stability to the air-bearing surface (ABS) design and slider's crown value.

A novel method is proposed to determine the relative movement of the slider in both vertical (flying height) and off-track directions. With the new method, further investigations on the slider flying height dynamics are carried out for both thermal actuated slider-disk contacting process and sliders at their full flying status. The thermal actuator controlled contact results show that the concurrent flying height and off-track measurements are well-decoupled.

Optical flying height tester is an industry standard method for flying height measurement of sliders. However, one of the biggest challenges for optical flying height testing is how to increase the accuracy of the corresponding calibration process. A method is proposed and demonstrated to increases the repeatability and accuracy of the flying height measurements by improving the repeatability of the optical calibration process. With the new calibration method and hardware setup, the slider absolute or static flying height was studied in this thesis.

Thermal flying-height control (TFC) is a new technology introduced for proper control of the flying height. The head disk spacing is reduced by a localized protrusion of the read/write head and this localized protrusion is achieved by introducing a thermal actuator. The thermal actuators have a critical role in ultra-low flying height adjustment. Experimental methodology is developed in this thesis to characterize the thermal actuator effectiveness in the presence of dynamic conditions especially the cooling effect.

New phenomena at ultra-low flying height are investigated which include the slider-lubricant interaction and tribologically induced electrical charge build-up in slider-disk interface. Such phenomena are studied by thermal actuated slider under different testing conditions: with/without mobile

lube on the disk surface and with/without electrical potential difference between slider and disk surfaces. The experimental results show that the electrical potential is highly dependent on the work functions of the material compositions of the slider, disk and lubricant.

Future ultra high density magnetic data storage requires extremely small grain size. In order to have thermal stability of recorded data, magnetic media must have high coercivity (Hc) which requires strong magnetic field to switch the magnetization of the magnetic grains. The magnetic field generated by current magnetic head is definitely not enough to make such a switching. Therefore, additional energy will be needed to assist the switching process.

A new energy assisted recording scheme is explored in this thesis. The magnetic writing process is enhanced by the combined field emission and moderate ionization between the write pole and magnetic media. The results show improvement in writing ability on perpendicular magnetic recording media using the proposed method.

Keywords: flying height, head-disk interface, high density, lubricant, magnetic data storage, slider technology, and tribology.

List of Tables

Chapter 2

Chapter 3

Chapter 5

List of Figures

CHAPTER 1

INTRODUCTION

1.1 Background

Information storage is one of the backbone technologies for the information society and magnetic hard disk drive (HDD) technology is the major information storage technology in the society. Since their introduction in 1957, the magnetic HDD has become the predominant device for storing digital information due to its capability in fulfilling the demand for inexpensive, highly-reliable, quickly-accessible and high-density data storage systems in today's information era. This makes HDD to be one of the most important components of the modern personal computer. Generally, no software application will run reasonably without the HDD. The technology behind the HDD is called magnetic recording, the principles of which will be discussed in paragraphs.

HDDs record data by magnetizing ferromagnetic material directionally, to represent either a 0 or a 1 binary digit. The process of writing the bit on the magnetic disk using a coil is drawn in Fig. 1.1. When writing, the coil is energized and a strong magnetic field forms in the gap of the write-pole, magnetizing the recording surface adjacent to the gap in the direction of the magnetic field.

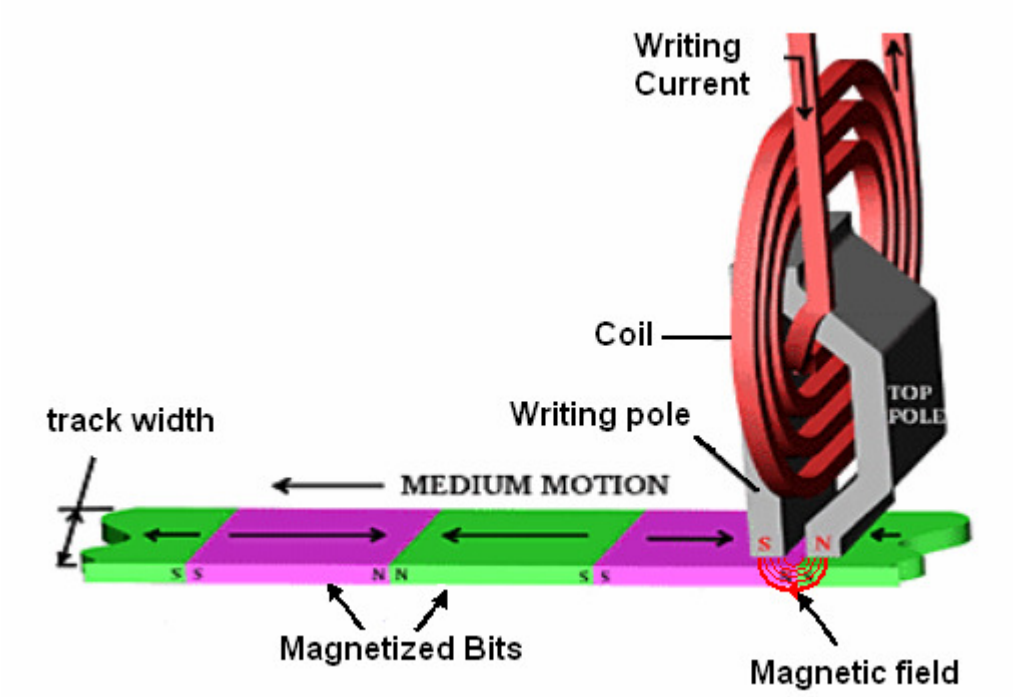

Figure 1.1 Process of writing data on magnetic medium

The written bits are permanently magnetized on the disk media. A magnetic field exists above the location of bit and the strength of the magnetic field weakens as the read/write head moves away. Thus, the reading heads need to fly extremely close to the surface of a magnetized disk to effectively detect the nano-sized data bits.

Current reading head's working principle is based on spin-valve or giant magnetoresistive (GMR) technology. The reading head is placed closely to a rotating magnetized storage disk, thereby exposing the reading element to magnetic bit fields previously written on the disk surface. When the reading element is biased with constant current, changes in the resistance of the element (corresponding to changes of magnetic states arising from written bits) are detected as voltage changes. These voltage fluctuations are referred to

as the readback signal. The schematic of the reading process is shown in Fig. 1.2.

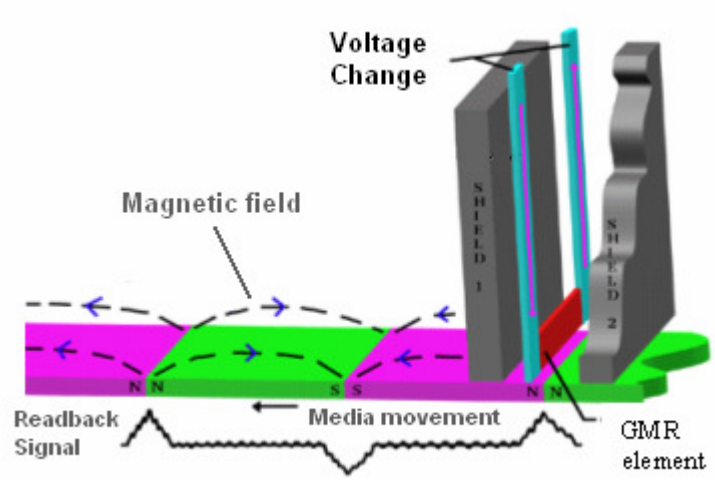

Figure 1.2 Process of reading data from magnetic media

The main components of hard disk drives (HDD) are shown in Fig. 1.3. The drive consists of several platters (magnetic disk) which are mounted to a spindle. The read/write sensors are embedded in the slider, which is loaded to the spinning platter (disk) by the actuator arm. The airflow between the slider and spinning platter generates a hydrodynamic air-bearing force that provides a small spacing between the head and disk. A suspension provides a spring action to the slider and balances the air-bearing force. The suspension is attached to the actuator arm. The arms are then fixed together to form a head stack assembly. The voice coil motor (actuator) positions the heads at any targeted track on the disk surface drives.

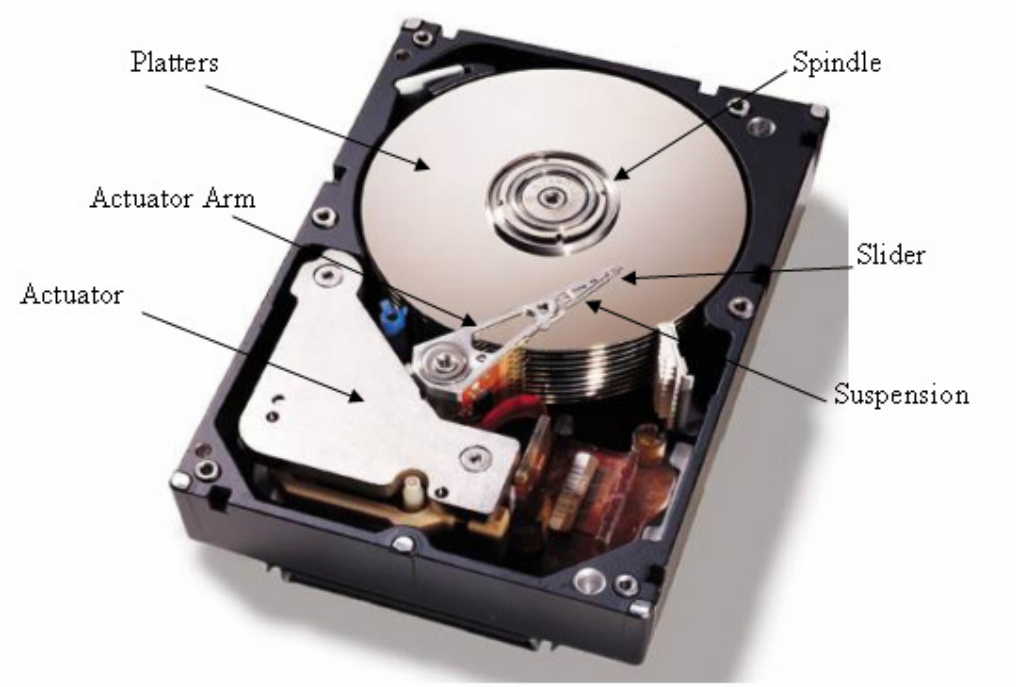

Figure 1.3 The overview and the main components of hard disk drives (HDD) with the top cover removed

In June 1957, IBM developed the first hard disk drive (HDD), which was called random access method of accounting and control (RAMAC). The areal density of system was 2000 bits/in^2 (100 bits/in and 20 tracks/in). The RAMAC system's magnetic read/write head was supported above the disk surface by a hydrostatic (pressurized) air bearing. This was the only time an externally pressurized air bearing was used to maintain the head-disk separation in the disk drive and a separation of 20μm between the heads and disks was achieved. All subsequent drives were to have flying air-bearing designs. These heads' surfaces are shaped such that the boundary layer of air just above the disk is compressed under the head, generating the necessary pressure. The compression of the air passing under the slider creates a lifting force that lifts the head-slider off the disk surface. Fig. 1.4 shows a typical air-

bearing slider with its main components, flying above the moving disk media. Some of the requirements for specific air-bearing designs include rapid take-off, close compliance to the disk's surface, stable flying, and minimal variation of flying height of the slider at different radial positions on the disk.

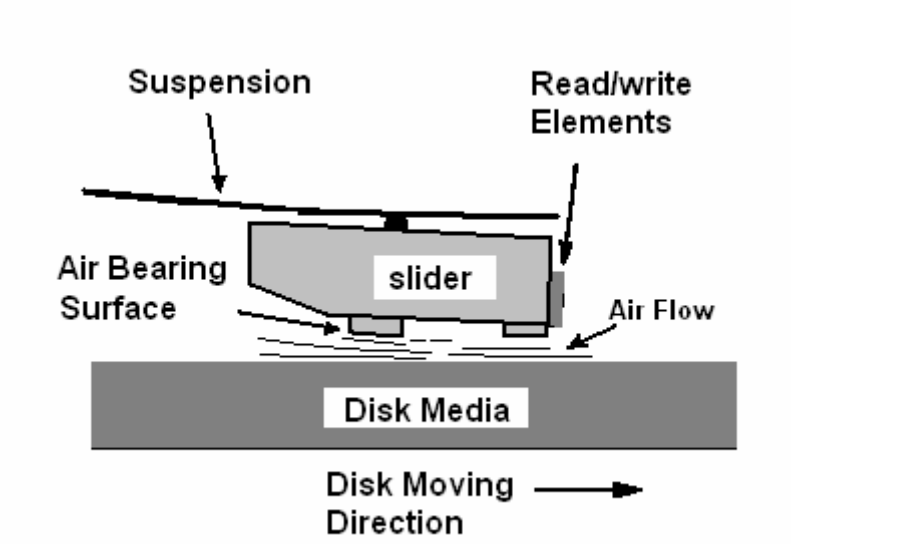

Figure 1.4 Schematic of an air-bearing slider flying above the disk media

One of the main reasons for the advancement in the areal density is attributed to the reduction of the spacing between the magnetic read/write head and the magnetic disk surface. The key role of the head-disk interface in determining the achievable areal density in a disk drive is illustrated in Fig.1.5. In the figure the areal density for a number of disk drive products is plotted against the nominal flying height of the head. The logarithmic scales for both areal density and flying height reflect the fact that magnetic recording is a "near-field" process; that is, reading and writing by a head occurs in close proximity to the head's gap. This leads to the exponential dependence of the

field on the spacing between head and disk and, consequently, areal density. Fig 1.5 also illustrates the important fact as areal density increases, tolerances in the head-disk spacing must also be reduced. These place significant constraints on both head and disk parameters, as well as drive design factors such as mechanical excitation by spindle bearings or external shock and clamping distortion.

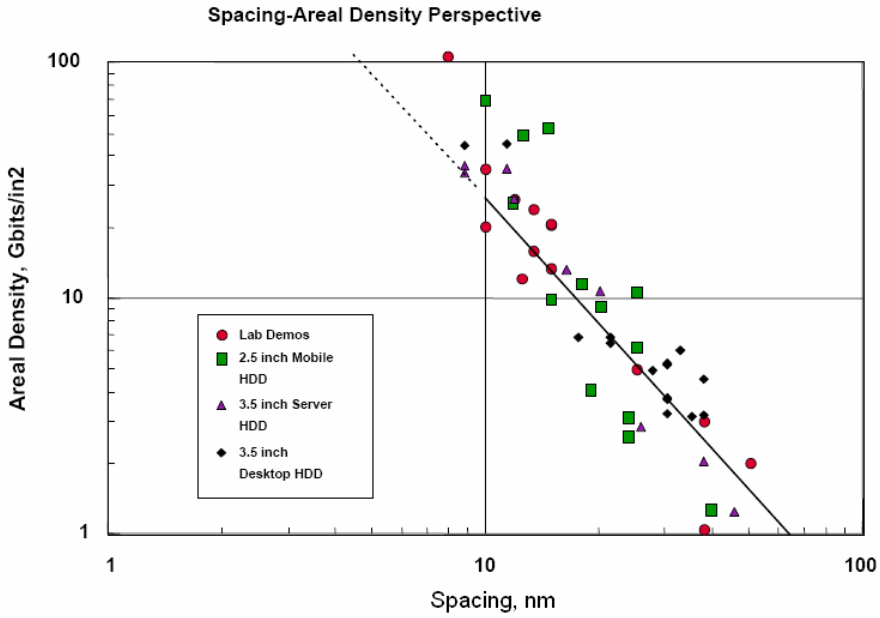

Source: Hitachi Global Storage Technologies.

Figure 1.5 Areal density of HDD product against the head-disk spacing

The magnetic head-disk spacing includes the following components: mean mechanical spacing (the flying height), slider overcoat thickness, disk overcoat thickness, lubricant, and pole tip recession of read/write transducer. Here, the mean mechanical spacing refers to the spacing between the mean plate of disk surface profile and the mean plate of slider surface profile, as shown in Fig.1.6. The mean spacing cannot be zero due to the non-zero surface roughness of both slider and disk media. Super smooth slider surface

(*Ra*: 0.3~0.4 nm) and super smooth disk surface (*Ra*: 0.2~0.3 nm) will be required to reduce the magnetic spacing below 10~12 nm. Currently, the areal density of magnetic data storage technology is increasing at an annual rate of 40% (Kryder and Gustafson, 2005). Higher areal density requires smaller spacing between magnetic read/write element and the disk media. The physical head-disk spacing have been reduced to 6-7 nm and it is expected that a physical spacing of 3-3.5 nm will be required to support the effort towards the areal density of 1 Tb /in^2 (Gupta and Bogy, 2005).

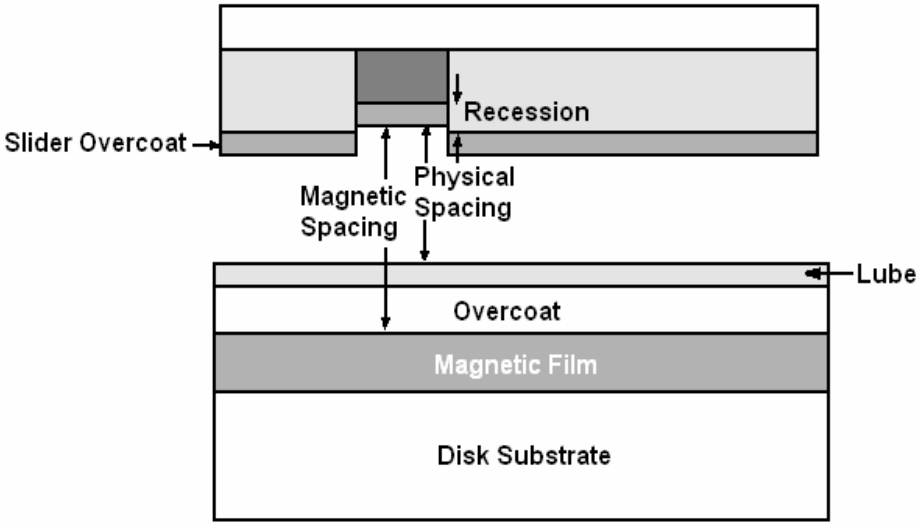

Figure 1.6 Head disk spacing components and definition of magnetic spacing and physical spacing

1.2 Characterizing Head-Disk Spacing for Achieving Extremely High Areal Density

Areal density is the main progress indicator for magnetic recording technology. Recent demonstration by TDK (2008) has pushed the areal density to 803 Gb/in^2 - the hard drive industry's highest demonstrated density to date. In order to achieve areal density beyond 1 Tb/in^2, the flying height will have to be reduced to 3-3.5 nm, with the tolerance no more than 10% (Dufresne and Menon, 2000), which is 0.3-0.35nm. This means that there may be likelihood of casual slider-lube interaction and slider-lube-disk interaction. A robust slider ABS and slider-gimbal suspension design will give a stable head disk spacing and minimize the possibility of slider-disk contact. Optimum design of the drive requires accurate measurements and understanding of the several parameters related to the head-disk interface:

1) The mean value of the flying height or physical spacing between a slider and the disk. This strongly influences head and disk design parameters.
2) The variations in the slider-to-disk air bearing spacing due to the changes disk flatness, disk topography, disk rotational variation, slider suspension variations, influence of external vibrations, and so on.
3) Electrostatic force and electrical potential between the slider and the disk where charges build-up due to the intermittent contact.
4) The optimization of the thermal protrusion induced by the embedded heater for on-demand flying height control.

The first two items are related with flying height and are generally considered together. The third item is related to the interaction forces between

two extremely close surfaces. As current flying height may reduce to sub-5nm, these interaction forces come into play. The last item is the latest technology in controlling the flying height during read and writing process. It is known as thermal flying height control (TFC) (Meyer et al., 1999; Machtle et al., 2001). TFC enable slider to perform on-demand flying height reduction. All of these factors will influence the technological advancement of the magnetic disk drive in achieving higher areal density. Thus, intensive research on these topics is necessary.

1.3 Flying Height and Its Characteristics in the Nanometer Head Disk Interface

Flying height (FH) is the key parameter for the achieving high linear density and read/write resolution. High flying height is unacceptable as this reduces the writing field gradient and results in broader transition and lower Signal to Noise Ratio (SNR) (Thomson and Best, 2000). Proximity contact is an ideal case to improve the read/write performance. For the proposed high density magnetic recording of 1 Tera-bit per square inch (Tb/in^2) (Wood, 2000; Mallary et al., 2002; Gao and Bertram, 2003), the allowed magnetic spacing is taken to be d = 6.5 nm, a value that must account for surface roughness, hard protective layers, lubricant, and maybe a few gas molecules in between (Wood, 2000). The targeted flying height is 3.5 nm for such a density (Gupta and Bogy, 2005). In such a low flying height, the tendency of head disk contact which could cause damages and deteriorate the read/write performance is extremely high as the slider is greatly influenced by external

factors. The reduction of the head disk contact and maintaining the flying stability of the slider had become an extreme challenge.

Although it is desirable to reduce the flying height for increasing the areal density, unjustifiable flying height reduction could deteriorate the head disk interface performance and thus, the read/write reliability. Therefore, accurate and repeatable measuring the slider's dynamics is of great importance in achieving the design target (Li et al., 2003). Generally, the measurement of the slider's dynamics can be divided into absolute and relative flying height. The absolute flying height is the average flying height whereas the relative flying height is the variation of the flying height in one disk revolution (Wang et al., 2000). Optical method is the most popular methodology in determining the absolute flying height of the slider (Zeng et al., 2001). It has been widely used by hard-disk drive industry and has been recognized as the standard tool in measuring the slider's flying height. However, the drawback of this method is the actual disk media must be replaced by glass disk. The measured flying height variation of glass disk would not be the same as that of the actual magnetic hard disk, each of which have different of disk distortions, surface topographies, lubricants and other variables (Li et al., 2003). Due to these limitations, another method has been explored. The *in-situ* triple harmonic method (Liu and Yuan, 2000) was explored and used to measure the flying height variation induced by the disk morphology. Unlike the optical method, the resolution of this method is not constrained by bandwidth limitation. Furthermore, the actual hard disk can be used in the measurement. It has been reported that high precision flying height in time domain can be achieved by such method (Yuan et al, 2002).

1.4 Flying Height Measurement Methodology

1.4.1 Reading Process Based Methods

The reading process based approach is established on the Wallace (1951) equation and Karlqvist head model (Mee and Daniel, 1990). The waveform method or PW_{50} method was reported by Klaassen and van Pepen (1990) which measures the variation of head disk spacing by the relationship between the head disk spacing and the shape of the isolated readback pulse at 50% of its amplitude. The general readback pulse of PW_{50} for the inductive heads can be expressed as

$$PW_{50} = \sqrt{g^2 + 4 \cdot (a+d) \cdot (a+d+\delta)} \qquad (1.1)$$

where g is the head gap, a is the transition parameter in the arctangent transition model and d is the magnetic head disk spacing. Head gap g and transition parameter a are fixed design parameters. As a result, the magnetic spacing d is totally dependent on PW_{50}. The above equations can also be applied to the MR heads.

The second type of readback based approach is the harmonic ratio method which is more sensitive to flying height changes compared to PW_{50} method. It was first introduced by Shi et al. (1985) and Brown et al. (1988). The method is based on the Wallace equation (Wallace, 1951), which shows that the harmonic readback signal reduces exponentially as the head disk

spacing increases. The Fourier transform of the readback voltage pulse is as follows:

$$V_{MR}(k) = C \cdot e^{-k(d+a)} \cdot \frac{1-e^{-k\delta}}{k} \cdot \frac{\sin(kg/2)}{kg/2} \tag{1.2}$$

where C is a factor independent on the wavelength vector $k = \frac{2\pi}{\lambda}$, λ is the recording wavelength and it is related to the MR head design and the medium properties, δ is the medium thickness, g is the MR-element-to-shield gap, d is the magnetic head disk spacing and a is the transition parameter. The harmonic measurement method uses the ratio between the fundamental wavelength λ and the third harmonic component 3λ from the readback signal of a recorded all-one pattern. By rearranging the equation 1.2, the flying height variation Δd can be derived as (Liu and Yuan, 2000):

$$\Delta d = -\frac{3\lambda}{4\pi} \cdot \Delta \ln\left(\frac{V_{MR}(k_1)}{V_{MR}(k_3)}\right) \tag{1.3}$$

where λ is the wavelength of recording signal, $V_{MR}(k_1)$ and $V_{MR}(k_3)$ are the intensity of the first and third harmonics, respectively.

It can be seen from the above derivation, the flying height variation is a function of the ratio of the first and the third harmonic amplitudes only. Such a harmonic ratio approach eliminates the dependence on the medium and head design values. The main drawback with this method is that the spectral power of higher order harmonic signal from all “1” pattern is too low compared with

that of the fundamental component, especially at high channel density (D_c) which refers to the ratio of PW_{50} to the physical bit interval (as shown in Fig. 1.7(a)). As a result, the signal-to-noise ratio (SNR) of higher order harmonic from all "1" pattern is significantly reduced.

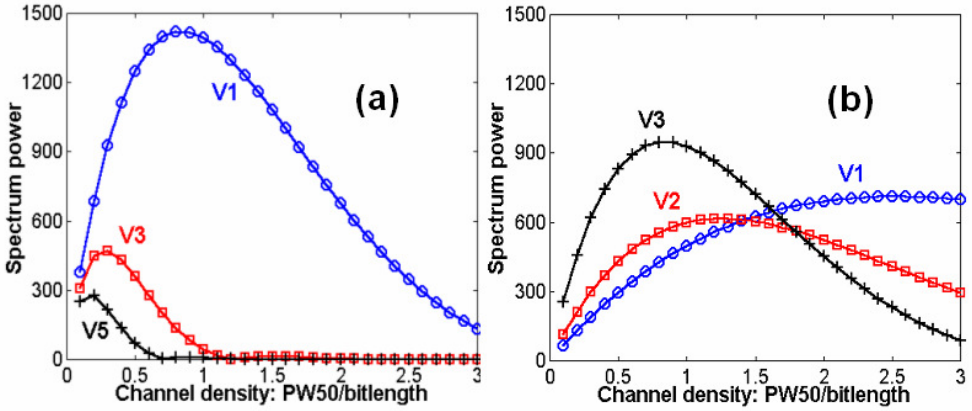

Figure 1.7 Spectrum power of the harmonics for the data pattern of (a) all "1" pattern and (b) "111100" pattern (Yuan et al., 2002).

1.4.2 Triple Harmonic Method

The problem with all "1" pattern in the harmonic reading based method is that the intensity of higher order harmonic signal is too low to sustain a sufficient signal-to-noise ratio (SNR) for achieving high accuracy of measuring flying height variation at high user density. Therefore, in order to improve the signal intensity of the higher order harmonic, Triple Harmonic Method, which uses (111100) code to test flying height in-situ has been proposed by Liu and Yuan (2000). The special code pattern provides three major harmonics and the signal intensity of both the first and the third harmonics, as shown in Fig. 1.7(b), are large enough to cover a very wide range of user density. As a result, this method can measure flying height at the higher user density up to 2.

The flying height measurement by the magnetic in-situ method is the function of some of the dimensional parameters. If the ratios of the dimensional parameters are not changed, the relative resolution, which is defined as the ratio of the absolute resolution to the nominal flying height, of the in-situ flying height measurement will be the same. It is claimed that the relative accuracy of the triple harmonic method can be within ± 2% of the magnetic spacing in the experiment (Yuan et al., 2002). The experimental results show that the flying height track profile is much wider than the signal amplitude profile and the flying height value is almost flat in a pretty wide region around the track center, as shown in Fig. 1.8. At certain off-track positions, the signal amplitude already drops 20%~30%, but the measured flying height value does not change so much. This property provides an opportunity for Triple Harmonic Method to measure both the flying height and the amount of off-track simultaneously.

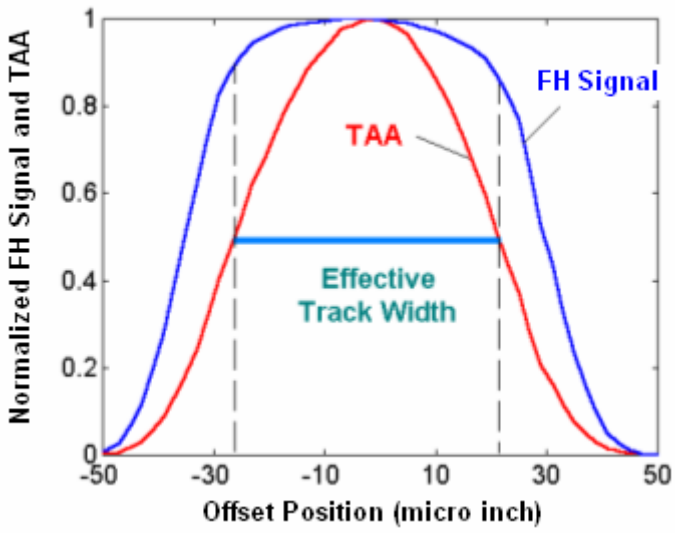

Figure 1.8 Flying height signal, track profile and the signal amplitude track profile (Yuan et al., 2002)

In a certain range, the flying height testing is not sensitive to off-track reading. The experimental results show that the Triple Harmonic Method is not sensitive to the conditioning change of the write process and the non-linear MR read process and the off-track reading. Furthermore, the relative testing accuracy of the developed setup can achieve ± 2% of the magnetic spacing. Therefore, it is a good solution to test the slider-lube-disk interaction for sub-10 nm flying height system.

1.4.3 Optical Interferometry Method to Evaluate Slider-Flying Characteristics

Different optical setups were reported by Best (1987) and Li (1996), Smith and Ganapathi (1993), Zhu et al. (1988), and Lacey et al. (1993). The dynamic behaviors of both the trailing and leading edges of a slider flying over a quartz disk was studied by Best (1987) using multiple beam interferometric theory. The dependence of slider optical constants on measurement angle of incidence and location, flying measurement repeatability, flying height tester calibration, and the effect of glass disk were studied by Li (1996). Lacey et al. (1993) introduced a white light interferometric system for flying height measurement using transparent disk. He described a theoretical solution and provided a phase shift measurement technique with several types of slider materials. The technique utilizes an ellipsometer to measure the slider's complex index of refraction from which the phase shift on reflection is calculated. Smith and Ganapathi (1993) and Zhu et al. (1988) used multi-channel heterodyne laser interferometer to measure the flying height of the slider. The main advantage of the method

compared to white light interferometry is that neither the disk nor the slider needs to be transparent. The only special requirement of the slider/disk assembly is that the back of the slider needs to be spectacularly reflective.

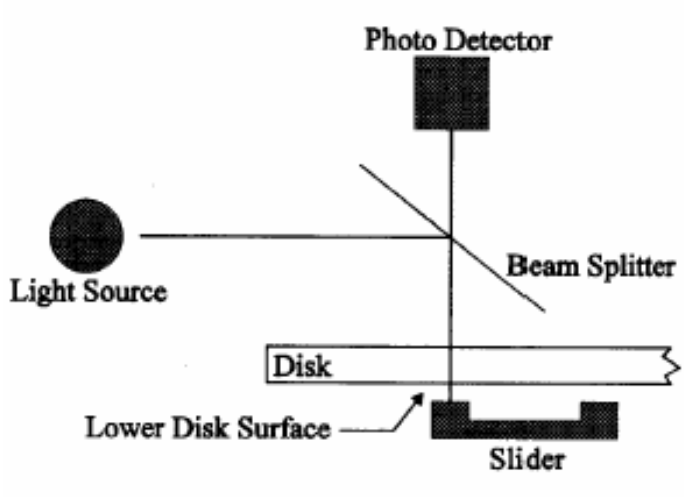

Figure 1.9 Optical Interferometry Setup

Optical interferometry has long been used for the accurate measurements of thin films. A monochromatic light beam is directed to pass through a transparent flat glass disk and it is focused on the slider. The light is reflected from the slider and is imaged into a photo detector (PD) or the charge-coupled device (CCD) camera. Fig. 1.9 shows the optical path focused to the slider and reflected at the detector. The intensity of resultant light detected at the detector varies as the distance between the disk surface and the slider surface varies from low to high value. The intensity of the light reflected from both surfaces considering multi-beam interference *I* is,

$$\frac{I_{out}}{I_{in}} = \frac{r_1^2 + r_2^2 + 2r_1 r_2 \cos\delta}{1 + r_1^2 r_2^2 + 2r_1 r_2 \cos\delta} \quad (1.4)$$

where r_1 and r_2 are intensities of the light reflected off the slider r_1 and the light reflected off the disk r_2 which can be derived as follow:

$$r_1 = \sqrt{\frac{(n_0 - n_1)^2 + k_1^2}{(n_0 + n_1)^2 + k_1^2}} \text{ and } r_2 = \sqrt{\frac{(n_0 - n_2)^2}{(n_0 + n_2)^2}} \qquad (1.5)$$

The phase angle difference δ between two reflections is a function of the phase shift ϕ_s on reflection off the slider surface. The value of δ can be derived as,

$$\delta = \frac{4\pi h}{\lambda} + 2\pi - \phi_s \qquad (1.6)$$

where λ is the wavelength of the light. The flying height h can be calculated after the phase shift ϕ_s is known. The phase shift which is the complex index of reflection $(n\text{-}ik)$ can be measured using the ellipsometer:

$$\phi_s = \tan^{-1}\left(\frac{2n_0 k_1}{n_0^2 - n_1^2 - k_1^2}\right) \qquad (1.7)$$

where n_o is the real index of the air above the slider, $(n_1\text{-}ik_1)$ and $(n_2\text{-}ik_2)$ is the complex index of the slider and disk material (Born and Wolf, 1989).

The dynamic flying height tester (Lacey et al., 1993) utilizes a white light source to provide three separate wavelengths of light (450nm, 550nm and 650nm). The lights are generated from the mercury arc lamp and they are

focused to the surface of the slider, through the transparent disk and they are reflected back though the disk on to the photo detectors. The lights reflected from the slider are directed through a sequence of optical lens. These include the pin-hole, beam splitter, wavelength filter and high-speed photo detector for each individual wavelength to be measured. A microscope which is connected to the CCD camera is used to monitor the position of the pin-hole and the slider interface condition. The calibration procedure involves unloading process where the head is lifted off the disk surface. The maximum and minimum intensity of each wavelength is measured during the unloading process. Once the maximum intensities for each wavelength are measured, the calibration process is completed. The maximum and minimum values of intensity measured during calibration are used in order to scale the measured value of intensity into units consistent with $\frac{I_{out}}{I_{in}}$ as used in (1.4).

$$\frac{I_{out}}{I_{in}} = \frac{(I_{Measured} - I_{CalMin})}{(I_{CalMax} - I_{CalMin})}(I_{TheoryMax} - I_{TheoryMin}) + I_{TheoryMin} \quad (1.8)$$

where

$I_{Measured}$ is the intensity measured for the desired spacing.

I_{CalMin} is the minimum intensity during calibration.

I_{CalMax} is the maximum intensity during calibration.

$I_{TheorylMin}$ is the minimum intensity based on Eqn. 1.4.

$I_{TheorylMax}$ is the maximum intensity based on Eqn. 1.4.

Solving Eqn. 1.4 for δ is given by

$$\delta = \cos^{-1}\left(\frac{r_1^{\,2} + r_2^{\,2} - \frac{I_{out}}{I_{in}} - r_1^{\,2} r_2^{\,2}\frac{I_{out}}{I_{in}}}{2r_1 r_2\left(\frac{I_{out}}{I_{in}} - 1\right)}\right) \qquad (1.9)$$

The solution from (1.9) is substitute to (1.6) which the flying height h is solved and is shown in (1.10).

$$h = \frac{\phi_s - \delta + 2\pi}{4\pi}\lambda \qquad (1.10)$$

1.5 Nano-Actuator for Flying-Height Control

In order to achieve sub-5 nm flying height, the contribution of intermolecular and electrostatic forces to the stability of the head disk interface is no longer negligible (Juang et al., 2006). Alternate air bearing slider designs have been introduced to minimize these nano-scale short-range forces by reducing the area of the sliders that is in close proximity to disks surface. This can be achieved by embedding a nano-actuator in the slider for on-demand flying height control. Example of these technologies includes micro-trailing pad slider (Juang et al., 2006), thermal flying height control slider (TFC) (Meyer et al., 1999; Machtle et al., 2001; Kurita et al., 2006), and piezoelectric flying height control slider (Kurita et al., 2002) for hard disk drives. TFC is the most effective way in reducing the flying height. Therefore, it is widely used in the hard disk drive technology development. The TFC is based on the concept that when a current is applied to the thermal actuator, a localized protrusion of the read/write head is generated due to the variation in

the thermal expansion coefficients of various materials. Atomic Force Microscope (AFM) (Li and Wang, 1998) or optical profiler (Gupta et al., 2000) are used to measure the static protrusion of the head without considering the dynamic conditions faced by the slider when it flies over the spinning disk. Research on dynamic thermal protrusion was limited to simulations by numerical calculations (Chen et al., 2000) or ANSYS modeling (Juang and Bogy, 2007). Up to now, the dynamic measurements of the slider protrusion (Wang et al., 2001; Kulkarni et al., 2000) were mainly focused on the pole-tip and alumina overcoat protrusion/recession. In fact, the thermal actuators have a critical role in ultra-low flying height (FH) adjustment; their effectiveness during flying in the presence of dynamic conditions, especially the cooling effect, should be studied. The exploration of experimental methodology and investigations on the cooling effect on the thermal actuator is an important topic for the head disk interface.

1.6 Effect of the Electrical Potential to the Head Disk Interface

In a hard disk drive, the electrical potential or electrostatic charging between the head and the disk have been studied and reported for some time (Fayeulle et al., 1993; Nakayama et al., 1997; Nakayama, 1999). This charging phenomenon is a result of the potential difference between the two plates that are made of different materials. For the case of a hard disk drive, the conducting part of the recording head is alumina composite (Al_2O_3-TiC) while the conducting part of the disk is a cobalt-based alloy magnetic layer. The work functions of these materials are further modified by the overcoats

and lubricants that are sandwiched between the two metal plates. The effects of the lubricants and carbon overcoats on tribological charging have been intensively reported (Feng et al., 1999; Oetelaar et al., 2001). Their studies have shown that tribological charging increases with an increase in relative humidity and lubricant thickness as well as a decrease in carbon overcoat. As the flying height reduces to sub-5 nm, this electrostatic force may cause the slider to come into contact with the media due to its attractive nature. Studies on the electrostatic force at near-contact were previously presented (Kiely and Hsia, 2002; Knigge et al., 2004). This electrostatic force will not affect the flying characteristics of a high-flying slider. However, they become increasingly important at the near-contact region.

1.7 Energy Assisted Magnetic Recording for Future Extremely High Density Magnetic Recording

The superparamagnetic effect (Lu and Charap, 1995) that causes the grains to be thermally unstable and susceptible to switching in their magnetic polarity is the main limitation for continuing grain size reduction to increase the areal density. To overcome this problem, future recording media must increase the media's coercivity (H_c) that requires a further increase in external energy to switch the magnetization of the bits. However, the conventional recording heads cannot generate high enough magnetic field for such future media, simply due to the limitation of material properties. Thus, different methods have been explored to introduce additional energy to assist the writing process of the magnetic head. One of which is Heat-Assisted Magnetic

Recording (HAMR). In HAMR, the medium's temperature is elevated by a laser light as the heat source to reduce its coercive field such that it is below the writing field (Ruigrok et al., (2000) Rottmayer et al., 2006). However, this practice is complicated as it involves mounting a laser source on the extremely small head structure. Field-emission current is another approach for energy assisted magnetic recording which was reported by Nakamura et al. (1995) and Zhang et al. (2006). Their studies have been focused on static measurements using the scanning tunneling microscope (STM) tip as the heating source. Therefore, their studies do not reflect the real situation in a hard disk drive. Till date, the implementation and dynamic measurements of the field emission assisted recording with actual recording head has not been studied.

1.8 Research Objectives

My works in this field include the methodology and research on the head disk system and integration for extremely high magnetic recording storage. In my works, two of the most widely used flying height measurement technologies had been utilized to explore and measure the tribological challenge for the high density magnetic recording. These two methods are the optical and the *in-situ* flying height measurement method. The *in-situ* flying height measurement method provides the relative flying height of the slider under different external influences. The measured flying height signal comprises different frequency components. The understanding and characterizing these frequency components are the main challenge in this

research. Suitable averaging and filtering methods need to be determined in order to categorize the measurement results. New method was developed to characterize the dynamics of the flying height. The optical method provides the absolute flying height of the slider. The challenge in this research is to improve the repeatability and accuracy of the measurement.. Novel measurement method has been proposed to further increase the repeatability and accuracy of the measurement, so that, is more suitable for sub-10nm flying height measurement.

Introduction of thermal actuated slider in the head disk interface is an important event in future HDD technology. In my study, thermal actuated slider was used to study the electrical potential between the head and the disk. Characterizing the thermal protrusion of head induced by the embedded heater was also carried out. Appropriate experimental methodology was developed to characterize the thermal actuator effectiveness in the presence of dynamic conditions especially the cooling effect.

Furthermore, the thesis also explores the new energy assisted magnetic recording to which enhanced the magnetic recording process by the combined field emission and moderate ionization between the write pole and magnetic media in experiment.

1.9 Dissertation Structure

The thesis consists of nine chapters. The first chapter is the introduction and the ninth chapter is the conclusion. In Chapter 2, the flying height variation of the slider induced by the disk clamping distortion is

described in detail. The experimental and theoretical explanations of such an effect are discussed. The measurement method for the flying height variation is introduced in this chapter. Chapter 3 reports the investigation on the correlation between the slider dynamic and the spindle motor vibration. Chapter 4 introduces a novel method for two-dimensional slider motion measurement. The measurement method determines the motion of the slider in flying height and off-track direction simultaneously.

In Chapter 5, optical method was used to determine the absolute flying height. A new calibration method is introduced. The setup for the optical calibration was developed for this measurement. Chapter 6 shows the study on the influence of lubricant to electrical potential using thermal actuated slider. The cooling effect on the thermal actuated slider was studied in Chapter 7 with greater sensitivity than magneto-resistive (MR) sensor measurements. Chapter 8 reports the enhancement of magnetic recording process by the combined field emission and moderate ionization between the write pole and magnetic media in an energy assisted magnetic recording experiment.

Results presented in chapter 2 to chapter 8 have been published in 2 patents and 6 journal papers as shown in the list of publications.

CHAPTER 2

FLYING HEIGHT VARIATION INDUCED BY DISK CLAMPING DISTORTION

This chapter reports the detail study on the flying height variation of sliders induced by the disk clamping distortion. The first part of the investigation involves methodology development that measures the flying height variation with *in-situ* flying height testing technology. Various shapes of disk deformation were studied in the experiment. Results obtained show that the flying height variation is a function of the amplitude of the disk clamping distortion. Results also exhibit that higher air bearing stiffness reduces the amount of flying height variation and lower flying height slider can present a higher percentage of flying height variation. Investigation is also extended to study the effect of slider's loading force on the flying height variation. The second part involves numerical simulation of the disk shape induced flying height variation and correlates the disk clamping distortion with slider's crown sensitivity. The developed numerical model suggests that static flying height variation depends not only on the amplitude of the disk distortion, i.e., flatness, but also on the disk shape and the sensitivities of the air-bearing slider design to the disk distortion. The measured experimental results were compared with simulated numerical results. Both results indicate that the disk clamping distortion has significant influence on the flying height

variation. Crown sensitivity of the sliders is one of the factors that determine the amplitude of the flying height variation. Higher crown sensitivity sliders exhibit greater flying height variation.

2.1 Background and Problem Definition

To achieve 1 Tb/in^2, the allowable flying height (FH) variation is merely 0.35 nm which is 10% (Dufresne and Menon, 2000) of the 3.5 nm mechanical spacing. Above 10-nm flying height, the magnitude of flying height variation, induced by the disk clamping distortion, is negligible when compared to the magnitude of the flying height. However, further reduction in the flying height had triggered the concerns as any flying height variation could lead to head disk contact (Thornton and Bogy, 2001; Qian, et al., 2003). In general, modern slider with proper air-bearing design is able to follow the disk deformation with slight shift (Zeng et al., 2001). The slider air bearing surfaces are designed to be with both high stiffness and high damping ratio to prevent excessive flying height variation caused by various reasons, including the clamping induced disk distortion. Many researchers had intensively studied the effect of these variations through simulation approaches. Bogy et al. (1993) study conformity of the slider crown to the disk geometry and its effect on the near contact flying performance. Qian, et al. (2003) showed that flying height variation induced by disk distortion could be calculated using mathematical models. Although flying height variation had been widely studied by these researchers, there is still a lack of appropriate numerical studies with experimental confirmation for better understanding of HDI and

designing a reliable interface. In this chapter, the flying height variation induced by the disk clamping distortion was investigated through experimental and theoretical approach. The dependence of flying height variation on flying height, suspension loading force and disk clamping distortion was investigated by experiment approach. Different disk clamping distortions and two types of sliders with different air-bearing surface (ABS) designs were used in the investigations. In order to have a theoretical explanation on these experimental results, a mathematical model was developed to explain the experimental results. The respective flying height variation induced by the disk distortion was simulated.

2.2 Description of Experiment

2.2.1 Methodology for Flying Height Variation Measurement

The Laser Doppler Vibrometer (LDV) has been widely used to measure steady and dynamic values of flying height. Thornton et al. (2001) has developed and utilized a LDV-based system to measure the flying height variation that could be associated with the disk clamping/warping/flutter. They reported that low frequency and high amplitude displacements such as disk clamping distortion pose resolution problem for the measurement system. The appropriate bandwidth of sub-nanometer resolution for this measurement system is from 7 kHz to 2 MHz. This has exceeded the bandwidth of interest on disk clamping distortion, which is less than 1 kHz. With a lower bandwidth, a 5 nm error is expected in this measurement system (Thornton et al., 2001). Therefore, the LDV system is not suitable for sub-nanometer

resolution measurement of the flying height variation induced by low-frequency disk clamping distortion. In this charter, the triple harmonic method (Yuan et al., 2001) was explored and used to measure the flying height variation induced by the disk clamping distortion. Unlike the LDV method, the resolution of the method is not constrained by bandwidth limitation. It has been reported that the high precision flying height in time domain can be achieved by such method (Yuan et al., 2002). The experiment setup is shown in Fig. 2.1. All the tests were conducted on the Guzik spinstand for writing the special code pattern onto and collecting the readback signals from the rotating disk. The readback signal was then sent to the self-developed *in-situ* flying height testing hardware that consists of two filter channels and one logarithmic processing unit. A spectrum analyzer and an oscilloscope were used to analyze the flying height signal of interest in the time and frequency domains, respectively.

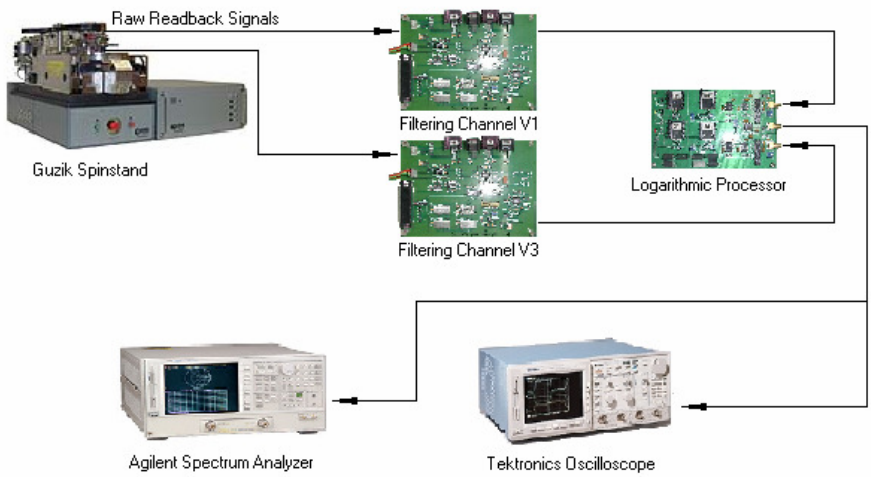

Figure 2.1 Experimental setup on the basis of the self-developed in-situ flying height testing electronics

The head-disk interfaces were maintained at a linear velocity of 25 m/s. The code pattern “111100” was written and sensed back each time via the *in-situ* flying height testing hardware. The flying height signals were captured in both time and frequency domains for analysis. The measured flying height signal comprises different frequency components. The low-frequency signal is associated with the disk clamping/warping/flutter, and the high frequency signal is related to the ABS vibration and disk waviness. Suitable averaging and filtering methods need to be determined in order to categorize the measurement results. For the study of flying height variation induced by clamping distortion, the low-pass filter with a cutoff frequency of 200 Hz was used to filter out flying height variation induced by ABS vibration and disk waviness. In this study, the experiments were conducted using the spinstand. Various disk distortions can be generated by modifying the clamping chuck shape of the spinstand. The amplitude and the types of clamping distortion used in the testing were uncommon comparing to the real drive. In fact, these distortions were generated for experimental study.

2.2.2. Disk-Clamping Distortion Measured by LDV

The disk distortion investigated in this work is in amplitude of microns. Therefore, LDV method can still be used to measure the clamping induced disk distortions. The labeling convention for the disk mode shapes designates -nodal circles and -nodal diameters (Qian, et al., 2003). Generally, changing the shape of the chuck can generate the out-of-plane disk displacement amplitude and frequency. These disk shape or distortions

measured by the LDV are shown in Fig. 2.2 for a 3.5 inch diameter aluminum disk. The 11 ms in the y-axis represents one revolution rotation with the spindle speed of 5400 rpm. The first spectral component of the out-of-plane (normal to the disk's surface) displacement of a spinning disk, as seen by a stationary slider, is the fundamental rotational frequency, ω_o, due to non-perpendicularity of the disk to the spindle axis [see Fig. 2.2(a)]. The next frequency component is twice the fundamental rotational frequency, $2\omega_o$, commonly called the "potato chip" clamping distortion of the disk as can be visualized in Fig. 2.2(b). The third disk mode shape and frequency is shown in Fig. 2.2(c). The corresponding 3-D drawing of the disk deformations for "potato chip" and third disk mode shape are shown in Fig. 2.3.

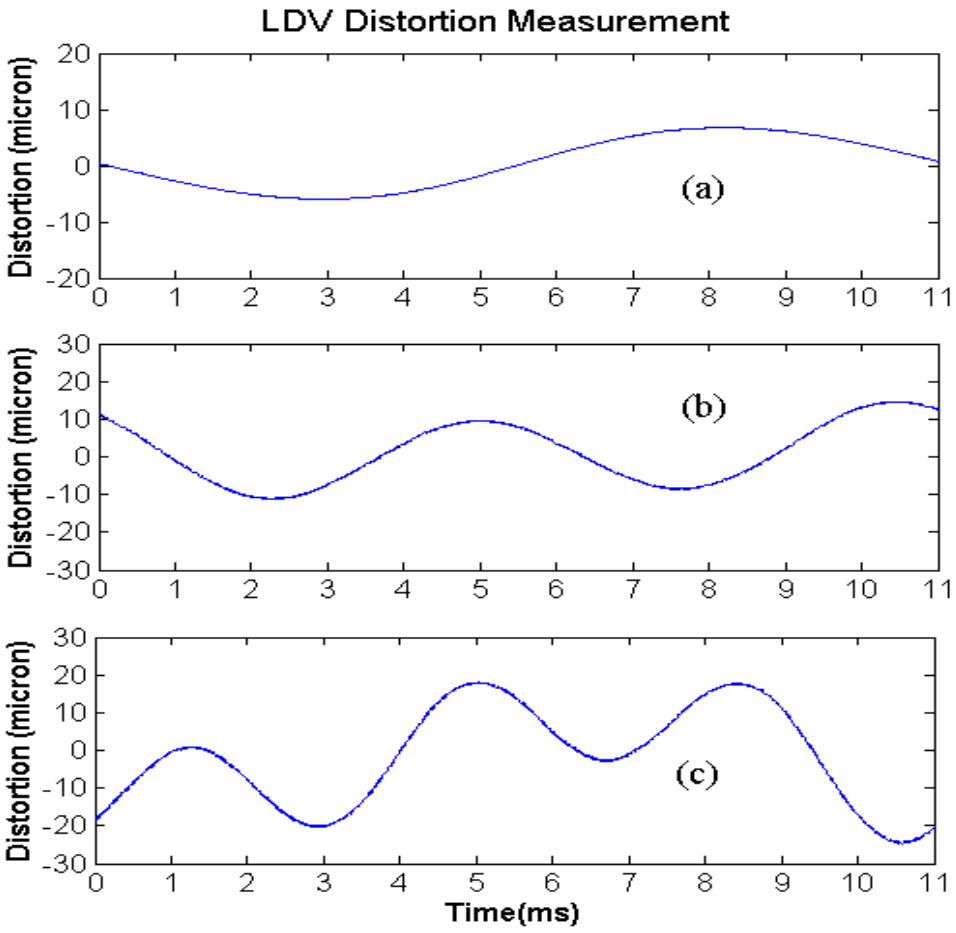

Figure 2.2 LDV measurement of disk clamping distortion. (a) First spectral component. (b) "Potato chip" clamping distortion. (c) Third disk mode distortion.

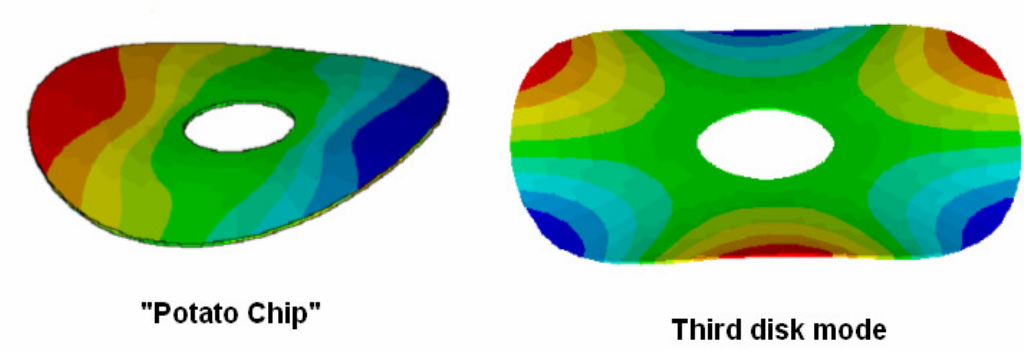

Figure 2.3 3-D drawing for the “potato chip” and third disk mode deformation.

2.3. Flying Height Modulation Study

2.3.1. Flying height Variation Induced by Clamping Distortion

The disk deformations that were used in the experiment had been identified by the LDV [see Fig. 2.2]. Fig. 2.4 shows the corresponding flying height variation measured by the *in-situ* method. Comparison between the diagrams shows that flying height variation, increases with the increase of the disk distortion amplitude. Apparently, the slider is able to follow more than 99.99% of the disk distortion amplitude. However, there still exist variations caused by the disk distortion, where positive disk distortion leads to the increase in the flying height and negative disk distortion results in the reduction of flying height. Furthermore, the flying height variation due to the disk distortion does not appear in the same phase as the disk distortion. The plot of phase shift against the distortion amplitude is shown in Fig. 2.5. The diagram indicates that phase shift remains almost unchanged when the distortion is increased.

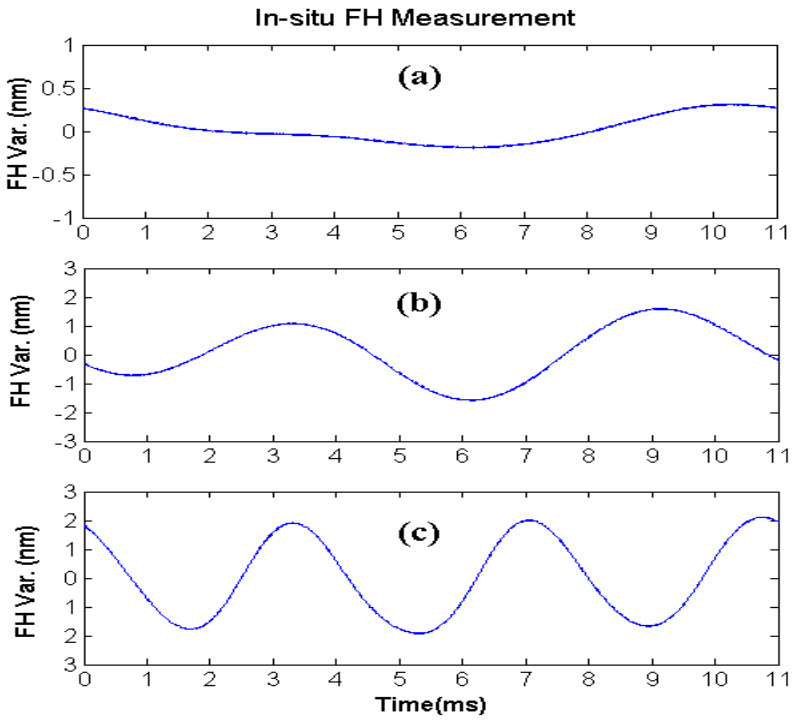

Figure 2.4 *In situ* flying height measurement of flying height variation induced by disk clamping distortion. (a) First spectral component induced flying height variation. (b) "Potato chip" induced flying height variation. (c) Third disk mode induced flying height variation.

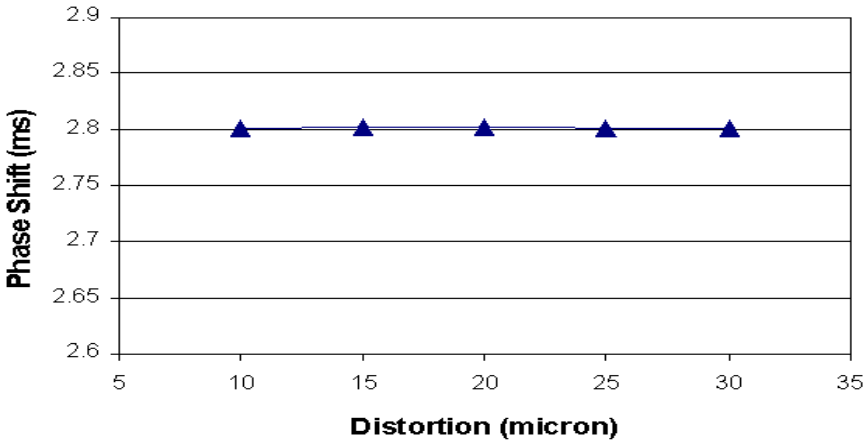

Figure 2.5 Phase shift comparison between the disk distortion and the flying height variation. Variation measured using the same slider and media.

2.3.2. Slider Design and Flying height Variation Caused by Disk Clamping Distortion

In order to understand the relationship between the air-bearing design and flying height variation induced by the disk clamping distortion, the experiment was continued with the comparison between two types of pico sliders with different ABS designs and flying height values. (Type A: 8 nm flying height and Type B: 24 nm flying height). The air pressure profiles for these sliders were simulated by the air-bearing simulator of the Computer Mechanics Laboratory, University of California, Berkeley (2000). The sliders' average stiffness was calculated as 0.27 and 0.08 gram/nm, respectively. The simulated air pressure profiles of the two types of sliders are shown in Fig. 2.6. Generally, 8-nm-FH-slider or slider A exhibits a higher average air pressure profile compared to 24-nm-FH-slider or slider B. The flying height variations of the sliders were also measured by the *in-situ* testing method. Both of the measurements were performed with the same disk and under the same disk clamping distortion. The results of the experiment are shown in Fig. 2.7 and 2.8. The variations in loading forces for different flying height are also included in the figures, which will be discussed later. The results show that the slider A has a smaller average flying height variation compared to the slider B. Generally, higher air bearing stiffness will lead to smaller flying height variation, as the case of slider A. However, in term of percentage, the slider type A is still of higher percentage of flying height variation as compared to the slider type B. The percentages of flying height variation are 7.5% and 5.8% for the two types of sliders which are based on the gram load of 2.5g respectively. This percentage difference indicates the presence of air-bearing

parameters that affects the flying height variation. Slider A's crown sensitivity is assumed to be main suspect due to its 2 times higher crown sensitivity value compared to slider B. This correlation between the crown effect and the flying height variation will be discussed in the modeling and theoretical section in this chapter.

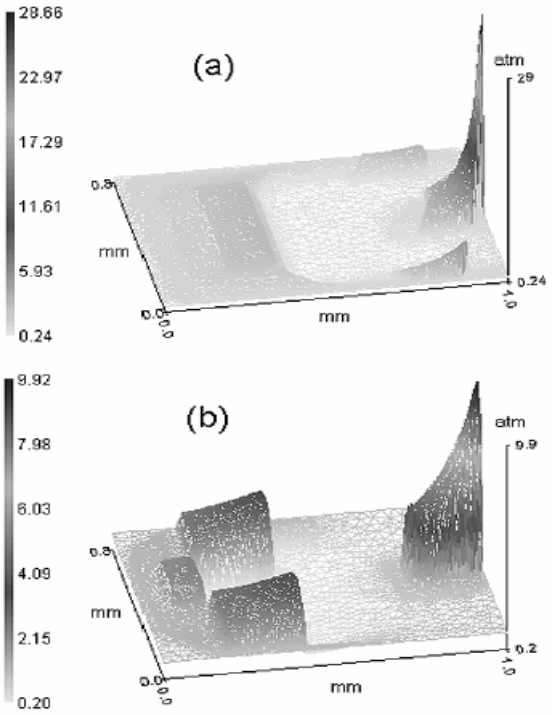

Figure 2.6 Pressure profile for two different ABS design pico slider (a) Low flying height Slider with flying height 8 nm and higher air bearing stiffness (0.27 g/mm). (b) Higher flying height slider with flying height 24 nm and lower air bearing stiffness (0.08 g/mm).

2.3.3. Effect of Loading Force

The nominal loading force for both sliders is 2.5 g. In order to explore the effect of loading force on the flying height variation, the loading force is

varied from 2.4 to 2.6 g. The results for these changes are shown in Fig. 2.7 and 2.8. Fig. 2.8 indicates that loading force changes do not have much influence on the flying height of the 24-nm-flying-height-slider as compared to that of the 8-nm-flying-height-slider. As shown in Fig. 2.7, it is obvious that changes of loading force for 8-nm-flying height-slider have intensified its flying height variation.

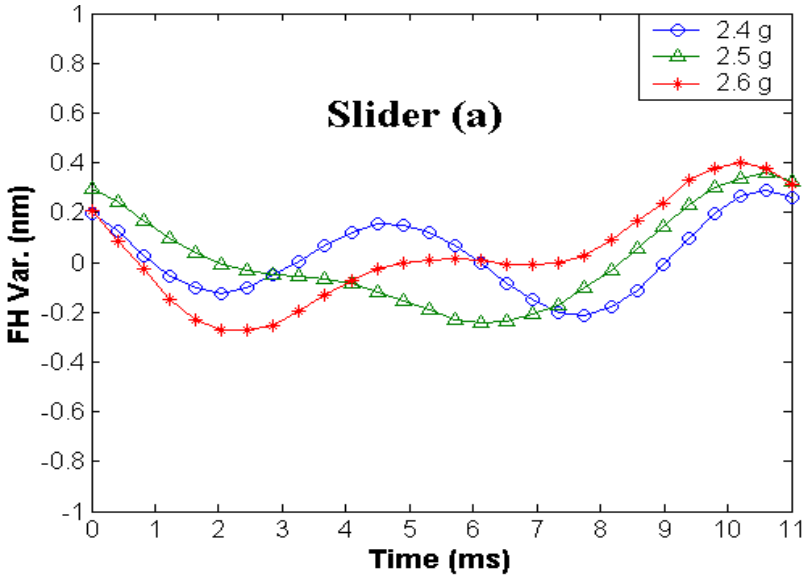

Figure 2.7 Flying height variation characteristic by changing the loading force for 8-nm flying height.

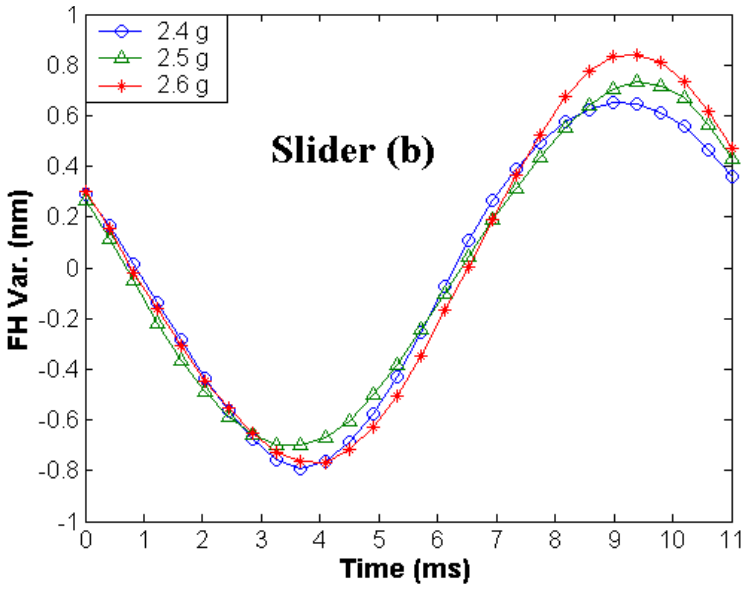

Figure 2.8 Flying height variation characteristic by changing the loading force for 24-nm flying height.

2.4. Theoretical Models of Static Flyability

Generally, disk distortion can lead to both static and dynamic flying height variation. The dynamic effect is generally associated with disk flutter and spindle induced vibration. For the case of static flying height variation, it is primarily induced by low frequency components such as the shape or curvature of the disk. The slider is designed to follow the dynamical changes of the disk. However, due to the changes in disk topography, the slider's static flying height is affected. Fig. 2.9 illustrates how the disk shape distortion affects the static flying height variation by comparing a slider that is flying on a flat disk surface with a slider that is flying on a distorted disk surface. Fig. 2.9 illustrates that the disk shape distortion is equivalent to crown changes of the slider. For the case shown in Fig. 2.9, the convex disk shape is equivalent to an increase in the slider crown.

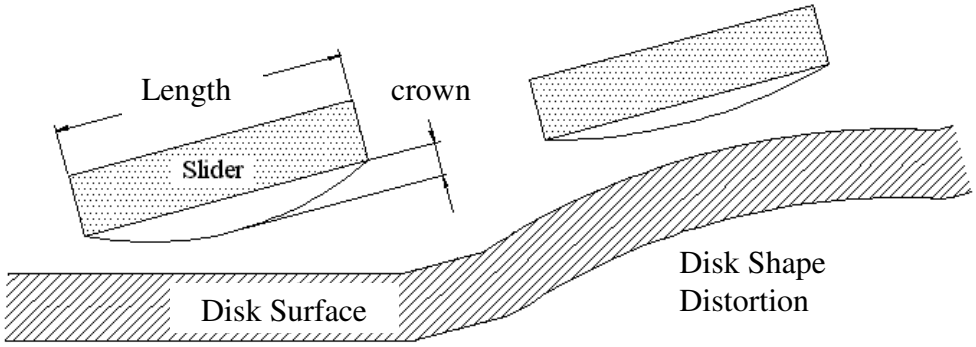

Figure 2.9 Illustration of slider flying over a distorted disk surface

In general, crown C over a given slider length L due to a very small curvature κ is given by

$$C = \frac{L^2}{8}\kappa \qquad (2.1)$$

The curvature κ is defined as

$$\kappa = \frac{d\phi}{ds} \qquad (2.2)$$

where ϕ is the tangential angle and s is the arc length. In two dimensions, let a plane curve be given by Cartesian parametric equations $x = x(t)$ and $y = y(t)$. Then the curvature κ is defined as

$$\kappa = \frac{\dfrac{d^2y}{dx^2}}{\left[1+\left(\dfrac{dy}{dx}\right)^2\right]^{3/2}} \qquad (2.3)$$

The mean flying height loss depends on both the tangential (or crown) and radial (camber) sensitivity of slider to the disk shape distortion (Qian, et al., 2003)

$$\Delta h = \alpha_{crown} \frac{L^2}{8} \kappa_t + \alpha_{camber} \frac{W^2}{8} \kappa_r \qquad (2.4)$$

where α_{crown} is the slider crown sensitivity, α_{camber} is the slider camber sensitivity, L is slider ABS length, and W is slider width. The radial curvature is defined as

$$\kappa_r = \frac{\dfrac{\partial^2 z}{\partial r^2}}{\left[1+\left(\dfrac{dz}{dr}\right)^2\right]^{3/2}} \qquad (2.5)$$

where z is the surface height and r is the radius. The tangential curvature is defined as

$$\kappa_t = \frac{\dfrac{\partial^2 z}{\partial x^2}}{\left[1+\left(\dfrac{dz}{dx}\right)^2\right]^{3/2}} + \frac{1}{r}\frac{\partial z}{\partial r} \qquad (2.6)$$

where x is the arc length of the disk. The first term in equation (2.4) is the circumferential component and the second term is the radial slope component

(coning). This equation (2.4) can be applied to disks of different form factors with concave or convex shape and to sliders of different form factors and air-bearing designs. The overall static flying height variation due to disk shape distortion is a combination of both crown and camber effects. However, in the case of constant radius, the radial components in the equation (2.5) and (2.6) will be omitted, i.e., $\frac{\partial z}{\partial r} = 0$. By substituting (2.6) into (2.4), the static flying height variation due to circumferential components can be rearranged as

$$\Delta h = \alpha_{crown} \frac{L^2}{8} \frac{\frac{\partial^2 z}{\partial x^2}}{\left[1 + \left(\frac{dz}{dx}\right)^2\right]^{3/2}} \qquad (2.7)$$

Noted in the above equations, if a first spectral component of disk shape is assumed, the relation between z and x can be estimated as $z = A\sin\omega t = A\sin\left(\frac{x}{r}\right)$. Therefore, equation (2.7) can be further simplified as:

$$\Delta h = -\alpha_{crown} \frac{AL^2}{8r^2} \frac{\sin\omega t}{\left[1 + \left(\frac{A}{r}\cos\omega t\right)^2\right]^{3/2}} \qquad (2.8)$$

where, A is the flatness and ω is the rotation speed of the disk. Equation (2.8) suggests that static flying height variation depends not only on the amplitude of the disk distortion, i.e., flatness, but also on the disk shape and the sensitivities of the air-bearing slider design to the disk distortion. The negative

coefficient in (2.8) shows the existence of a 90-degree phase difference between the disk distortion and the static spacing loss.

It is not surprising that, the static flying height variation due to disk shape depends strongly on the slider geometry and air-bearing design. To illustrate this, the negative air bearing pico-sliders in Fig. 2.6 are used again in the following flying height variation calculations. From the air-bearing simulation, the slider crown sensitivity can be computed using the CML simulator (2000). Fig. 2.10 shows the simulated flying height against the crown changes for both of the sliders. From the simulation results, it is noticeable that the crown sensitivity is not always linear to the flying height changes. From the regression analysis, the graphs are fitted with a polynomial equation. The slider crown and chamber sensitivity can be calculated as the differential of the graph, i.e., $\alpha = \frac{\partial FH}{\partial C}$. Table 2.1 lists the obtained sensitivities for above two designs.

Sensitivity	**Slider A**	**Slider B**
α_{crown}	0.001C+0.1155	0.0004C+0.0664
α_{camber}	0.0005C-0.0283	$0.0015C^2$-0.0302C+0.0788

Table 2.1 Crown and camber sensitivity for slider A and B

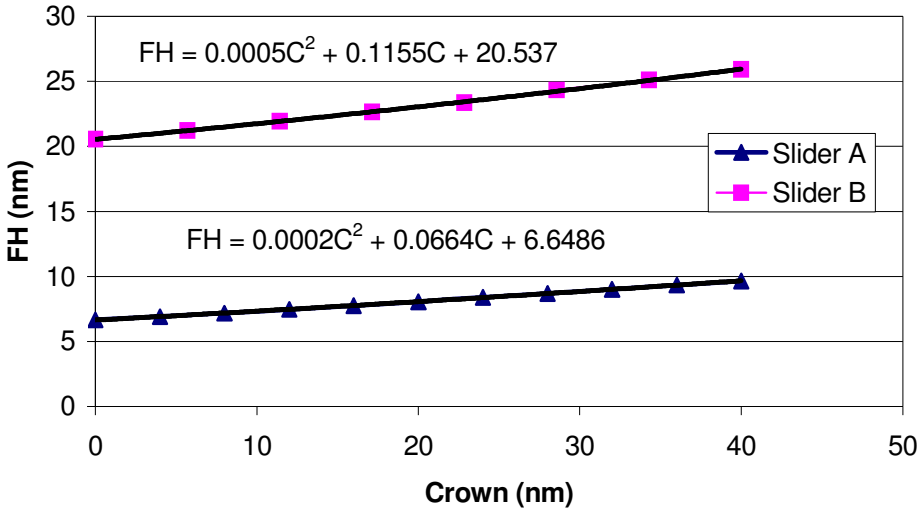

Figure 2.10 Sensitivity of the flying height to crown changes for Slider A and B

To illustrate how disk distortion affects the spacing loss, the well-known "potato chip" clamping distortion of the disk which can be visualized in Fig. 2.2(b) with 10-μm flatness is taken as an example for a detailed analysis. The flying height variation induced by the disk distortion was simulated by (2.8) and the results are shown in Fig. 2.11. Both slider A and B were used in the simulation. Note that the derived result in Fig. 2.11 conforms to the experimental results in both amplitude and phase difference. The results witness the highest flying height variation occurred at the peak and valley of the disk distortion where the curvature of the disk is at the maximum point. It is interesting to note that Slider A with lower crown sensitivity has a small flying height variation compare to Slider B. This example underscores the importance of crown sensitivity to the flying height variation of the slider.

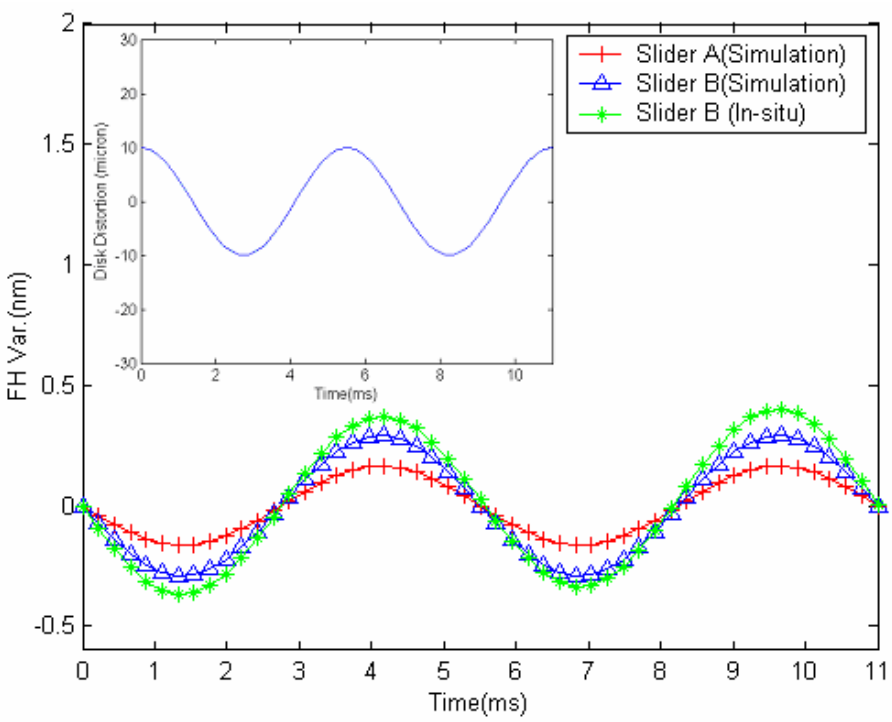

Figure 2.11 Static flying height loss simulation and measured results for Slider A and B

2.5. Summary

Reducing the flying height to sub-10 nm triggered the concerns of flying height variation induced by disk clamping distortion as any flying height variation could lead to head disk contact and affecting the head disk interface stability. The testing results of flying height variation induced by disk clamping distortion are presented using the *in-situ* testing method. The measured results reviewed that flying height variation increase proportionally to the intensity of the disk distortion. Higher air bearing stiffness will reduce the amount of flying height variation of the slider. Also, it is interesting to notice that the lower flying height slider can introduce a higher percentage of

flying height variation compared with the slider of higher flying height. Furthermore, the changes of loading force at lower flying height case may correspond to higher percentage of flying height variation, comparing with higher flying height case. A theoretical model was also developed to explain the flying height variation induced by the disk clamping distortion. The simulation results show the correlation between the flying height variation induced by the crown sensitivity of the slider and the disk clamping distortion.

CHAPTER 3

SPINDLE MOTOR VIBRATION AND SLIDER'S FLYING

Spindle motor vibration is the other external factor apart from the disk deformation that induces flying height variation and affecting the stability of the head-disk spacing and readback performance of the disk drive. This chapter reports the study on the relationship between slider's dynamic flying height stability and spindle motor vibration. The investigations were carried out with *in-situ* flying height testing technology introduced by the authors. The unbalanced modes, which are the rocking motion of the spindle, were studied in the experiment. Results obtained show that the dynamic stability of slider is a function of the spindle vibration. It is interesting to notice that higher frequency vibration of spindle motor has a greater effect on slider dynamics. Investigations are also extended to characterize the dynamic behavior of the sliders with two types of air-bearing surface (ABS) designs. Results indicate that sliders with higher roll stiffness are of better dynamic performance and flying height stability under the unbalanced modes vibration of spindle motor.

3.1 Introduction and Problem Definition

As the areal density of the magnetic recording increase to 1 Tb/in^2, the flying height is predicted as 3.5nm with a variation less than 0.35 nm. There are numerous parameters that could increase the flying height variation and

affect the stability of the head-disk spacing and readback performance of the disk drive, the effects of some of which are still unknown. The spindle vibration induced flying height variation is one of them that are not properly addressed. Above 10-nm flying height (FH), the magnitude of spacing variation, induced by the spindle vibration is negligible compared with the magnitude of the flying height. However, further reduction in the flying height had triggered concerns as any spacing variation could lead to head disk contact. In the past, some investigations were carried out to characterize the spindle vibration and its impact on the stability of the head-disk interface (HDI). The objective of their studies was to investigate the contribution of the spindle vibration to overall track misregistration (TMR) (Guo and Chen, 2001). Recent studies by Lee et al. (2003) revealed the correlation between the slider dynamic and the spindle vibration. His experimental studies show that flying height variation increases when the measurement location is closer to the spindle motor. Many researchers have intensively studied the dynamic of the slider through simulation approaches (Lida et al., 2002; Ono and Takahashi, 1998). Ono and Takahashi (1998) simulated the bouncing vibrations, tracking ability, and wear durability of sliders with respect to air bearing stiffness, contact force, contact stiffness, and damping. Although the flying stability of the slider can be investigated using numerical simulation coupled with actual spindle vibration, the measured experimental data is much more useful for better understanding of the HDI and for designing a more reliable interface. Until now, appropriate experimental methodology to investigate this phenomenon is still lacking.

This chapter presents the exploration of characterization methodology and investigations on the dynamic flying stability of the slider induced by the spindle vibration. The experimental setup is developed and the triple harmonic ratio method is introduced to predict the forced responses of the systems. Two types of sliders with different ABS designs were used in the experiment.

3.2. Description of Experiment

3.2.1. Measurement Methodology for Flying height Variation

Laser Doppler vibrometer (LDV) is the most popular tool used in measuring flying height variation. However, due to the testing principle and signal to noise ratio (SNR) limitations, signal averaging is a requirement for LDV measurement. As a result, only averaged or static flying height modulation (FHM) can be tested (Zeng et al., 2001; Thornton et al., 2002). The triple harmonic method (Yuan et al., 2001) described in section 2.2.1 of chapter 2 was explored and used to measure the flying height variation. There are multiple frequencies in flying height signals; the low-frequency signal is associated with the disk clamping/flutter/vibration as discussed in chapter 2; whereas the high frequency signal is related to the air-bearing surface (ABS) vibration and disk waviness. An appropriate averaging and filtering method is needed in order to categorize the measurement results. In the study of spindle vibration induced flying height variation; the low-pass filter with a cutoff frequency of 5 kHz was used to filter out flying height variation induced by ABS vibration, disk waviness and suspension vibration. The frequency

response function (FRF) of the flying height variation, which provides detail of the slider dynamic behavior, is calculated by spectrum analyzer.

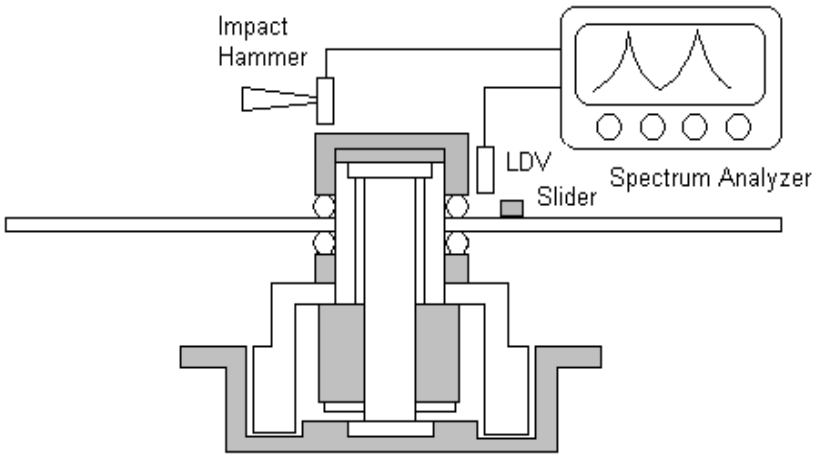

Figure 3.1 Schematic of the experimental setup

3.2.2. Disk/spindle Vibration Measurement

In general, disk/spindle vibration has both balanced and unbalanced modes (Shen et al., 1995). For balanced modes, no vibration results at the spindle and base structure. The vibration of disk moves out-of-phase and is balanced with each other. For the unbalanced modes, the disk moves in-phase and the vibration exists at the spindle and base. The unbalanced modes usually appear in pairs, which are known as forward and backward procession. Often, the unbalanced vibrations are excited by spindle bearing defects and external shock. In contrast, the balanced modes primarily result from the deflection of the spinning disks. Therefore, it can be predicted accurately by classical vibration analysis of rotating disks (Shen et al., 1995). The experimental setup

consists of an impact hammer, a LDV for axial disk vibration measurements and a spectrum analyzer to calculate FRF; see Fig. 3.1. The primary objective of using an impact hammer to simulate the spindle vibration is to differentiate the balanced and unbalanced modes. The amplitude of the shock impulse, which is approximately 30 mg and 50 mg, is manually controlled by the height and the weight of the impact hammer to obtain repeatable and consistent FRF. To minimize the contribution from the balanced modes, the setup adopts the following modifications. Firstly, the hammer applies the impact force near the inner rim of the spindle. Secondly, the axial vibration is measured near the inner rim, where the disk vibration is minimal. Fig. 3.2 shows the LDV measurement of the disk vibration and comparison is made between those with hammer excitation and those without. The waterfall plot was used to identify the vibration mode of the disk/spindle system (Shen et al., 1995). Here, (0,1)U and (0,1)B devote the unbalanced and balanced modes, respectively. Whereas, (0,0) denotes the axisymmetric mode and (0,2) denotes 2-nodal-diameter mode, and so on. Theoretically, all modes split into forward and backward resonance (Tseng et al., 2003). For example, the peak around 400 Hz forms the first (0,1)U, which is also known as rocking modes or gyro modes and 550 Hz is the second (0,1)U mode. The peak around 900 Hz is the (0,0)U mode, where the spindle and disk vibrate in axial direction. Since the excitation is conducted near the inner rim of the spindle, (0,0)U generates the highest vibration as compared to the other modes. The (0,0)U and (0,1)U modes are the main focus for this experiment because they show a significant displacement component in the disk plane. This directly affects the dynamic

flying stability of the slider and eventually degrades the read/write performance of the HDD.

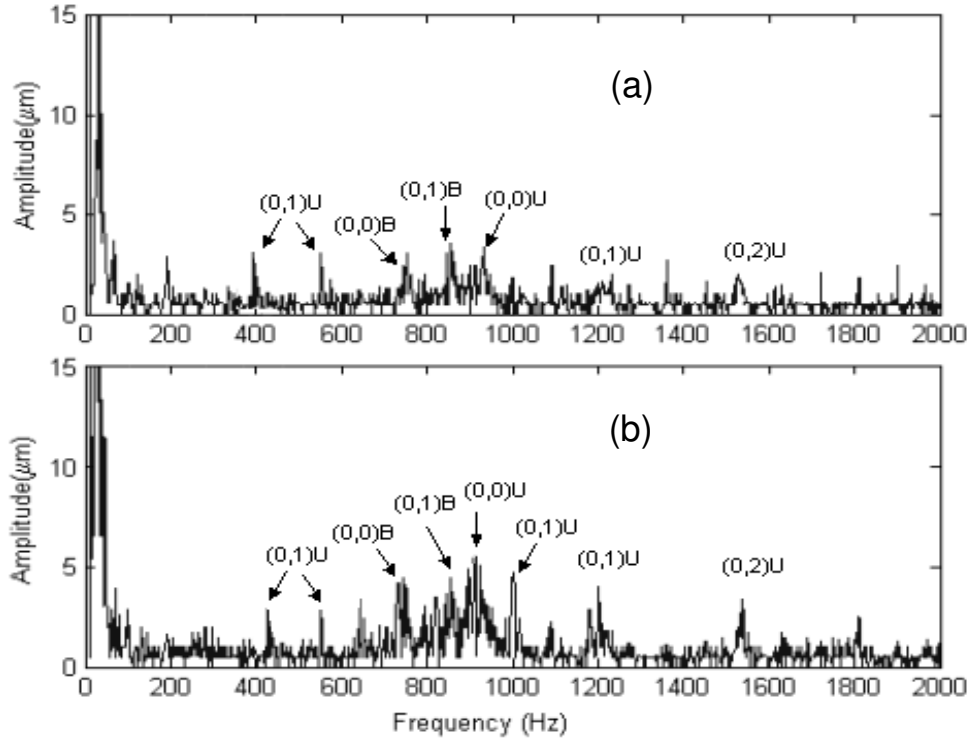

Figure 3.2 FFT representation of disk vibration for (a) without excitation and (b) with excitation (30mg) experimentally measured.

3.3. Results and Discussion

3.3.1. Flying height Variation Induced by Spindle Vibration

The purpose of the experiment is to identify the effect of this spindle vibration to the flying height variation of the slider. A pico slider was used in the disk/spindle system. The same slider in chapter 2 was used in the experiment. This slider was designed and developed to fly at flying height of 7 nm. The air pressure of the slider (Slider A), as shown in Fig. 3.3, was

simulated using the interface simulator developed by Computer Mechanics Lab., University of California at Berkeley (2000).

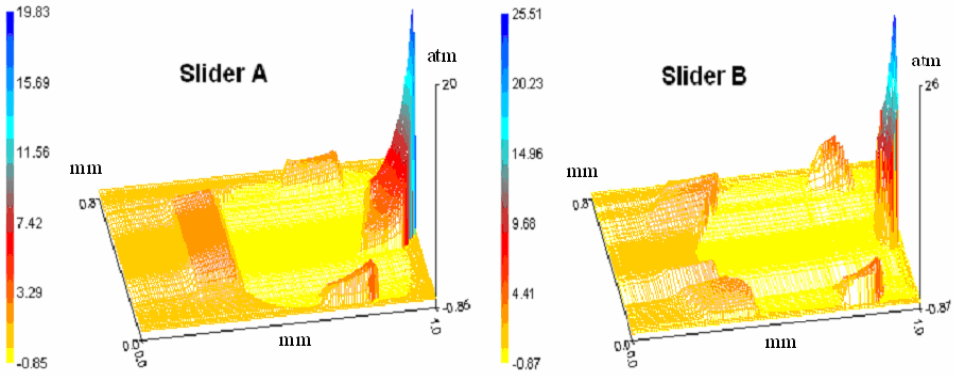

Figure 3.3 Simulated air bearing pressure for Slider A and Slider B.

In this experiment, the slider was positioned at the inner diameter (ID) of the disk to reduce the effect of the balanced modes which was discussed in section 3.2.2. The flying height variation of the slider measured in time and frequency domain by *in-situ* method are shown in Fig. 3.4 and Fig. 3.5, respectively. Fig. 3.4 shows the flying height variation before and after the excitation. Before the excitation (thicker line), the flying height variation was induced by disk clamping distortion with a typical S-shape (one revolution). This is correlated to the slanted disk deformation. The explanation for this type of flying height variation was discussed in chapter 2. During the excitation (thinner line), the results indicate an increase in flying height variation compared with the results before excitation. Details of the flying height variation can be explained by frequency domain analysis.

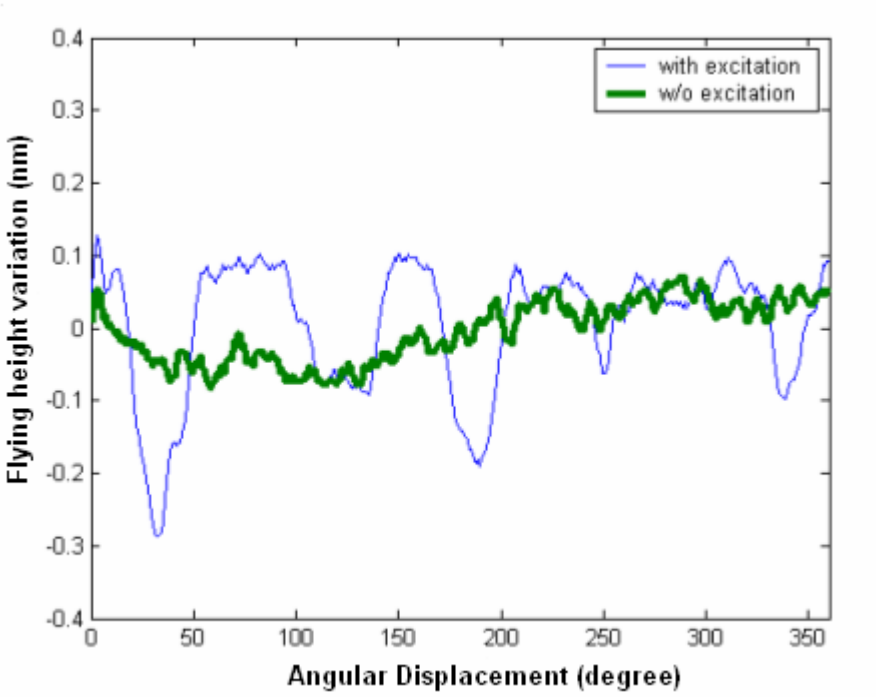

Figure 3.4 Time domain representation of slider's flying height variation with and without excitation experimentally measured.

The frequency domain representation of the flying height variation in Fast Fourier transform (FFT) is shown in Fig. 3.5. Fig. 3.5(b) shows that the peaks around 450 Hz and 600 Hz form the first pair of the (0,1) unbalanced mode, whereas the peaks around 950 Hz and 1200 Hz form the second (0,1) unbalanced mode. The denotations of the modes were defined in section 3.2.2. The disk vibration and flying height variation were measured in two different systems which have different triggering time. Therefore, frequency shifts are observed in the results.

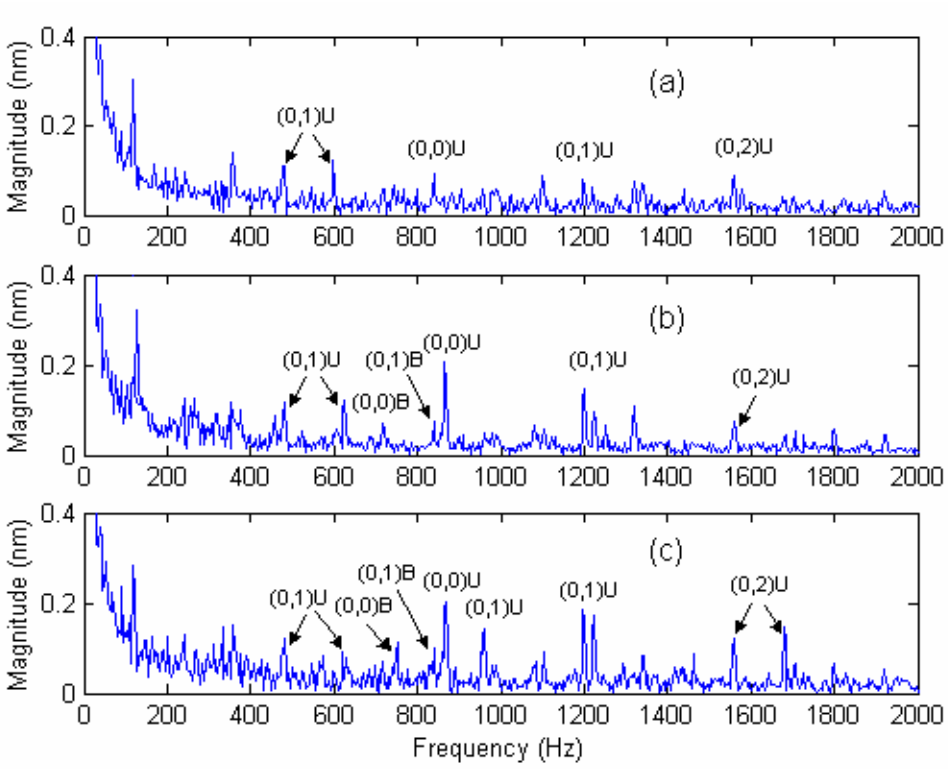

Figure 3.5 FFT representation of slider A flying height variation for (a) without excitation, (b) with excitation (30mg) and (c) with excitation (50mg) experimentally measured.

Generally, the flying height results coincide with the LDV measured spindle vibration as shown in Fig. 3.2. This indicates a correlation between the spindle vibration and the flying height variation. In Fig. 3.5(b), the unbalanced modes, which were contributed by the radial vibration of the spindle motor, are affecting the flying height variation significantly. The experiment continued by increasing the excitation force to 50 mg, which is shown in Fig. 3.5(c). It is interesting to see that the magnitude of second (0,1)U and first (0,2)U modes increase, as the magnitude of the excitation increases. However, the lower frequency components are unaffected by the excitation. This revealed the

variation of the slider following ability to different vibration modes. It is believed that higher frequency vibration modes will have a greater effect on the flying height variation as compared to lower frequency components. Some of the resonances split into 3 or multiple peaks, as shown in Fig. 3.5(b) and 3.5(c). These multiple peaks represent the slightly different resonance frequencies of the disk vibration resulting from the acoustic coupling between the disk and the surrounding air (Tseng and Wickert, 1998). The results also indicate that the balanced modes do not have a significant impact on the flying height vibration. It can be seen that (0,0)B and (0,1)B are not significantly affected by both of the excitations.

3.3.2. Sliders Performance Comparison

To characterize the dynamic behavior of the sliders under the effect of spindle vibration, another type of slider (Slider B) was used. The air pressure of Slider B is shown in Fig. 3.3. Table 3.1 shows the simulated stiffness matrix for the two types of sliders. The stiffness matrix, K shows the relationship between the slider's altitude, U (flying height, pitch and roll) and the slider's acting forces, F (gram load, pitch torque and roll torque). The equations of the relationship are as follow:

$$\boldsymbol{K} \cdot \boldsymbol{U} = \boldsymbol{F} \qquad (3.1)$$

$$\begin{bmatrix} \boldsymbol{k}_{11} & \boldsymbol{k}_{12} & \boldsymbol{k}_{13} \\ \boldsymbol{k}_{21} & \boldsymbol{k}_{22} & \boldsymbol{k}_{23} \\ \boldsymbol{k}_{31} & \boldsymbol{k}_{32} & \boldsymbol{k}_{33} \end{bmatrix} \cdot \begin{bmatrix} \boldsymbol{h} \\ \boldsymbol{p} \\ \boldsymbol{r} \end{bmatrix} = \begin{bmatrix} \boldsymbol{L} \\ \boldsymbol{PT} \\ \boldsymbol{RT} \end{bmatrix} \qquad (3.2)$$

where, *h*, *p* and *r* represent the flying height, pitch and roll. *L*, *PT* and *RT* are the gram-load, pitch torque and roll torque respectively. Generally, both sliders' pitch stiffness is almost the same (Slider A, 1.1 μrad and slider B, 1.16 μrad). However, roll stiffness of Slider B is 2 times higher than that of Slider A (Slider A, 0.0689 μrad and slider B, 0.140 μrad). The differences were used in the experiment to determine the influence of roll stiffness on the flying height variation.

SIMULATED STIFFNESS MATRIX (SLIDER A)

	Height (nm)	Pitch (μrad)	Roll (μrad)
Load (gram)	3.98E-01	2.18E-01	-2.82E-03
P-Torque (μN-M)	1.79E+00	1.10E+00	-4.90E-03
R-Torque (μN-M)	-5.31E-03	5.79E-03	6.89E-02

SIMULATED STIFFNESS MATRIX (SLIDER B)

	Height (nm)	Pitch (μrad)	Roll (μrad)
Load (gram)	4.63E-01	2.45E-01	1.74E-04
P-Torque (μN-M)	1.90E+00	1.16E+00	-4.99E-03
R-Torque (μN-M)	-4.49E-03	-2.92E-03	1.40E-01

Table 3.1 Simulated stiffness matrix for slider A and B.

Fig. 3.6 shows the FFT of the flying height variation measured by *in-situ* method. Comparing the results in Fig. 3.6 with Fig. 3.5, it is noticed that both (0,0) and (0,1) unbalanced modes do not have a significant impact on the flying height variation of Slider B as compared to Slider A, even though both of the sliders were under a similar spindle vibration. The unbalanced modes dissipate a vibration, which is parallel to the roll angle of the slider movement. It is believed that unbalanced vibration modes could affect the roll movement

and the overall dynamic performance of the slider. The result also shows that higher roll stiffness could reduce the flying height variation induced by the spindle vibration.

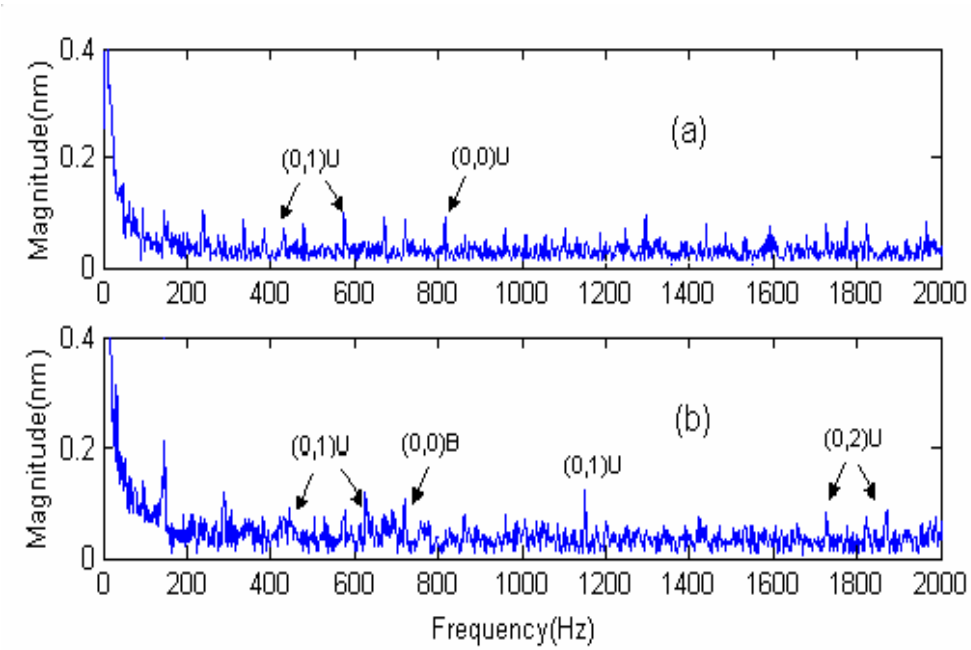

Figure 3.6 FFT representation of slider B flying height variation for (a) without excitation and (b) with excitation (30mg) experimentally measured.

3.4. Summary

Spindle vibration is one of the main external factors that induce flying height variation and affecting the read/write reliability of the magnetic recording storage. The disk deformation has been investigated in chapter 2, this chapter discussed about the dynamic variation of slider's flying height induced by spindle motor vibration using the *in-situ* testing method. A pair of (0,1) unbalanced modes with a frequency split was detected in flying height variation when the impact hammer excited the spindle. The measured results

revealed that the balanced modes relatively do not have a significant impact on the flying height variation. Higher air bearing roll stiffness will reduce the amount of flying height variation induced by spindle vibration.

CHAPTER 4

EXPLORATION OF THE IN-SITU MOTION OF HEAD-SLIDER IN BOTH FLYING HEIGHT AND OFF-TRACK DIRECTIONS

The slider dynamics discussed in the previous chapters was focused on one-dimensional measurement that was perpendicular to the disk or the flying height variation. The flying dynamics and stability of the slider is not limited to flying height. The off-track direction or the in-plane movement could also jeopardize the read/write performance in the data recording if it is not properly controlled. In this chapter, a novel method to determine the motion of the slider in flying height and off-track direction simultaneously is presented. The results show the relative movement of the slider in two dimensions, both during thermal actuator controlled contact and full flying condition. A method for separating the position error signal (PES) and the flying height signal from the readback signal is introduced. The method includes writing dual-frequency pattern tracks adjacently, and with the readback signals from the tracks filtered for the in-situ motion measurement. The harmonic ratio method was used to determine the flying height variation of the head whereas the conventional servo burst detection method was used to determine the PES.

4.1 Introduction

In order to achieve the targeted areal density of 1 Tb/in^2 in hard disk drives, the linear density and the track density must be increased to around 1.85 Mbpi and 540 ktpi respectively (Wood, 2000). The increases in linear and track density require smaller head-disk clearance and improvement of track registration for the head. As the clearance is subsequently reduced to sub-5nm, the slider tends to contact the disk and exhibit track misregistration and flying height variation (Wang et al., 2001; Ono et al., 1998). Therefore, it is important to verify the off-track and flying height variation *in-situ* so that the performance in terms of slider motion can be analyzed. Numerous techniques have been developed to measure the off-track (Mamun et al., 2003; Serrano, 2000) and flying height variation using the readback signal (Smith, 1999; Brown et al., 1988). However, there is little methodology which measures both of the motions simultaneously (Wang et al., 2001). In this chapter, we will introduce a novel method to analyze these motions. The measurement technique is based on the harmonic ratio method (HRM) (Brown et al., 1988; Yuan et al., 2002). The techniques utilize the ratio of the first harmonic (fundamental) amplitude and the harmonic amplitude of the readback signal to measure the displacement, clearance and spacing of the slider in respect to the track. These measurement techniques are reported to be sensitive only to the readback signal amplitude of the harmonics (Yuan et al., 2002). A thermal actuator head was used in the experiment. The contact intensity was controlled by the protrusion of the thermal actuator.

4.2 Description of Experiment

Numerous researches have used in-situ flying height measurement method to study the single-dimensional parameter of the slider motion (Smith, 1999; Brown et al., 1988). The proper interpretation of two-dimensional slider's motion measurement is now described. The measurement method is primarily based on the harmonic ratio method (HRM) which is a continuous, instantaneous readback signals measurement of the ratio of two spectrum's amplitudes. Special adjacent tracks are prewritten on the disk using the spinstand as shown in Fig. 4.1.

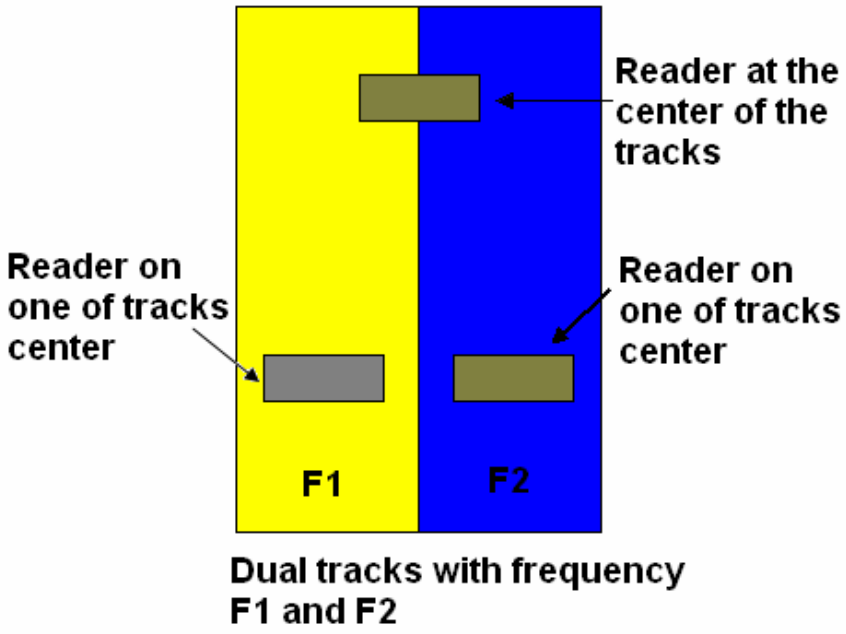

Figure 4.1 Schematic of the adjacent tracks that were prewritten on disk with frequency *F1* and *F2*.

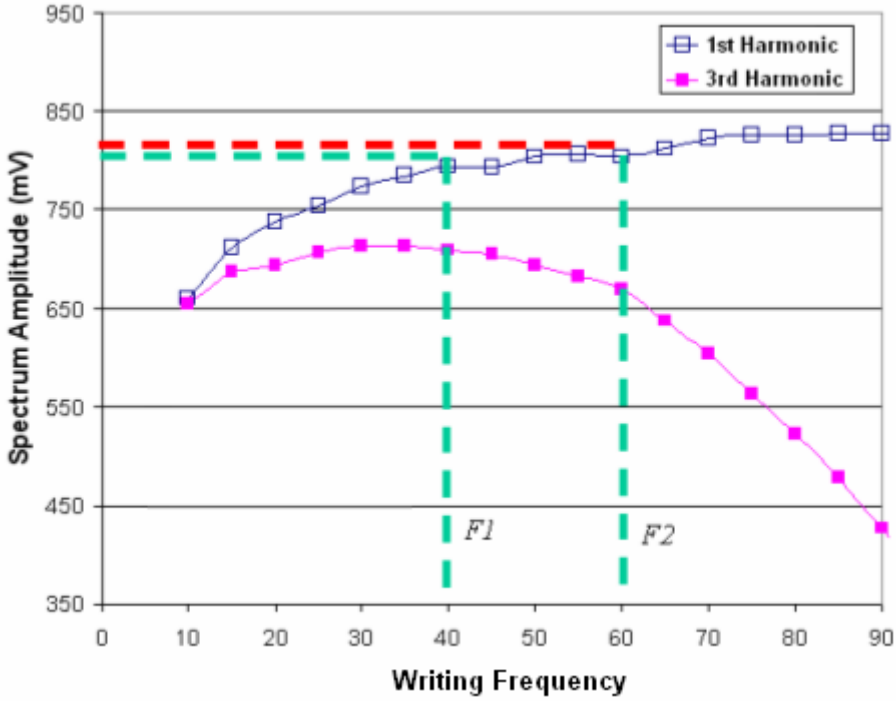

Figure 4. 2 Spectrum amplitude of first and third harmonics of the readback signal at different writing frequencies (MHz)

The tracks are written using all-one pattern signals at two different frequencies. The writing frequencies of the tracks can be determined by the readback spectrum of the head. Fig. 4.2 shows the spectrum power for the first and third harmonics of the readback signals, which is plotted against the writing frequency. These two harmonics are the largest two odd harmonics in the readback spectrum. For higher sensitivity in flying height measurement, the readback signal's frequency *F1* and *F2* should be chosen in such a way that the amplitudes of the harmonics are both as high as possible. Furthermore, it is desired to get the comparable signal amplitudes for both tracks, so that the amplitude deviation due to the effect of frequency response of the electronics can be minimized. In this example, the tracks can be written at frequency *F1*

(40 MHz) and *F2* (60 MHz) respectively. The relation between these two tracks is determined by the ratio of the readings, which is calculated as

$$\alpha = \frac{V_2 - V_{ns}}{V_1 - V_{ns}} = \frac{\Delta V_2}{\Delta V_1} \qquad (4.1)$$

where V_{ns} is the background noises and V_1, V_2 are the amplitudes of the respective readback signals of the tracks for frequency *F1* and *F2* respectively. In a more generalized form, the relation between V_2 and V_1 is derived as

$$\Delta V_2 = \alpha \Delta V_1 \qquad (4.2)$$

After we have determined the relation between these two tracks, the sensor of the head is positioned in the middle of the two tracks as shown in Fig. 4.1. The center of the tracks is determined by the track profile measurement using the spin-stand application. In this case, each track contributes a portion of the readback output of the sensor. The readback signal is filtered by two separate narrow band-pass filters and the voltage amplitudes of the readback signals are recorded simultaneously. The respective output signals for one revolution recorded by both of the narrow band-pass filters are shown in Fig. 4.3. The signals measured and recorded are comprised of both position error and flying height signal. The PES is the measurement of the head on-track positioning. The readback amplitude varies as the head moves away from the center of the track. The flying height signal is the measurement of the clearance between the head and the disk. The readback amplitude varies as the head moves away (or close) to the disk surface.

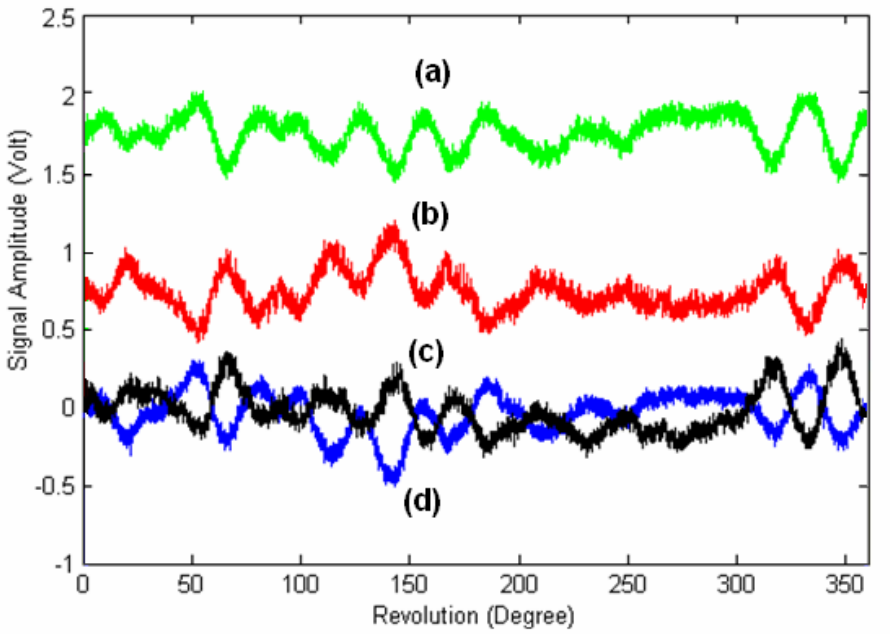

Figure 4.3 Readback signals with writing frequency of (a) 60MHz and (b) 40 MHz in *DC* voltage, (c) 40 MHz and (d) 60 MHz in *AC* voltage.

The readback signal is an inaccurate means to measure flying height variation unless the off-track position of the head is known. Off-track motion of the head will generate apparent flying height variation by modulating the amplitude of the readback signal. However, our modified HRM (dual wavelength), which is similar to multi-frequency method (Zhu and Liu, 2006), is less sensitive to the signal fall-off due to the off-track motion of the head. Furthermore, minimum head-disk contact intensity was generated in the testing which was controlled by the thermal actuator. The flying height harmonics are obtained by integrating the readback signals and removing the PES components associated with track mis-registration. First, the original *DC* offset readback signals are converted into *AC* mode. Assuming that the gains at both frequencies are the same, and then in general, the increase in amplitude

at one frequency is accompanied by a corresponding decrease at the other frequency. Hence the PES signal can be removed by adding the *DC* signal with the *AC* signal at the other frequency. In this case, V_{1DC} is added to V_{2AC} and vice versa.

The output of the results is shown in Fig. 4.4. The results show that the PES is successfully eliminated from the readback signal. The remaining outputs are the changes of readback signals caused by changes in the vertical direction, and can be used to determine the flying height variation.

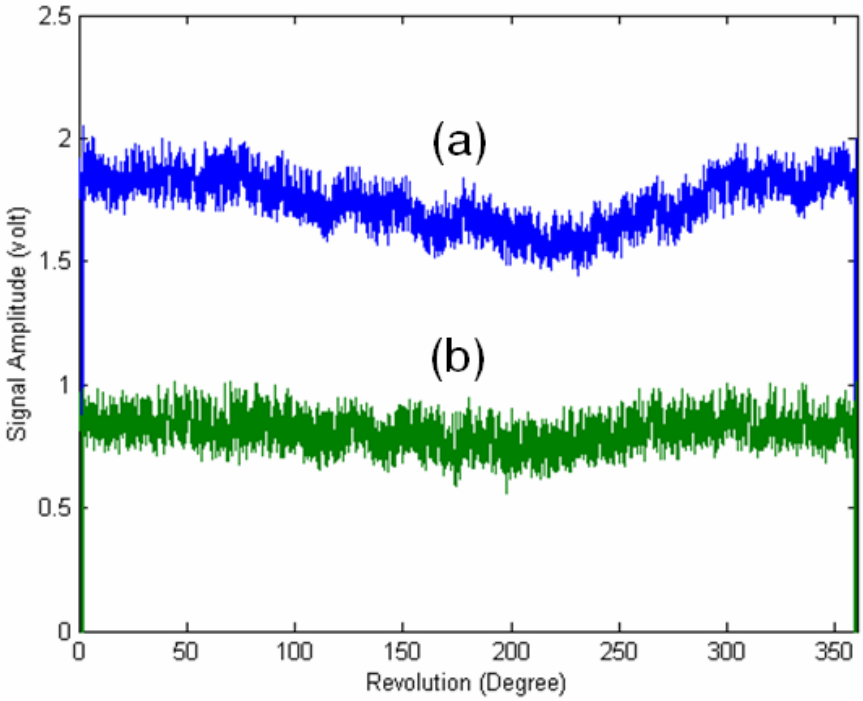

Figure 4.4 Readback signal after PES elimination process for (a) 60 MHz and (b) 40 MHz.

4.3 Flying Height Measurement

The flying height variation for the slider can be determined by the harmonic ratio method (HRM) method introduced by Shi et al. (1985) and Brown et al. (1988). The method shows the harmonic readback signal reduces exponentially as the head disk spacing increases. The Fourier transform of the readback voltage pulse is as follows (Brown et al., 1988):

$$V_{MR}(k) = C \cdot e^{-k(d+a)} \cdot \frac{1-e^{-k\delta}}{k} \cdot \frac{\sin(kg/2)}{kg/2} \qquad (4.3)$$

$$V_1(\lambda_1) = C_1 \cdot e^{-\frac{2\pi}{\lambda_1}(d+a)}; V_2(\lambda_2) = C_2 \cdot e^{-\frac{2\pi}{\lambda_2}(d+a)} \qquad (4.4)$$

where C is a constant, k is the wavelength vector ($2\pi/\lambda$), λ is the recording wavelength, δ is the medium thickness, g is the MR-element-to-shield gap, d is the magnetic head disk spacing and a is the transition parameter. Since δ and g are constants; equation (4.3) can be written as (4.4) where λ_1 and λ_2 are the respective wavelengths of the dual tracks. By taking the ratio between V_1 and V_2, equation (4.4) can be rearranged and the flying height variation d can be derived as:

$$\Delta d = -\frac{\lambda_1\lambda_2}{2\pi(\lambda_1-\lambda_2)} \Delta \ln \frac{(\Delta V_2)_{DC} + (\alpha \Delta V_1)_{AC}}{(\alpha \Delta V_1)_{DC} + (\Delta V_2)_{AC}} \qquad (4.5)$$

where, constant, C is eliminated in (4.5) by considering the changes of the flying height ($\Delta d = d(t_1) - d(t_2)$). The PES is eliminated in (4.5) when DC signal and AC signal is added up, i.e. $(\Delta V_2)_{DC} + (\alpha \Delta V_1)_{AC}$. In order to increase

the sensitivity of the measurement signal, $\lambda_1\lambda_2/2\pi(\lambda_1-\lambda_2)$ should be as small as possible (Yuan et al., 2002). Thus, larger frequency difference between λ_1 and λ_2 is desirable.

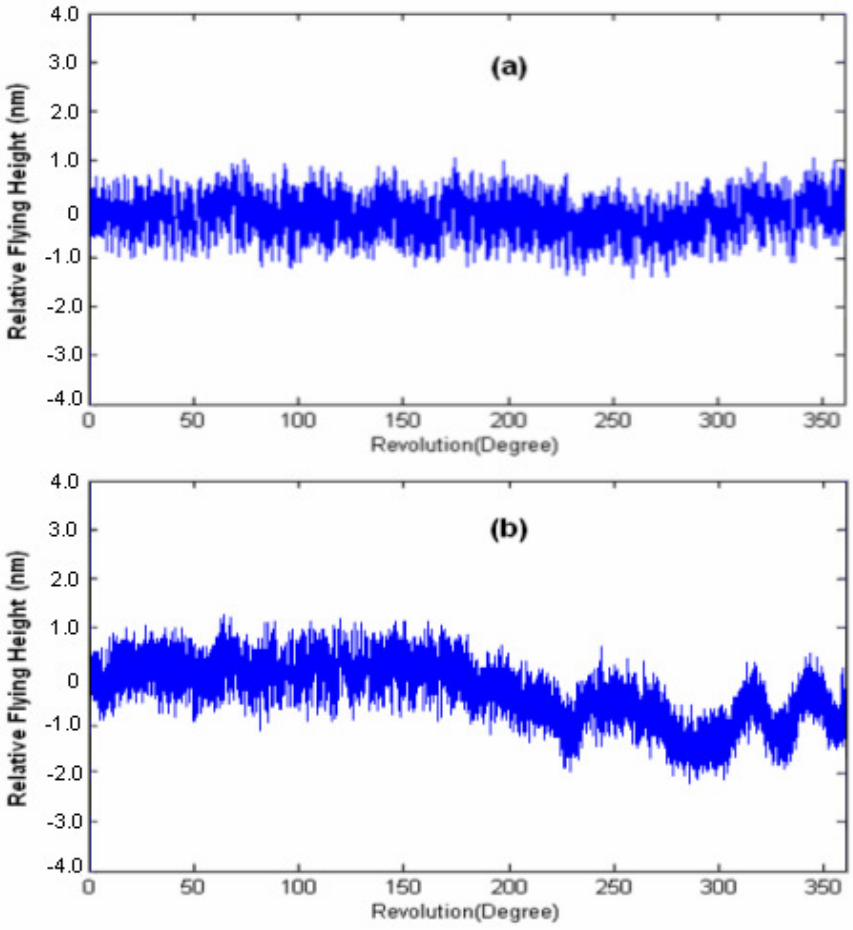

Figure 4.5 Flying height variation measured by harmonic ratio method for (a) fully flying, (b) with head-disk contact.

Fig. 4.5 illustrates the measured flying height variation of the slider where (a) representing the results derived from Fig. 4.4 and the head is at flying condition. The flying height of this commercial slider is 7 nm. The conversion and the calibration of the measurement are done by the spin-up (or spin-down)

of the spindle motor (Brown et al., 1988). The peak to peak flying height variation is less than 1 nm when the slider is in full flying condition. Fig. 4.5 (b) shows the flying height variation where the thermal actuator is activated and the slider comes into contact with the disk. The head-disk contact is closely monitored with AE sensor. Minimum contact is generated to prevent excessive off-track. Peak to peak flying height variation of 3 nm is observed in the one revolution testing. The results show a small flying height variation in the beginning of the contact that slowly intensifies (after 200 degrees) as the contact prolongs.

4.4 Head Position Error Measurement

The mis-registration of the head from the center of the dual-track can be measured by the position error signal (PES). In this experiment, the feedback controlled servo is switched off during the testing so that full PES changes can be observed. The PES signal is used to generate the corrective signal that is applied to the read/write head positioning circuitry. The position of the head can be distinguished by its relative position to the dual-tracks. The dual-tracks were written at two different frequencies. When the read head is positioned on the center of the tracks, the read head can detect the magnetic transitions from both of the tracks at one time. The signals difference from each of the tracks should be zero when the head is exactly position along the track center of the dual-tracks, because the read head will detect the equal amounts of signal from both of the tracks. As the head is affected by contact and runout which causes off-track, the difference between these two signal

amplitudes is known as the *in-phase* PES (Mamun et al., 2003). Since our measurement method detects the relative position of the head with regards to the dual-tracks, the PES for the slider can be determined by the following expression:

$$\boldsymbol{PES} = (\Delta \boldsymbol{V}_2)_{AC} - (\boldsymbol{\alpha}\Delta \boldsymbol{V}_1)_{AC} \qquad (4.5)$$

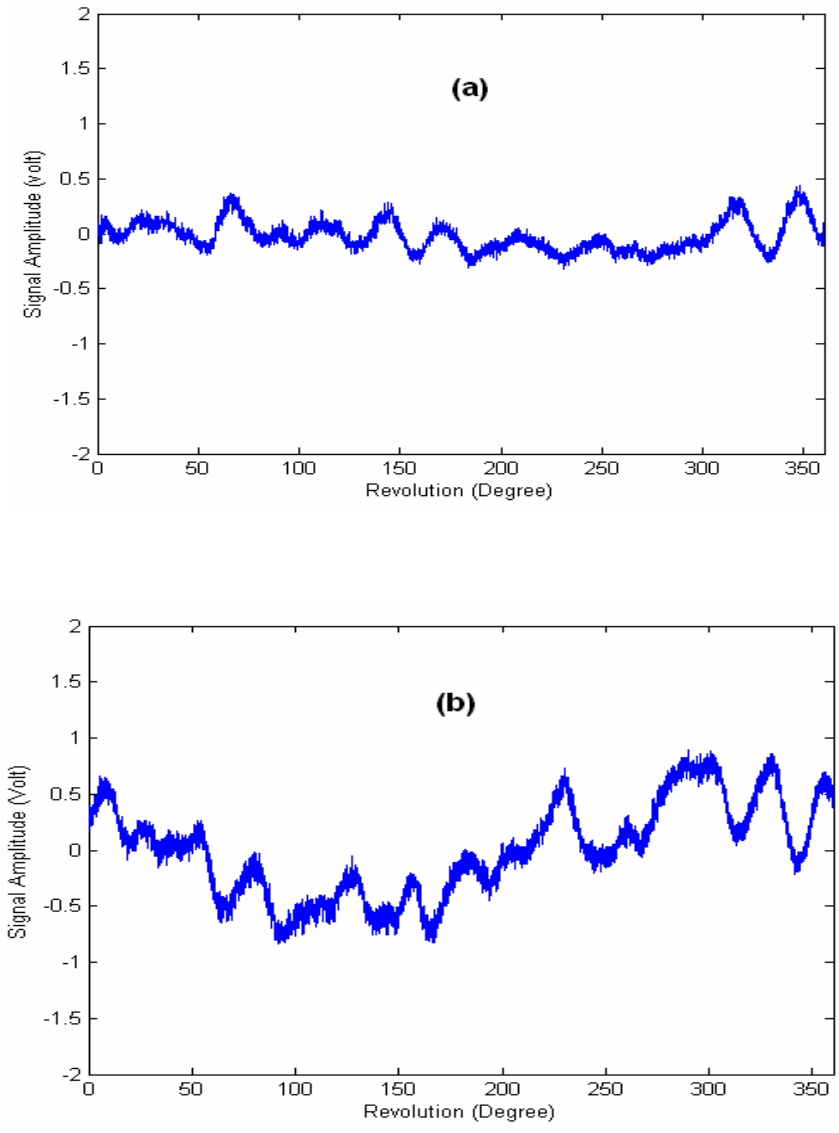

Figure 4.6 Position error measurement results derived from the readback signal for (a) fully flying, (b) with head-disk contact.

The PES measurement is illustrated in Fig. 4.6. The results show slider's in-plane movement due to external factors such as disk vibration or air-flow excitation on the suspension. These PES measurement results are comparable to dual frequency servo burst pattern (Mamun et al., 2003). The dual frequency servo burst pattern is similar to our proposed method where it consists of adjacent servo bursts written in two different frequencies and the *in-phase* PES signal is determined by the difference of burst A and burst B. Fig 4.6(a) shows the PES signal for a fully flying slider where small PES changes were detected. In contrast, higher PES signal were detected when there was head-disk contact as shown in Fig 4.6(b). The results indicate that the slider moved away from the track center in the beginning and returned to the center after 200 degrees where upon larger amplitudes of high frequency PES variation ensued. The larger amplitudes closer to the end of contact is attributed to intensified head-disk contact that also shows up as a larger flying height variation in Fig. 4.5(b). The large off-track movement did not affect the measured flying height as shown in Fig 4.5(b), evidence that the concurrent flying height and off-track measurements are well-decoupled.

4.5 Summary

Additional to the one-dimensional flying height that is widely studied in the previous two chapters, the two-dimensional slider motion was investigated in this chapter. A novel method to analyze the flying height and off-track direction motions of the slider simultaneously was introduced. The

techniques utilize the ratio of the first harmonic (fundamental) amplitude and the harmonic amplitude of the readback signal to measure the displacement, clearance and spacing of the slider in respect to the tracks. The method includes writing dual-frequency pattern tracks adjacently, and with the readback signals from the tracks filtered for the in-situ motion measurement. A method for separating the position error signal (PES) and the flying height (FH) signal from the readback signal is introduced. The relative movement of the slider in two dimensions, both during thermal actuator controlled contact and full flying condition was measured in the experiment.

CHAPTER 5

METHOD AND TESTER FOR OPTICAL FLYING HEIGHT MEASUREMENT

Other than readback based flying height measurements that were discussed in previous chapters, optical measurement is another method that is widely used to determine the flying height. However, currently available optical flying height measurement suffers poor repeatability and accuracy. A method and testing setup for improving the repeatability and accuracy of the optical flying height measurement are introduced in this chapter. The optical measurement method comprises of two adjacent slider flying (dummy and testing slider) on a transparent disk. The optical maximum and minimum calibration is done by varying the rotational speed of the disk relative to the dummy slider. The flying height of the testing slider is calculated using the measured maximum and minimum calibration of the dummy slider, the measured reflected light intensity and the light signal portion reflected from a surface of the disk at a fixed rotational speed between the disk and the testing slider.

5.1 Introduction

The optical calibration process for interferometry based flying height measurement is an important process in determining the accuracy and repeatability of head-disk spacing measurements. The light intensity

calibration is typically performed by measuring the maximum and minimum fringe intensity of a light signed while changing the head-disk spacing by at least ¼ wavelength of the light signed. Existing calibration methods use loading and unloading method to alter the spacing of the disk and slider, such as the method disclosed in U.S. Patent 5,457,534, Lacey et al., (1993). The intensity I_{out} of the light reflected from both the slider and from the glass surface of a transparent test disk based on multi-beam interference is given by:

$$\frac{I_{out}}{I_{in}} = \frac{r_1^2 + r_2^2 + 2r_1 r_2 \cos\delta}{1 + r_1^2 r_2^2 + 2r_1 r_2 \cos\delta} \qquad (5.1)$$

where r_1 and r_2 are fringe intensities of the light reflected off the slider r_1 and the light reflected off the disk r_2, and I_{in} is the incident light intensity. The phase angle difference δ between two reflections is a function of the phase shift ϕ_s on reflection off the slider surface. The value of δ can be derived as,

$$\delta = \frac{4\pi h}{\lambda} + 2\pi - \phi_s \qquad (5.2)$$

where λ is the wavelength of the light, h is the flying height and ϕ_s is the phase shift. The intensity of the resultant light detected at the detector changes as the distance h between the disk surface and the slider surface varies from a low (loaded) to high (unloaded) value. Fig. 5.1 shows a typical plot of intensity changes against time for the load/unloading process.

As the flying height (FH) is reduced to the sub-10 nm region, a higher negative pressure air-bearing is typically required to generate a high suction

force which pulls the slider closer to the disk surface and increases the flying stability of the slider. As a result, the suction force, which is contrary to the unloading force, causes the slider to vibrate when the slider is forced to withdraw from the disk. This vibrational behaviour is clearly discernable in the example curves shown in Figure 5.1 for different light signal wavelength, in the region between the loaded position, and the unloaded position. This vibrational behaviour results in a "smearing" of the periodic intensity changes corresponding to the interference fringes, making a determination of the intensity values for the maxima and minima difficult and inaccurate. This can affect the calibration and measurement accuracy.

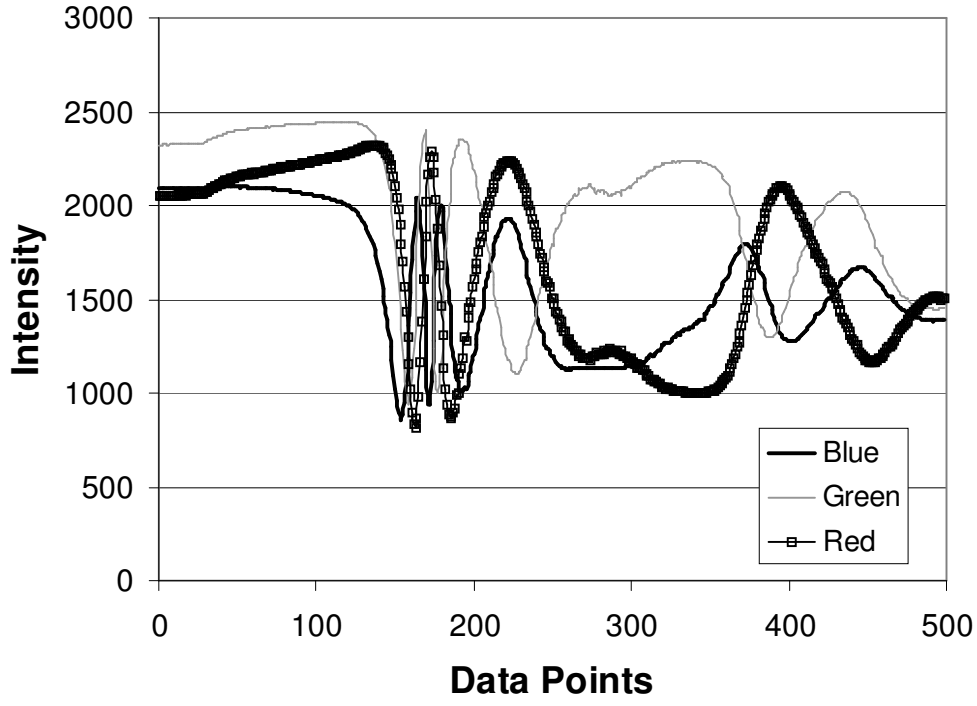

Figure 5.1 Measured intensity changes for load/unload calibration.

The unloading position of the slider is another important factor which can affect the measurement accuracy. Due to the pivoting position of the suspension, the unloading process will affect the pitch angle of the slider. A higher pitch angle will increase the fall-off of the maximum and minimum of the intensity and consequently increase the error in the measurement. Another drawback for the load/unload calibration method is that repeated landing of the slider on the disk may damage and contaminate the air bearing surface (ABS) of the slider. The damages are more significant when an extremely low flying height slider is used in the measurement.

Generally, other than the load/unload method, any mechanism which unloads the head from the disk by a quarter wavelengths or more can be used for the maximum and minimum intensity calibration. For example, in the disk drive system, the relative linear speed between the head and recording media is controlled by the rotational speed of the spindle motor. Increasing the spindle speed will increase the separation of the head and media by changing the air-bearing pressure of the slider. By changing the separation between the head and media, the interferometric intensity varies enough to detect at least one maximum and minimum fringe intensity which can be used for the calibration process, as disclosed in T. Ohkubo et al. (1987). Fig. 5.2 shows the intensity plot of what is termed the RPM calibration process. Curves for different light signal wavelength, show that lower slider vibration can be achieved by using the RPM calibration process compared to the load/unload calibration. Consequently, this will reduce the calibration noise and increase the measurement accuracy.

However, in the RPM calibration process the slider ABS design must be such that the flying height will increase to above λ/2 by changing the RPM of the spindle. Current ABS slider with extremely low flying height, say less than 10 nm, are not able to fly as high as λ/2 even at very high spindle speed.

A need therefore exists to provide an optical flying height calibration and measurement technique that seeks to address at least one of the above mentioned disadvantages.

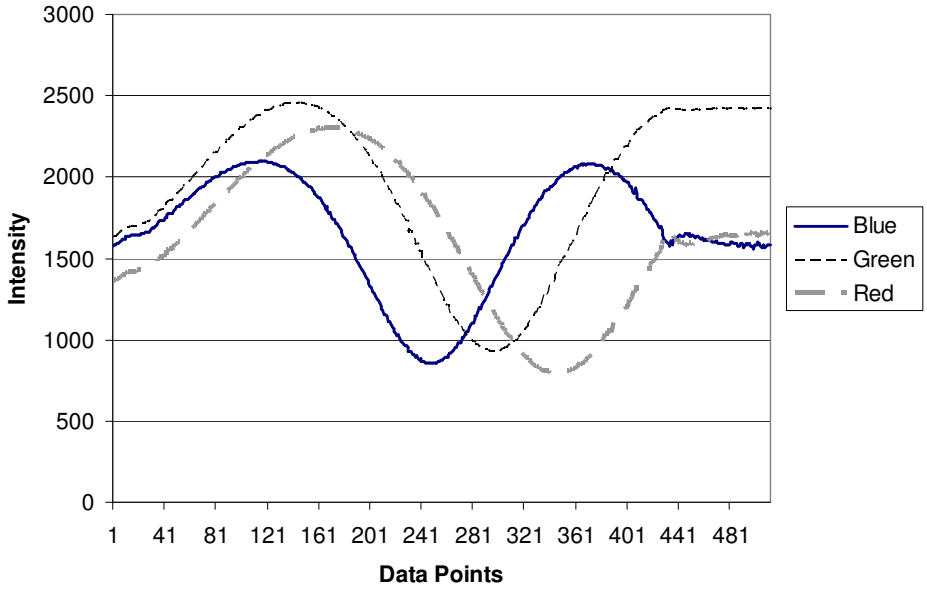

Figure 5.2 Measured intensity charges for RPM calibration.

5.2 Experimental Setup

Fig. 5.3 shows a cartridge which accommodates a dual slider assembly where one of the sliders is a dummy slider and the other slider is a testing slider. Both sliders are mounted side by side such that the flying height calibration and the measurement process can be done simultaneously without

displacement of the cartridge. The dummy slider can be repeatedly used with different testing sliders by merely changing the testing slider.

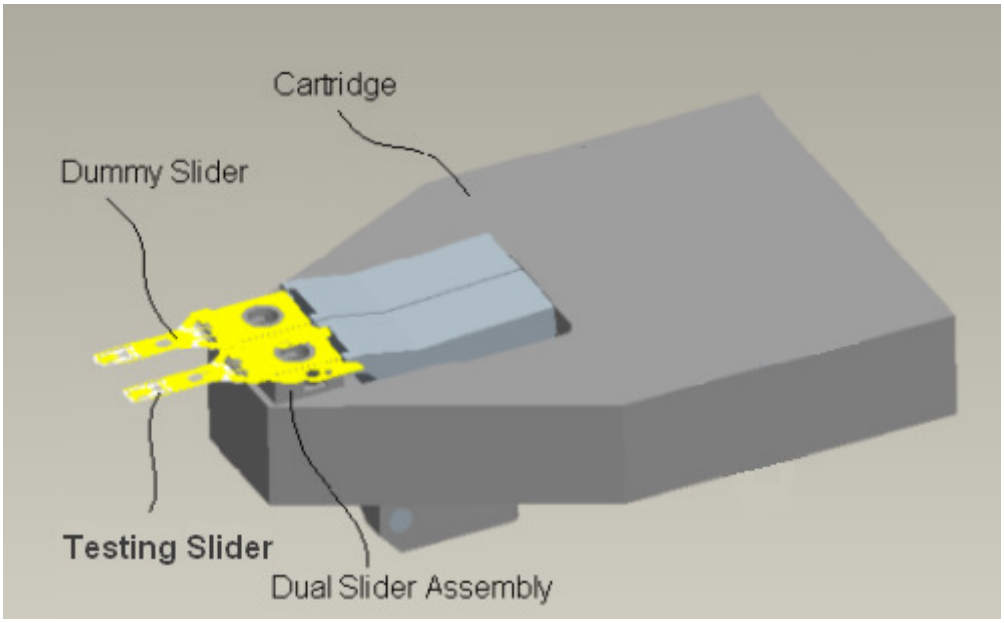

Figure 5.3 A dual slider assembly cartridge used in flying height measurement according to an example embodiment.

Figure 5.4 shows a schematic diagram illustrating a flying height tester in the example embodiment. The flying height tester comprises a transparent disk coupled to a spindle motor which controls the rotational speed of the disk. An X-Y-Z stage is provided for mounting a dual dummy and testing sliders cartridge in the example embodiment. The spindle motor and X-Y-Z stage are mounted on an anti-vibration granite base. It will be appreciated that in different embodiments, single slider cartridges may be provided for the dummy and the testing slider respectively, each mounted on independent X-Y-

Z stages. In such embodiments, a potential interaction between the behavior of the dummy slider and the testing slider may be reduced.

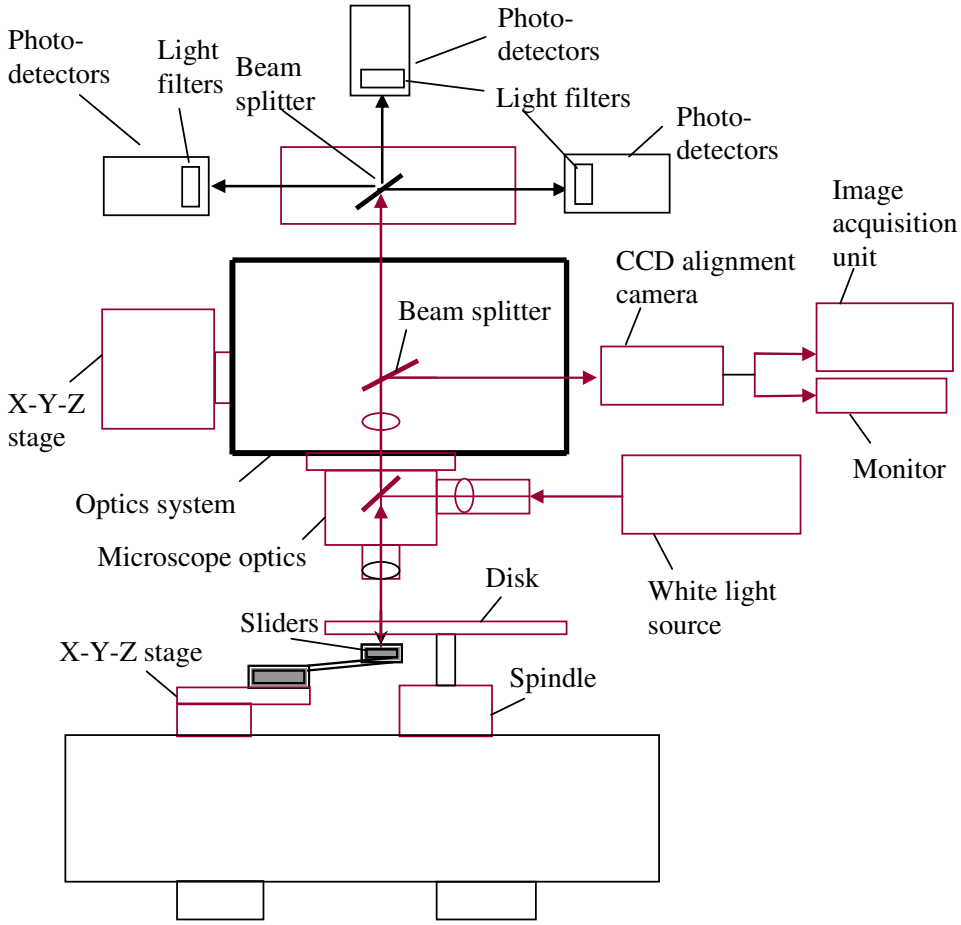

Figure 5.4 A schematic diagram illustrating a flying height tester according to an example embodiment.

The flying height tester comprises a white light source, and an optics system for directing a light signal from the light source towards the surface of the disk and the air bearing surfaces of the dummy and testing sliders. The optics system further comprises optical components for filtering different

wavelengths prior to the detection optics system for performing measurements at different wavelengths.

A microscope system including a CCD alignment camera, microscope optics, image acquisition unit and monitor is also provided to facilitate aligning of the incident light signal from the light source on the respective air bearing surfaces of the dummy and testing sliders.

In operation for calibration and measurement, the dummy and testing sliders are mounted on the cartridge using mounting assemblies, and the cartridge is mounted on the X-Y-Z stage. Next, the pinhole of the optics system, coupled to an X-Y-Z stages unit, is positioned such that the incident light beam from the light source is positioned at the trailing pad of the air bearing surface of the dummy slider. For the calibration measurement, the spindle motor speed is varied from about 1500 to about 20000 rpm while the intensity is captured in the detection optics system via the optics system. The measured intensity is recorded and stored in the detection optics system. The detection optics system in the example embodiment includes wavelength discriminating beam splitters, respective light filters for each individual wavelength of interest, and respective low-noise photo-detector elements in the photo-detectors for each wavelength to be measured.

In the example embodiment, the dummy slider is designed such that for a variation of the rotational speed between about 1500 to about 20000 rpm, the dummy slider undergoes a height variation of just more than half the respective wavelengths to be measured with the flying height tester, thus covering one maximum and minimum fringe intensities pair for the respective wavelengths. The maximum and minimum fringe intensities are determined

by scanning through the measured intensity data over the rotational speed range, and saving the determined maximum and minimum intensities at the individual wavelengths for flying height measurement.

The pinhole of the optics system is then shifted to the sensors on the trailing pad of the air bearing surface of the testing slider. The light intensities measured from the testing slider are then measured at one or more rotational speeds within the operational range of the testing slider, and for the respective wavelengths. The flying height of the testing slider can then be calculated using the maximum and minimum fringe intensities of the dummy slider and the measured intensity of the testing slider at the respective wavelengths. The testing slider can then be replaced by another testing slider for a next measurement, while the dummy slider may be re-used for a number of different testing slider measurements. In the described example, the calibration measurements using the dummy slider are made for each respective optical condition at the time of measurement with different testing sliders, since the optical conditions may vary over time, to increase the accuracy of the respective calibration and flying height measurements.

In the following, the mathematical details of the calibration and measurement method described above are provided. In the described example, there are three measured parameters that are used in the mathematical details. These parameters can be measured directly from the optical system. These parameters are as follow:

1. R_{cal_min} is the reflectivity derived from the minimum fringe intensity measured from the dummy slider;

2. $R_{\_measure}$ is the reflectivity derived from the measured intensity from the testing slider (or the dummy slider), at a particular rotational speed, and
3. R_{cal_max} is the reflectivity derived from the maximum fringe intensity measured from the dummy slider.

Other than the measured parameters, the theoretical values for the maximum and minimum reflectivity, R_{theory_max} and R_{theory_min}, can be calculated as follows:

$$R_{theory\_max} = \frac{r_1^2 + |r_2|^2 + 2r_1|r_2|}{1 + r_1^2|r_2|^2 + 2r_1|r_2|}$$
$$R_{theory\_min} = \frac{r_1^2 + |r_2|^2 - 2r_1|r_2|}{1 + r_1^2|r_2|^2 - 2r_1|r_2|} \qquad (5.3), (5.4)$$

where r_1 is reflection coefficient of the disk-air, r_2 is reflection coefficient of the air-slider:

$$\boldsymbol{r}_1 = \frac{\boldsymbol{n}_1 - \boldsymbol{n}_0}{\boldsymbol{n}_1 + \boldsymbol{n}_0},\ \boldsymbol{r}_2 = \frac{\boldsymbol{n}_0 - (\boldsymbol{n}_2 + \boldsymbol{ik}_2)}{\boldsymbol{n}_0 + (\boldsymbol{n}_2 + \boldsymbol{ik}_2)} \qquad (5.5), (5.6)$$

where n_o the real index of the air above the slider, n_1 is the real index of the disk material and $(n_2\text{-}ik_2)$ is the complex index of the slider material.

In order to relate a theoretical reflection value, R_{theory}, at a particular rotational speed to the measured parameters, the following equation can be utilized:

$$\frac{R_{theory} - R_{theory\_min}}{R_{theory\_max} - R_{theory\_min}} = \frac{R_{measure} - R_{cal\_min}}{R_{cal\_max} - R_{cal\_min}} \qquad (5.7)$$

From equation (5.5), the following equation can be derived, relating R_{theory} to the measured parameters as follows:

$$R_{theory} = \frac{R_{measure} - R_{cal\_min}}{R_{cal\_max} - R_{cal\_min}} \times \left(R_{theory\_max} - R_{theory\_min}\right) + R_{theory\_min} \qquad (5.8)$$

From equations (5.1) and (5.2), the following equation for R_{theory} can be derived:

$$R_{theory} = \frac{I_{out}}{I_{in}} = \frac{r_1^2 + |r_2|^2 + 2r_1|r_2|\cos\left(\frac{4\pi FH}{\lambda} + \phi_s\right)}{1 + r_1^2|r_2|^2 + 2r_1|r_2|\cos\left(\frac{4\pi FH}{\lambda} + \phi_s\right)} \qquad (5.9)$$

where ϕ_s is the phase shift on the reflection:

$$\phi_s = 2\pi - \tan^{-1}\left(\frac{2n_0k_2}{n_0^2 - n_2^2 - k_2^2}\right) \qquad (5.10)$$

From equation (5.9), flying height can be calculated from the following equation:

$$FH = \frac{\cos^{-1}\left[\frac{r_1^2 + |r_2|^2 - R_{theory}\left(r_1^2|r_2|^2 + 1\right)}{2r_1|r_2|\left(R_{theory} - 1\right)}\right] - \phi_s}{4\pi}.\lambda \qquad (5.11)$$

Using equations (5.6) to (5.11), it will be appreciated by a person skilled in the art that flying height can be calculated based on the measured parameters R_{cal_min}, $R_{measure}$, and R_{cal_max}.

Returning to Figure 5.4, the rotational speed is controlled by the acceleration of the spindle motor, which is a constant value. Rapid acceleration can generate excessive heating, sliding and wear to the spindle motor bearing and may eventually disrupt the stability of the acceleration. Therefore, smooth and steady acceleration is preferably used in the measurement so as to maintain the robustness of the spindle motor. This can reduce the jittering and noise in the spindle speed variation.

The dummy slider used in the described example for the maximum and minimum calibration process can fly from as high as 450 nm to as low as 10 nm. Fig. 5.5 and Fig. 5.6 show the ABS design and the flying height plot against the spindle speed variation respectively. Fig. 5.6 shows that the flying height varies from about 10 nm to about 450 nm as the spindle speed changes from about 1500 to about 10000 in an example speed range. The ABS design of the dummy slider is an important factor to determine the stability of the flying height changes against the spindle speed. A preferred design for the dummy slider will minimize the fluctuation in the flying height. A linearly and repeatable change of flying height is preferable compared to non-linear and non-repeatable flying height changes. The range of the spindle speed variation is preferably designed to accommodate the acceptable flying height changes for the testing slider so that no slider-disk contact occurs during the measurement. Typically, the testing slider will have a pre-determined acceptable spindle speed range, e.g., 7000-12000 rpm. Higher or lower speeds

than the acceptable spindle speed range can cause the testing slider to crash. Therefore, the dummy slider is preferably designed to have a flying height variation that can accommodate this acceptable spindle speed range.

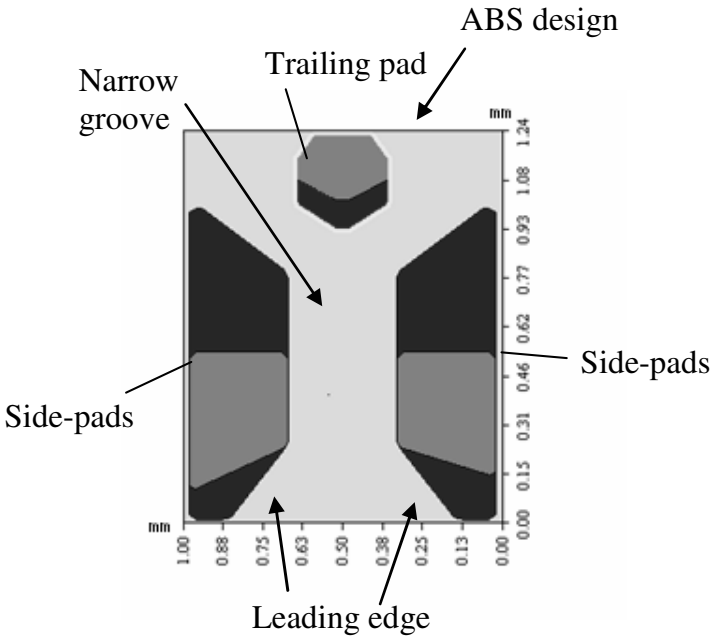

Figure 5.5 ABS design of a testing slider of the dual slider assembly cartridge of Fig. 5.3.

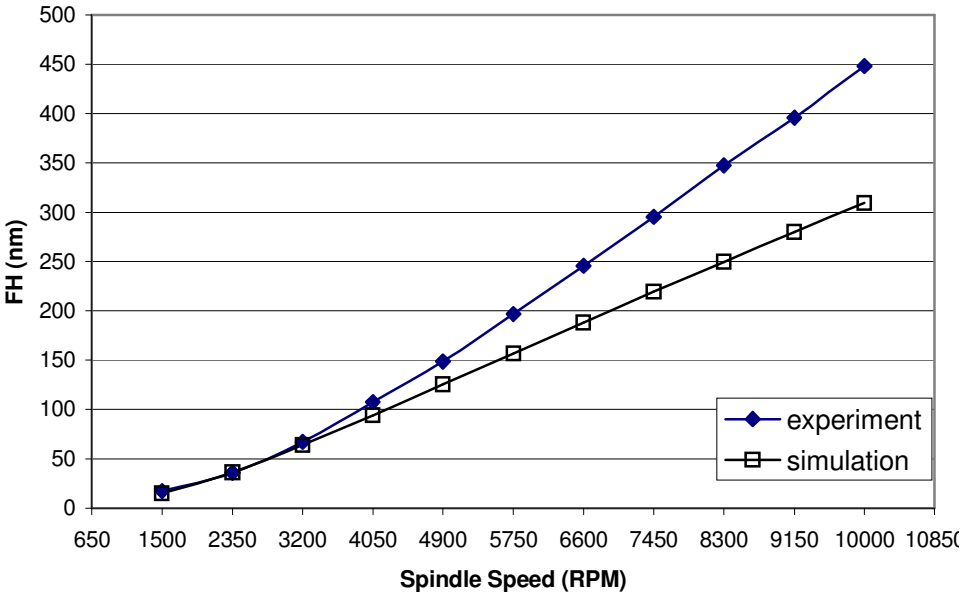

Figure 5.6 Flying height variation as a function of spindle speed for the dummy slider under the dual slider assembly cartridge of Fig. 5.3.

Figures 5.7 (a) and (b) show schematic side and top views respectively illustrating a mounting assembly design for the dummy and testing sliders. The mounting assembly for a slider comprises a base plate and a suspension coupled to the base plate via a hinge. The slider is mounted at the trailing end of the suspension, and has the air bearing surface facing towards the disk (not shown).

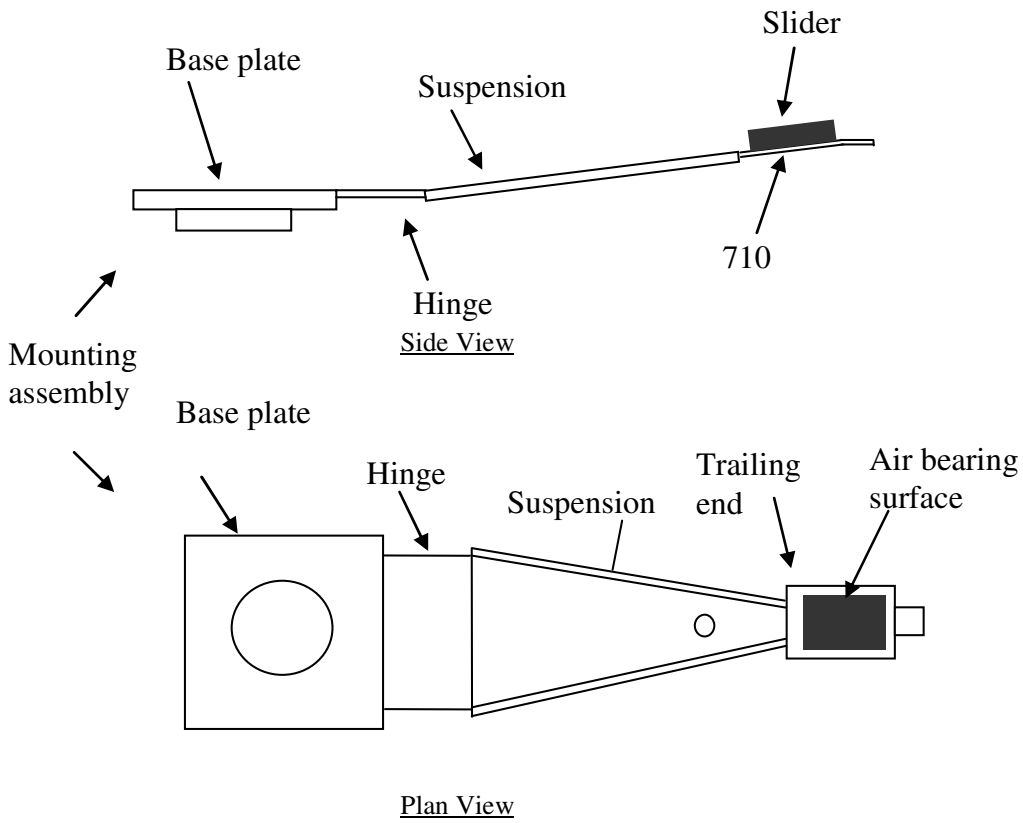

Figure 5.7 (a) and (b) show schematic side and top views respectively of a mounting assembly for a slider.

With reference to Figure 5.5, the design concepts for the dummy slider in the example embodiment are:

i) A positive pressure instead of negative pressure slider design. The existence of negative pressure in the dummy slider design increases the suction force when the velocity of the air-flow rate increases; eventually reducing the ability of the slider to fly higher.

ii) Include a shallow step trailing pad and side-pads for both sides of the slider. This increases the air-pressure of the slider when the linear velocity increases.

iii) Include a narrow groove between the two side pads to generate a small amount of negative pressure which can reduce the flying height to about 10nm.

iv) Include a V-shape or chamfer at the leading edge for both of the side-pads to allow acceleration of the air-flow when the linear velocity of the slider increases.

The design of the dummy and testing sliders is different in functionality. The testing slider is typically designed to have an extremely low flying height and thus a high negative pressure design is typically used. On the other hand, the dummy slider is designed to have a wide range of flying height variation with respect to the linear velocity or the spindle speed to capture the maximum and minimum fringe intensity pair, as described above.

The optical constants (n and k) for the dummy and testing sliders are preferably similar as both of them can be fabricated from the same wafer and material. Both sliders are preferably fabricated in the same row-bar where they undergo the same etching, lapping, grinding, DLC over-coating and other fabrication processes. This can ensure that the optical constants do not vary significantly between the dummy and testing sliders due to the fabrication tolerances in the processes. The optical constants are an important factor in the measurement because of the light reflection dependency on the optical constant for different materials. The n and k differences between the dummy slider and the testing slider are preferably compensated accordingly in order to retain the measurement accuracy. Table 5.1 shows the optical constants for both of the sliders in an example embodiment.

Optical constant	*n*@450	*n*@550	*n*@650	*k*@450	*k*@550	*k*@650
Dummy Slider	2.1351	2.146	2.1108	0.57193	0.50505	0.47724
Testing Slider	2.129	2.1381	2.0955	0.61661	0.54079	0.52469

Table 5.1 Optical constants for dummy slider and testing slider

The determination of, and compensation for the different optical constant values can be based on a number of techniques, for example the technique described in Leong et al. (2006). More particular, the *n*, *k* values for the dummy slider can be obtained through direct measurement. For the testing slider, an *n*, *k* map is first obtained, and the flying height measurement performed at a location having the closest n, k values compared to the ones determined for the dummy slider.

5.3 Measurement Results

Fig. 5.8 shows a comparison of flying height measurement results for both a conventional testing slider load/unload calibration technique and the RPM calibration of the example embodiment. The results show that the load/unload method with high fluctuation resulted in a variation in the flying height measurements, whereas the RPM method of the example embodiment provides measurement results.

	L/UL	RPM
Std dev	1.151	0.263
Average	7.805	7.195

Table 5.2 Standard deviation for the flying height measurement

Table 5.2 shows the standard deviation for the respective flying height measurements of Figure 5.8. Better standard deviation can be achieved using the RPM method of the example embodiment, which provides a higher repeatable measurement, especially for low flying height sliders and extremely high negative air-pressure ABS design sliders.

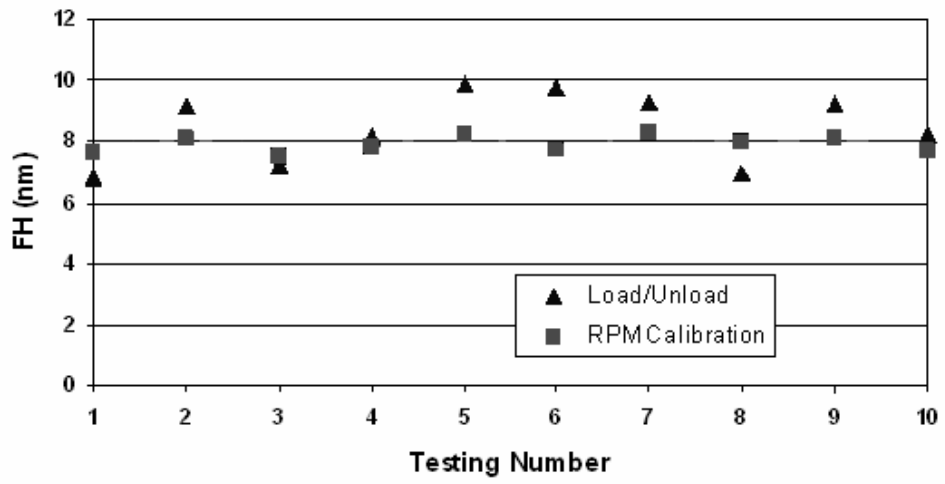

Figure 5.8 Graph showing a comparison of flying height measurement for conventional sliders load/unload method and for the RPM calibration method using the slider assembly cartridge of Figure 5.3.

5.4 Testing Procedure

Figure 5.9 shows a flow chart illustrating a method for optical flying height measurement according to an example embodiment. At step one, a first slider and a second slider are aligned adjacent a transparent disk. At step two, a rotational speed of the disk relative to the first slider is varied whereby a spacing between the first slider and the disk changes. At step three, changes in a first reflected light intensity caused by interference of a light signal portion reflected from the first slider and a light signal portion reflected from a surface of the disk are measured, wherein the rotational speed is varied over a range such that one maximum and minimum intensities pair is measured in the reflected light intensity. At step four, a second reflected light intensity caused by interference of a light signal portion reflected from the second slider and a light signal portion reflected from a surface of the disk is measured at a fixed rotational speed between the disk and the second slider. At step five, a flying height of the second slider is calculated using the measured maximum and minimum intensities pair and the measured second reflected light intensity.

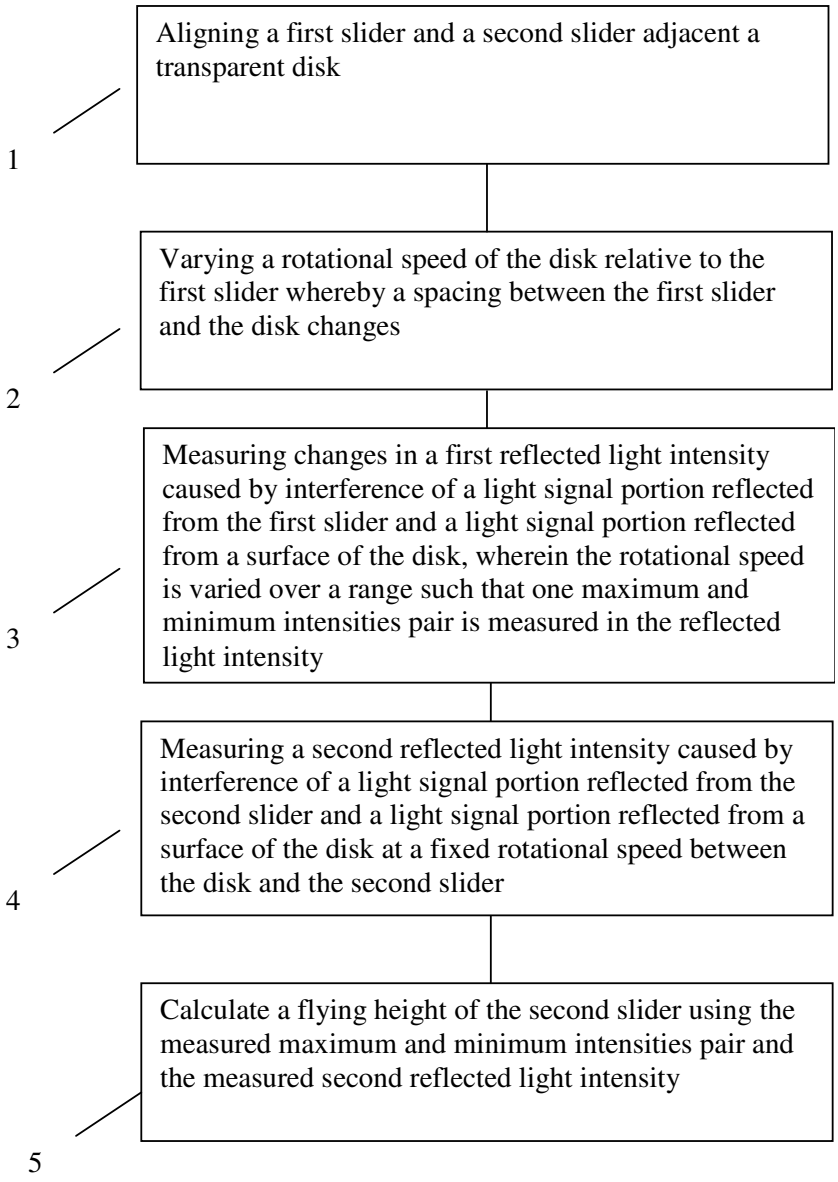

Figure 5.9 Flow chart illustrating a method for optical flying height measurement according to an example embodiment.

The described embodiments provide a method for optical flying height measurement. The described method provides a novel way in separating the head and the disk in the calibration process by utilizing a dual slider assembly where one of the slider is a dummy slider. The flying height of the dummy

slider is preferably designed such that when the spindle speed is varied from about 1500 to about 20000 rpm; the flying height is linearly changed in the first order range of the light wavelength of 10 to 450nm.

5.3 Summary

Apart from the readback based flying height measurements that were discussed in the previous chapters. This chapter introduces a method for optical flying height measurement. The flying height tester comprising a transparent disk; means for aligning a dummy slider and a testing slider adjacent a transparent disk; means for varying a rotational speed of the disk relative to the dummy slider whereby a spacing between the dummy slider and the disk changes; means for measuring changes in a first reflected light intensity caused by interference of a light signal portion reflected from the dummy slider and a light signal portion reflected from a surface of the disk, wherein the rotational speed is varied over a range such that one maximum and minimum intensities pair is measured in the reflected light intensity; means measuring a reflected light intensity caused by interference of a light signal portion reflected from the testing slider and a light signal portion reflected from a surface of the disk at a fixed rotational speed between the disk and the testing slider; and means for calculating a flying height of the testing slider using the measured maximum and minimum intensities pair and the measured second reflected light intensity.

By using the above mentioned methods, better standard deviation can be achieved which provide a higher repeatable measurement, especially for

low flying height sliders and extremely high negative air-pressure ABS design sliders.

CHAPTER 6

STUDY OF THE COOLING EFFECT OF THE THERMAL ACTUATOR ON A FLYING SLIDER

One of the most significant progresses in the development of low flying height technology is the embedding of the thermal actuator into slider for on-demand flying height control. Thermal actuator is the most effective way in controlling the flying height and it is widely used in current hard disk drive. This chapter and the followed chapter will focus on thermally actuated flying height control and its relationship with slider dynamics. A method that can be used to study the cooling effect on the thermal actuator of a flying slider with greater sensitivity than magneto-resistance (MR) sensor measurements was introduced. By monitoring the 1^{st} and 2^{nd} harmonics of the readback signal associated with the *AC* excited thermal protrusions, the 2^{nd} harmonics signal diverges from the linear 1^{st} harmonic signal as cooling effect intensifies. This is attributed to distortion of the readback signal envelope with increased cooling. Results also indicate that disks with bonded lubricant only produces a higher cooling effect compared with disks with both bonded and mobile lubricant. An ANSYS simulation model was developed to explain the non-linearity in the 2^{nd} harmonic.

6.1 Introduction

Thermal flying-height control (TFC) was introduced (Meyer et al., 1999; Kurita et al., 2006) to secure the head-disk spacing at the targeted value. The TFC is based on the concept that when a current is applied to the thermal actuator, a localized protrusion of the read/write head is generated due to the variation in the coefficients of the thermal expansion of various materials. Such protrusion effectively reduces the magnetic spacing and is therefore widely introduced into recent commercial hard disk drive. Previous research studied the relationship between the heating elements and the head protrusion using static and dynamic measurement methods. The static measurements of the head protrusion using Atomic Force Microscope (AFM) (Li and Wang, 1998) or optical profiler (Gupta et al. 2000) did not consider the dynamic conditions faced by the slider when it flies over the spinning disk. Therefore, these do not accurately reflect the actual protrusion conditions on the slider. Research on dynamic thermal protrusion was mostly limited to simulations by numerical calculations (Chen et al., 2000) or ANSYS modeling (Juang and Bogy, 2007). The dynamic measurements of the slider protrusion (Wang et al., 2001; Kulkarni et al., 2000) were focused on the pole-tip and alumina overcoat protrusion/recession rather than the thermal actuator. Currently the relationship between the dynamic flying height and the thermal protrusion is measured by the magneto-resistance (MR) sensor and the in-situ flying height method (Y. Li et al., 2004). However, this measurement does not consider the heater and air cooling effect on the MR sensor, which is highly sensitive to the temperature change. Given that thermal actuators have a critical role in ultra-low flying height (FH) adjustment; their effectiveness during flying in the

presence of dynamic conditions, especially the cooling effect, should be studied.

This chapter presents the exploration of experimental methodology and investigations on the cooling effect on the thermal actuator. The experimental setup was developed and the harmonics signal method was introduced to predict the thermal response of the actuator. Two types of disk with different lubricants were used in the experiment.

6.2 Description of Experiment

The thermal effect of a magneto-resistive (MR) head is well known in head-disk interface (HDI) measurements, notably the thermal asperity (TA) and pole-tip protrusion (PTR) measurements. However with the embedded heater in the slider, the heat generated by the heater has a significant influence on the readback signal of the MR head and the electrical resistance of the MR sensor is highly temperature dependent (Tian et al., 1997). Therefore, the dynamic readback signal is a coupling between magnetic signal by head-media and the thermal effects due to the proximate heater. Hence, an accurate study of the thermal actuator protrusion using the MR method tends to be inaccurate. Here, a new method is introduced which is able to decouple the effects and detect the actual dynamic changes of the thermal actuator. This new method, hereby named as the “harmonics method”, measures the first and second harmonics of the flying height variation using the read/write sensor.

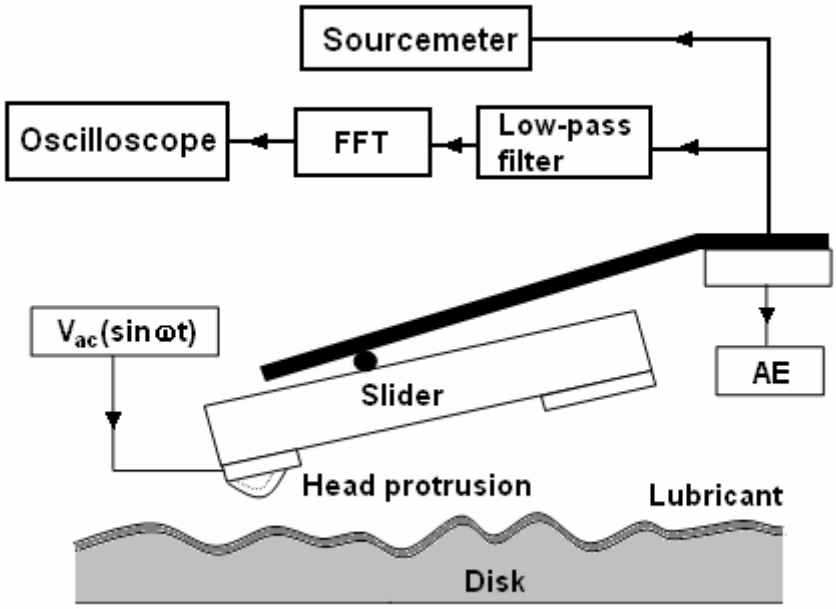

Figure 6.1 Schematic of the experimental setup.

Fig. 6.1 shows the experimental setup for the testing. The setup comprises of a spinstand with read/write functionality. A commercial read/write head come with commercial thermal flying-height controlled (TFC) slider was used to write a 60MHz track on the disk. The slider has a nominal flying height of 10nm. The slider's flying height was varied using a 1 kHz sinusoidal voltage applied to the thermal actuator and the resultant readback envelope was filtered with a 10 kHz low-pass filter. The signal was then translated into frequency domain using Fast Fourier transform (FFT) function of the oscilloscope. The magnitudes of the harmonics were recorded as the heater power was varied. The principle of the harmonics method is based on the concept that "magnetic contrast" or influence of written magnetic information may be decoupled from influence of temperature variations if the latter contributes in a decidedly non-linear manner to the MR signal (Abraham, et

al., 1996). The non-linearity can be detected by higher harmonics such as in a case of 2nd harmonic measurement. Here, the harmonic content by varying the magnetic spacing via thermal actuation is introduced. The thermal variation could be separated from magnetic information by acquiring the 2nd harmonics component of the readback signal. Any non-linear contribution of the cooling effect to the temperature variation can similarly be determined by measuring the 2nd harmonic component of the readback signal. As a comparison, the resistance changes of MR sensor were also measured using Sourcemeter by applying a constant 0.6mA current. The temperature coefficients of the MR read sensor was calibrated in a temperature controlled oven, with sensitivity in the neighborhood of -0.1 %/^{o}C.

6.3 Results and Discussion

6.3.1. Cooling Effect Measurement Using Magneto-Resistive (MR) Sensor

The MR resistance measurement is used to investigate the cooling effect on the thermal protrusion at near contact regime. Two types of test conditions were used: bonded + mobile lube disk (Z-dol, 12Å lube thickness), and bonded lube (Z-dol, 6Å lube thickness). Figure 6.2 (a) shows the resistance reduction as a function of the *DC* heating power for both cases. For tunneling giant magneto-resistive (TGMR) heads, a negative temperature coefficient of resistance applies (Mao et al., 2004). The resistance of the sensor was measured while the heater power was varied from 50 mW to 98 mW. A reference value of the static (unload) measurement was done for the

case where there is no cooling effect of the spinning disk. Delta resistance change ΔR, at heater power P_i, defined here as

$$\Delta R(P_i) = \left[R(L, P_i) - R(UL, P_i)\right] - \left[R(L, P_0) - R(UL, P_0)\right] \qquad (6.1)$$

where P_0 is the initial heater power, UL and L refer to unloaded and loaded conditions respectively, was calculated in Fig 6.2 (b). The results indicate that head temperature rise in the flying condition is significantly less than that of the static condition (unload). The static (unload) resistance reduction is linearly proportional to the heater power whereas the dynamic (loaded or flying) case is slightly non-linear --- a small divergence from their corresponding linear fitted lines is observed in Fig 6.2 (b). Given the few nanometers head-media clearance, the gas molecule interaction is in the order of single molecule (Peng et al., 2004) which indicates possible heat conduction instead of convection between the media and the slider. High pressure corresponds to more molecules per unit volume for heat transport. Simulation results (Juang and Bogy, 2007) show that pressure change in the protrusion area is non-linear, and thus, as the protrusion moves closer to the media, the heat generated is dissipated through the air bearing to the media non-linearly. A greater non-linearity was observed for the bonded lube disk compared to the bonded + mobile lube disk. Since the former is a poorer thermal insulator, the cooling effect played a more dominant role. From the ΔR *curve,* it is difficult decouple the linear and non-linear effects. Thus, in order to measure more directly on the cooling effect, a new method is developed.

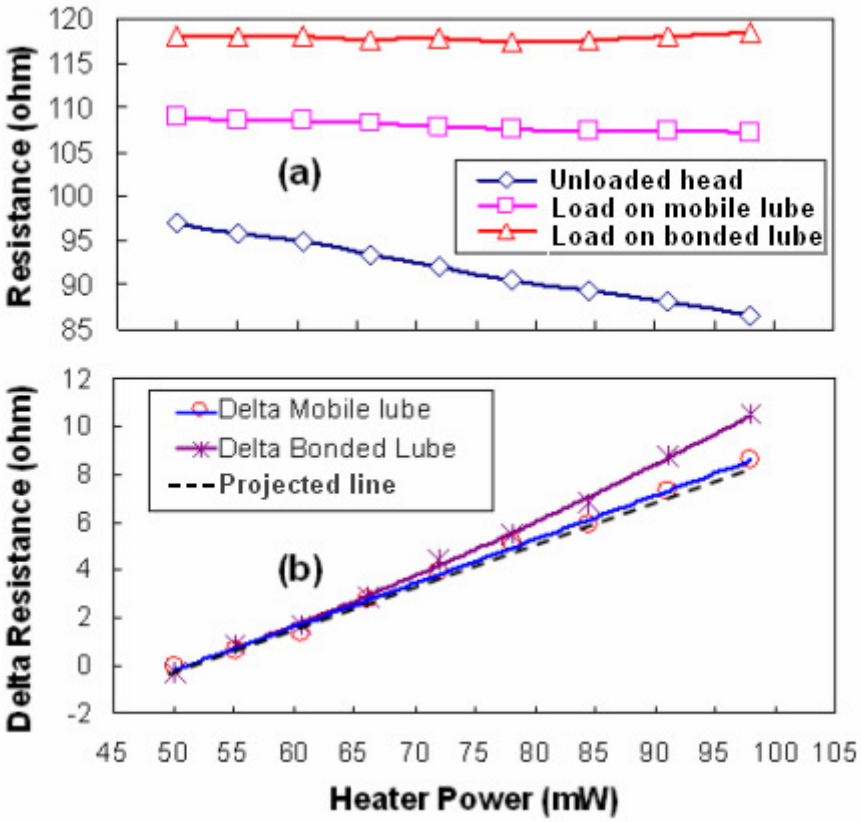

Figure 6.2 Static and dynamic resistance measurement of the TGMR sensor for (a) actual resistance change and (b) delta resistance change.

6.3.2. Characterizing the Thermal Actuator Cooling Effect with Harmonics Method

Fig. 6.3 shows the harmonics measurement as a function of the applied *DC* heating power. The readback signal associated with the sinusoidal thermal protrusion generated by a 1 kHz alternating current (*AC*) ripple that is added to the *DC* heating power was measured while the *DC* heater power was varied from 50 mW to 98 mW. Generally, the protrusion of the slider matches the waveform of the sinusoidal current. However, higher harmonics signals are detected when the envelope of the readback signal is distorted upon significant

cooling effect on the slider. In our experiment, only 2nd harmonics is used as higher harmonics signals as 3rd or 4th is too weak to be used in the detection. Fig. 6.3 shows the interaction between the thermal actuator and a) bonded + mobile or b) bonded lube disk. Initially, the 1st first harmonics signal increases proportionally with the 2nd harmonics signal due to the thermal protrusion (heater temperature rise). However, as the cooling effect intensified, the 2nd harmonic signal starts to diverge from the 1st harmonics signal when heater power is more than 80 mW. This non-linear change indicates that the cooling starts to increase significantly when the protrusion is closer to the disk. The explanation for this is as followings. There are two components in the measurement, the linear component is from the heater (heat generated by the heater affecting the MR sensor) and non-linear component is from the cooling effect (interaction between the MR sensor and the air). The 1st harmonics measures the amplitude of the sine-wave envelope which response better with linear component (Abraham et al., 1996). The higher harmonics i.e. 2nd harmonics, which measures the deformation of the sine-wave relates to the non-linear component (cooling effect). In the beginning of the protrusion, the cooling effect on the protrusion is minimal; the heater (linear) component dominates the measurement results as shown in Fig. 6.3. As the air cooling intensifies, the non-linear component or the 2nd harmonics will start to response to the cooling and diverges. Fig. 6.3(b) shows the results of the bonded lube measurement. It shows that the divergence starts as early as 50 mW. This implies that the bonded lube disk has a more significant cooling effect compared with the bonded + mobile lube disk.

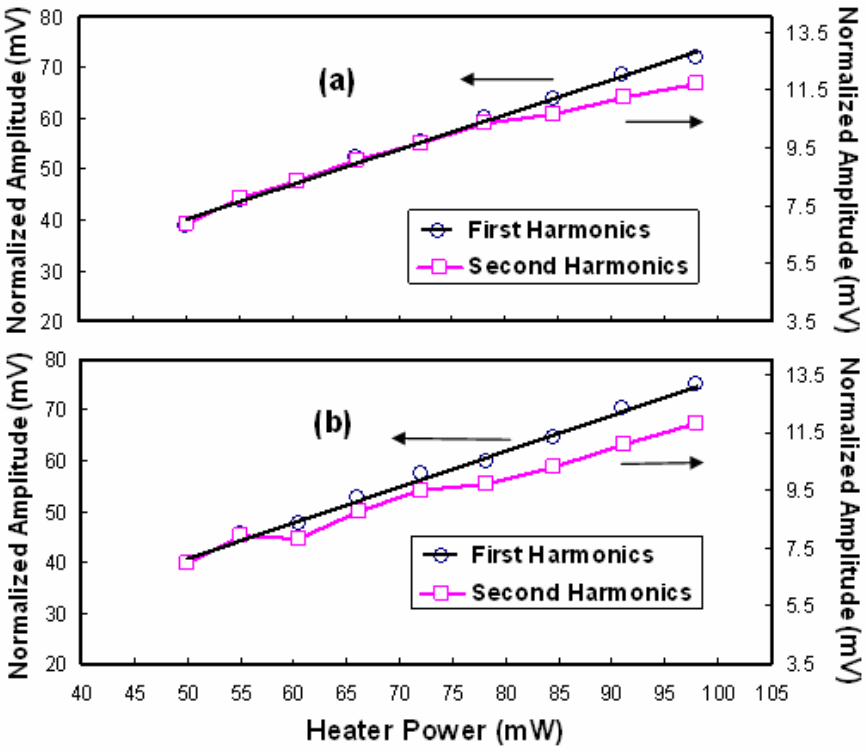

Figure 6.3 Comparison between (a) bonded + mobile lube and (b) bonded lube for harmonics measurement.

In General, the results of the harmonic method draws similar conclusions as the MR method. The different nature of cooling provided by the different lube conditions is clearly seen by the former, and the trend coincides with those from the MR measurements. However, the 2nd harmonic measurement generates greater sensitivity to the cooling effect compared to the MR method as shown by the greater divergence seen in the results. This increased sensitivity is in part to the ability of the harmonics measurement method to decouple heater and cooling contribution --- the 1st harmonic signal (measures changes from heater contribution) is linear, and the 2nd harmonic signal (measures cooling changes) diverges in a non-linear fashion.

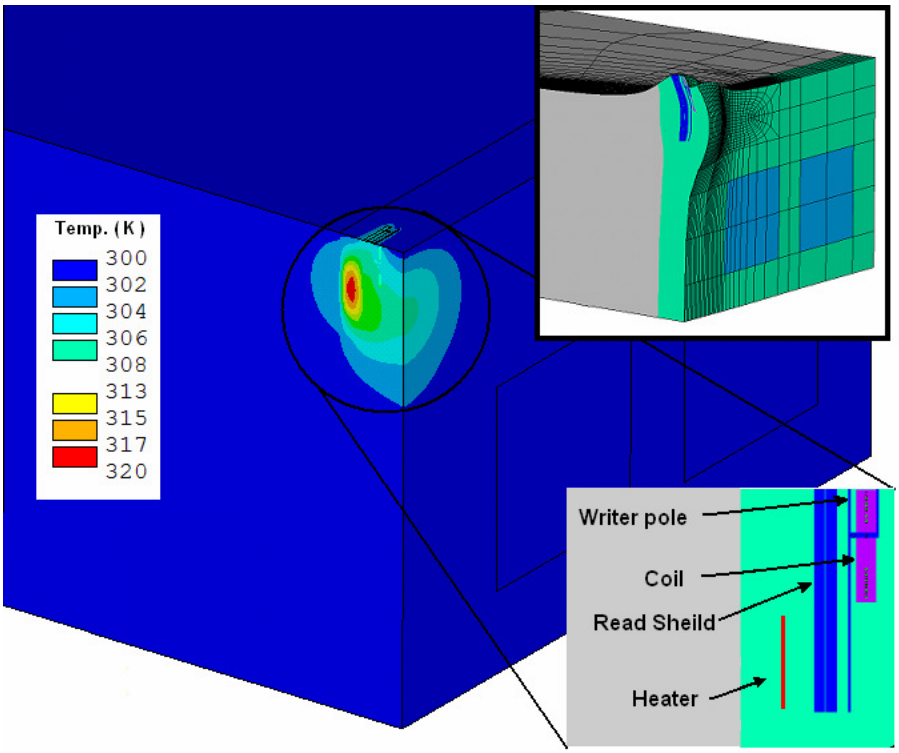

Figure 6.4 ANSYS simulation model for the thermal flying control (TFC) slider

6.3.3. Cooling Effect Study Using ANSYS Simulation

Fig. 6.4 shows the finite element model for the TFC slider carried out in ANSYS. In order to simulate the heat flux that is conducted from the air bearing surface to the air bearing, a large convection value (from 100,000 W/m^2K to 500,000 W/m^2K) was used as the boundary condition. It is worthy to note that larger convection values on the air bearing surface as the boundary condition in the simulation model represent a larger cooling effect of the air bearing. The thermal actuator response due to the 1 KHz sine-wave is shown in Fig. 6.5. The bandwidth of thermal actuation is of great importance because it determines the response time of the thermal protrusion to the heating power.

Fig. 6.5(b) shows the phase difference between the temperature and protrusion which indicates the time needed for thermal expansion of the material when subject to certain applied power. Fig. 6.6 shows the thermal protrusion when the slider is subjected to different conditions of cooling. The frequencies applied in this case were 1 and 2 KHz. The results show that for 1 KHz thermal protrusion, a response with very slight non-linearity is observed as the cooling effect increases. When a 2 KHz excitation was used, a more quadratic or non-linear nature was observed. In this case, the thermal actuator response time for 2 KHz is unable to keep-up to the cooling of the slider and demonstrates a distinct non-linear form in the simulation results.

Ideally, a material expands linearly and the response to a sine-wave (single frequency) input is a single component (1^{st} harmonic) at that frequency. In the real case, due to different coefficient of expansion and finite expansion time, the resulting thermal protrusion may not follow the sine-wave exactly, and the non-ideal response contains higher harmonic components. The 1^{st} harmonic measures the envelope, while the 2^{nd} harmonic detects deviation from the ideal sine-wave response. The harmonic results were obtained by Fast-Fourier transform (FFT) on the readback signal. Extensive number of points (10K data points) is needed to generate accurate FFT measurement to obtain 2^{nd} or higher harmonics component. In ANSYS simulation, this is extremely time consuming and computationally expensive. Therefore, the response at different frequency (1 kHz and 2 kHz) was used instead to show greater non-linearity at higher frequencies.

The simulation shows greater non-linearity at 2 KHz, or at higher frequencies, greater non-linear effects result. Thus, detection at 2^{nd} harmonic

(higher) frequency provides greater sensitivity to the non-linearity from cooling. This special characteristic can be used to detect the cooling effect on the protrusion. However, due to variations in head material, thermal coefficients, structures and interfacial properties, different heater and head designs have different frequency response, and this needs to be considered.

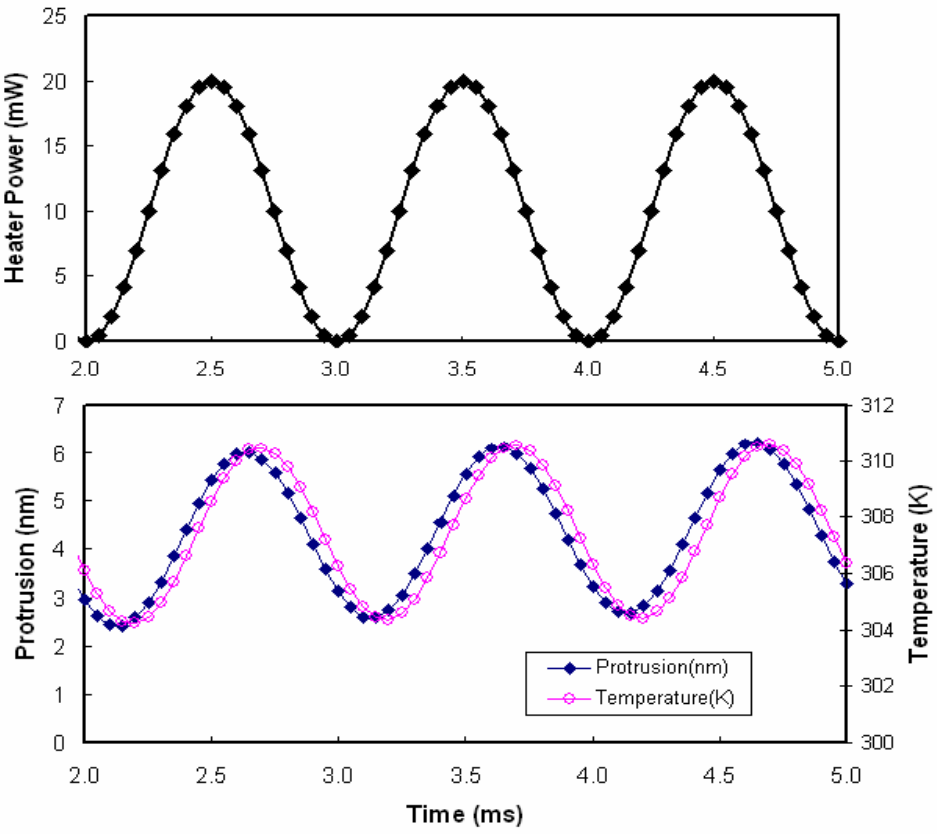

Figure 6.5 Simulation results for (a) sine-wave power supply to the heater and (b) frequency response analysis of the thermal actuator.

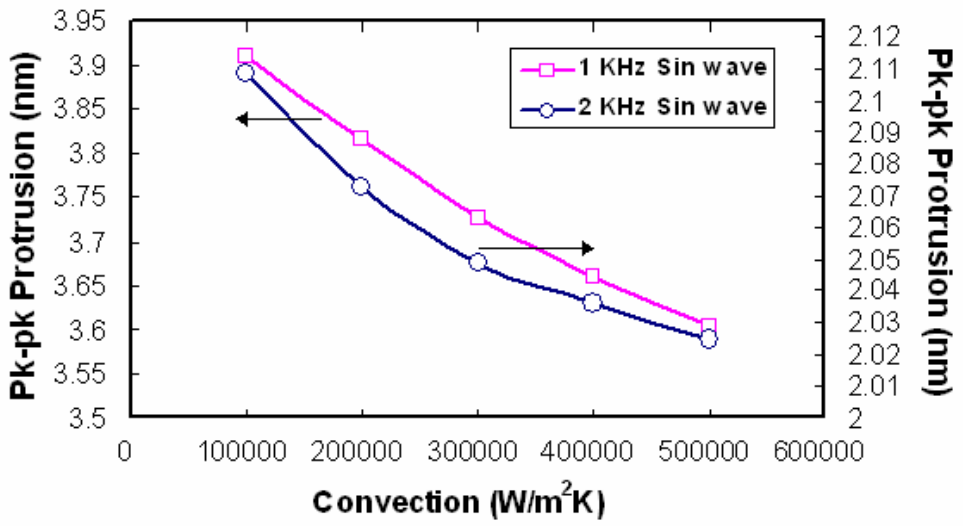

Figure 6.6 Response of the thermal actuator with different convection (cooling)

6.4 Summary

Previous chapters are focused on the studies of static and dynamic flying height stability. In this chapter, the focus is on flying height control technology and thermally actuated slider. The cooling effect on the thermal actuator of a flying slider was investigated using the developed harmonics method. Using the 2nd harmonics signal, the non-linearity associated with the cooling effect was successfully detected with greater sensitivity than the conventional MR measurement method. This non-linearity was also observed in ANSYS simulations. The experimental results also show a comparison of cooling effect for bonded + mobile lube and bonded lube disk.

CHAPTER 7

STUDY ON THE INFLUENCE OF LUBRICANT TO ELECTRICAL POTENTIAL

In order to increase the magnetic recording density to beyond 1 Tb/in^2, the flying height has to be reduced to sub-5 nm. Due to this reduction, the tribocharge buildup or the electrical potential between the head and disk can result in electrostatic forces. The electrostatic force does not have significant effect on the flying characteristics of a high-flying slider, but they become increasingly important especially at near contact region. Unlike chapter 6 which studies the cooling effect of the thermal actuator, this chapter is focused on studying the slider-lubricant interaction at near contact region and determining the electrical potential using a thermal actuator. The experiment was conducted using a low flying height slider with a built-in thermal actuator. In order to prevent wear and excessive contact during touchdown, flying height was adjusted by the thermal actuator driven with a sine-wave drive voltage. As the power of the thermal actuator increased and minimum flying height reduced, the touchdown point was determined by measuring the Acoustic Emission (AE) signal. When the testing conditions were varied: with/without mobile lube on the disk surface and with/without external bias voltage applied to the slider, the results indicate that lower actuator power or head protrusion is required for touchdown in the existence of mobile lube,

suggesting the variation of electrical potential caused by different lube conditions. A modified Kelvin force method (KFM) was also developed to compare with these measurement results. Further study on the electrical potential difference was conducted using two different lubricants.

7.1 Introduction

The electrical potential or electrostatic charging between the head and the disk have been intensively studied and reported (Fayeulle et al., 1993; Nakayama et al., 1997; Nakayama, 1999). This charging phenomenon is formed by the potential difference between the slider body and the disk (Kiely and Hsia, 2002). The work functions of these materials can be modified by the overcoats and lubricants between the two metal plates (Feng et al., 1999; Oetelaar et al., 2001). Feng et al. (1999) studies shows that the tribological charging increases with an increase in relative humidity and lubricant thickness as well as a decrease in carbon overcoat. On high flying slider, the electrostatic force does not have significant effects on the flying characteristics. However, they will be come into play at the near-contact region. As the flying height (FH) reduces to sub-5 nm, due to its attractive nature, this electrostatic force may cause the slider to come into contact with the media.

Studies on the electrostatic force at near-contact were previously presented (Kiely and Hsia, 2002; Knigge et al., 2004). Here, we focus instead on the use of a thermal actuator to study the influence of the lubricant in the head-disk interface and to determine the electrical potential at the near-contact

region. This chapter will introduce a method of measuring the electrical potential using the thermal actuator. The study attempts to differentiate the electrical potential for two different lubricants used in the head-disk interface and these results are compared with other measurement methods.

7.2 Experimental Setup

Fig.7.1 illustrates the experimental setup for measuring the electrical potential due to the slider-lubricant interface. A thermal actuator was used to control the thermal protrusion of the slider in this experiment. The actuator reduced the flying height gradually until touchdown, and the Acoustic Emission (AE) signal was measured during the process. A thermal actuator is proposed due to its localized protrusion which will reduce the area of contact and have a negligible effect on the pitch and roll of the flying height. Here, we named this proposed method as AE method. The thermal-actuated slider that was used in the testing has a 7 nm flying height. The maximum thermal protrusion generated by the embedded thermal actuator in the slider is 9 nm.

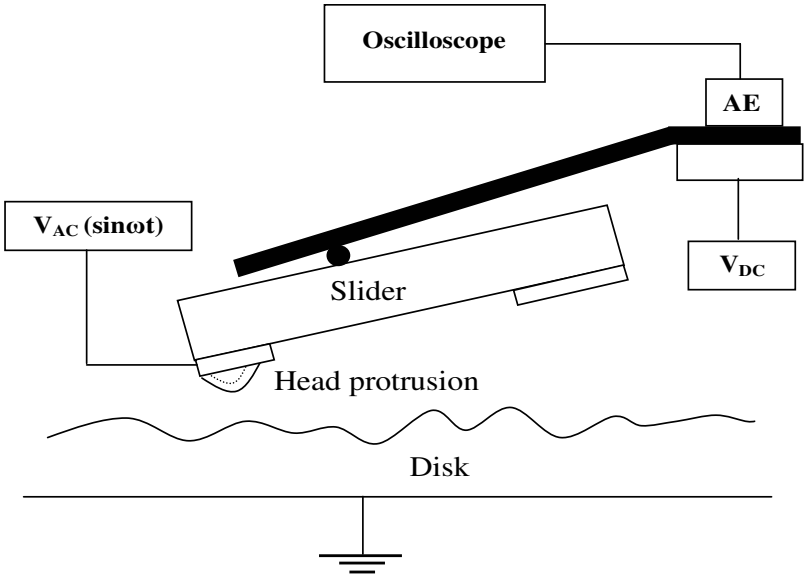

Figure 7.1 Schematic of the experimental setup.

Fig. 7.2 shows the thermal protrusion of the slider against the power of the heater. The protrusion was measured using a Zygo optical profiler. A linear relationship between the protrusion and the power of the heater was observed. Since non-linear thermal protrusion may misrepresent the actual flying height reduction that is needed to generate the AE signal in the electrical potential measurement, the linearity of the protrusion is an important factor that contributes to the accuracy of the testing.

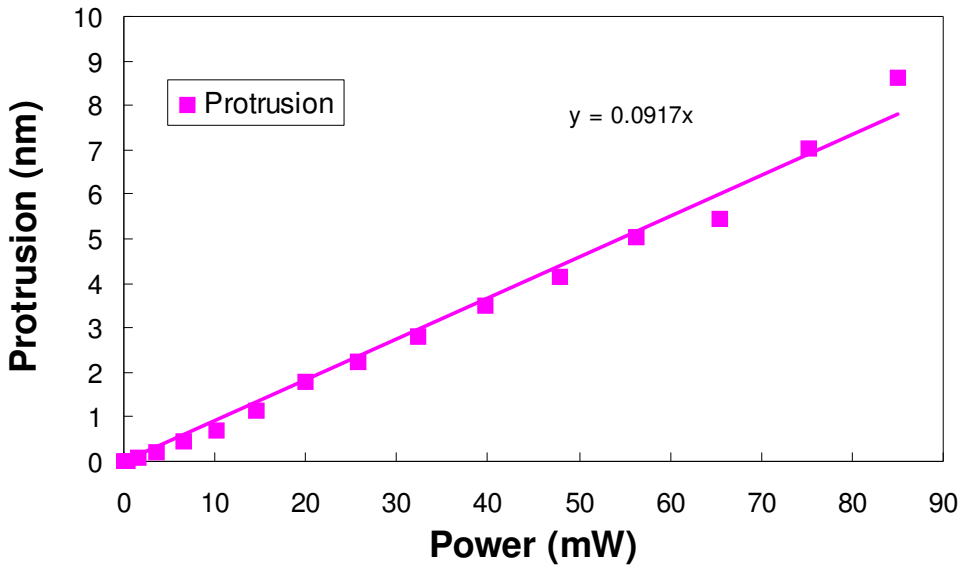

Figure 7.2 Thermal protrusion of the head against the heater power.

Fig. 7.3 shows the measured AE signal using the AE method described. Flying height was adjusted at the same frequency as the sine-wave applied to the thermal actuator. The frequency of the sine-wave used in the flying height adjustment was 1 KHz. This translated to a 1 millisecond touchdown interval for the slider on the disk. The root mean square (RMS) value of the AE signal was recorded for comparison between different tests. Our previous research indicated a problem of wear and excessive contact during touchdown which may influence the repeatability of the measurement. Using this periodic contact approach, continuous contact between the slider and the media can be avoided. In general, the localized protrusion has negligible effect on the pitch and roll. Thus, adjusting the flying height at the applied sine-wave frequency produced predictable and periodic intermittent contact, thereby increasing the repeatability and accuracy of the measurement.

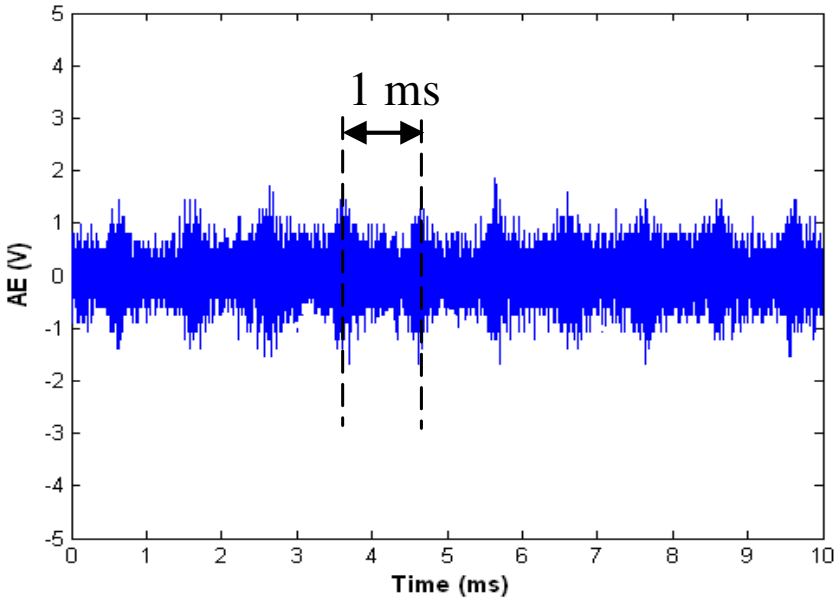

Figure 7.3 AE signal during head-disk contact.

7.3 Results and Discussion

Two types of test conditions were set up in this present work: (a) with and without mobile lube, and (b) with and without *DC* bias. The first condition was used to determine how the electrical potential varies between a disk with mobile lube and another that was washed and left with residual bonded lube on the disk surface. The second was to obtain an estimate for the change in electrical potential as a result of the mobile lube.

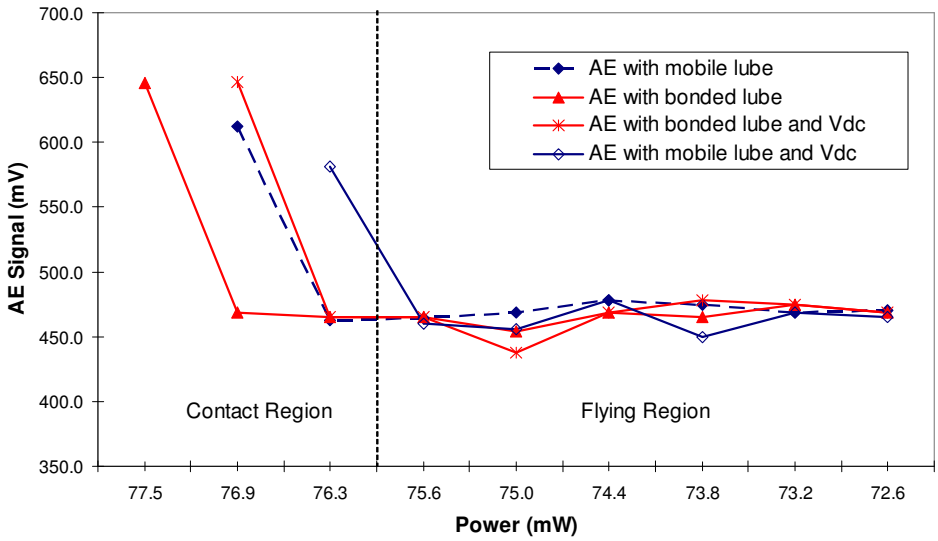

Figure 7.4 AE signal comparison (with/without *DC* bias, bonded and mobile lube).

Fig. 7.4 details the change in the RMS value of the AE signal against the power of the thermal actuator as the thermal protrusion of the slider (with an initial flying height of 7 nm at zero heater power) was gradually increased until the AE signal was detected. The results show that in all cases, more than 75mW was needed for the slider to touch down. In addition, lower thermal actuator power or head protrusion was required to generate a touchdown AE signal for the disk with mobile lube. The different actuator power required to induce touchdown indicates different electrical potential for the two cases, i.e., the disk with and without mobile lube (or bonded lube). This difference was measured by introducing a *DC* bias voltage in the experiment. The *DC* voltage was adjusted until similar touchdown AE conditions were recorded. In this case, the *DC* voltage needed for the disk with bonded lube to achieve the same AE touchdown condition as those with mobile lube was 0.3 V. The presence

of electrical potential difference can be explained by the dielectric difference between the slider and disk (Giancoli, 2000). The mobile lube, which has a higher density compared to bonded lube, will have higher dielectric. This dielectric generates higher electrical charges between the slider and the disk, in which, it is proportional to electrostatics force. With the present of higher electrostatic force, the mobile lube disk will have lower flying height and the thermal actuator power needed for touchdown is smaller compared to bonded lube.

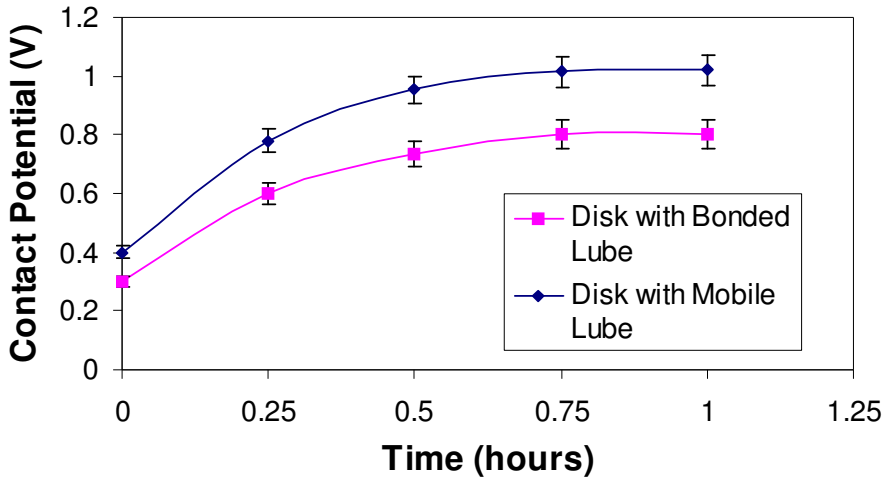

Figure 7.5 Time variation of electrical potential.

Fig. 7.5 shows the time variation of the electrical potential using the proposed AE method for both the mobile and bonded lube case. It is observed that the electrical potential increases over time. However, this increase starts to tapers off after 0.75 hour. The measured results follow an exponential model of the form $a + b\exp(-t/\tau)$. Such exponential charging and discharging was also observed by others (Kiely and Hsia, 2002). Faster potential increase was also

seen for the disk with mobile lube, and the values were higher than for a disk with bonded lube, indicating that mobile lube has a significant effect on the increase in electrical potential difference. The repeatability of the measurements was tested with 5 identical ABS sliders for both the bonded and mobile lube case. Fig. 7.5 shows the error bar for the repeatability test. A high percentage of repeatability of 94-95% for both cases of testing was achieved.

In order to verify this proposed AE method, a modified and improved electrical potential measurement method based on the conventional Kelvin force microscope was used. The Kelvin force microscope is based on an Atomic Force Microscope (AFM) setup, while its work function measurement is dependent on the changes of the electrostatic forces between the small AFM tip and the sample. Here, the method is adapted so that it can be used to measure electrical potential between a flying slider and disk. This new method, hereby named as the "harmonics method", measures the first harmonic of the flying height variation using the read/write sensor. The first harmonic component of the electrostatic force between the slider and the disk (Yasutake et al., 1996) is given by

$$F_e = \frac{\mathrm{dC(z)}}{\mathrm{dz}}(\mathrm{V_{dc}} - \mathrm{V_S})\mathrm{V_{ac}}\sin(\omega \mathrm{t}) \qquad (7.1)$$

where F_e is the resulting electrostatic force between the slider and disk, V_{dc} and $V_{ac}\sin(\omega t)$ are the *DC* and *AC* voltages applied between the slider and the disk, *C(z)* is the slider-media capacitance at a flying height of *z,* and V_s is electric surface potential. The electrostatic force causes the slider to oscillate when the

AC voltage bias is applied between the slider and the disk. Here, the *AC* voltage bias was fixed at 10 KHz frequency. This flying height variation is measured by the in-situ flying height measurement method (Yuan et al., 2002) using the read/write sensor. The written readback signal was 60 MHz. The amplitude of the voltage bias/potential applied between the disk and slider was 0.5V *DC* and 0.5V (peak to peak) *AC* at 10 KHz respectively. The readback signal was low-pass filtered at 20 kHz and a spectrum analyzer was used to determine the first and second harmonics of the signal. The electrical potential (V_{DC}= V_s) was determined by monitoring when the first harmonic signal goes through null as the applied *DC* voltage was scanned through a certain range.

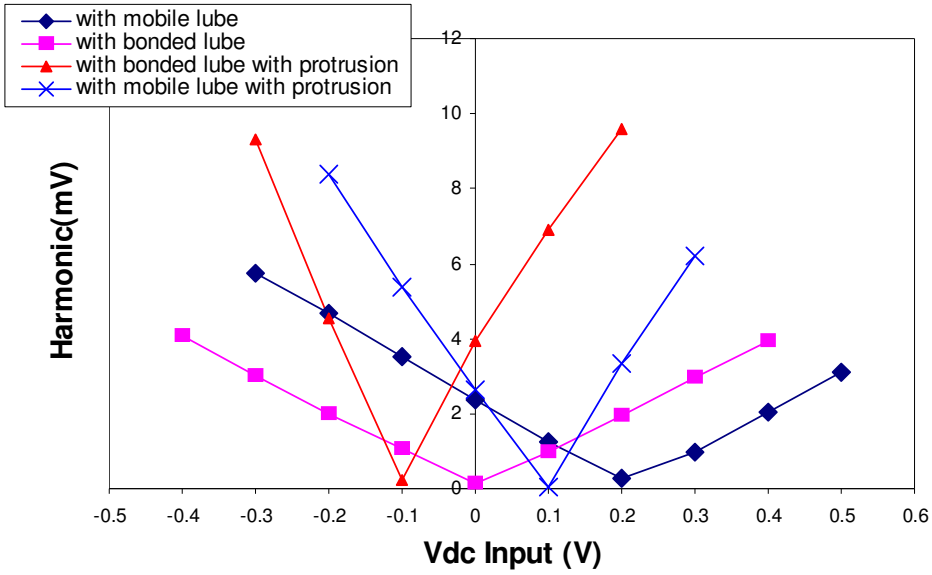

Figure 7.6 Measured electrical potential with harmonics method.

Fig. 7.6 shows the measurement of the first harmonic signal as the *DC* bias was scanning from -0.4 V to 0.5 V. The *DC* voltage at the minimum point of the plot corresponds to the electrical potential to be measured.

Comparing the case with mobile and bonded lube, the results indicate a 0.2V difference in electrical potential. This is a 0.1V difference compared to the previously proposed AE method. Fig. 7.6 also shows the electrical potential measurements with a fixed thermal protrusion. The thermal protrusion used is less than half of the value for the proposed AE method so that head-disk contact can be prevented. The results show a shift in electrical potential from 0.2V to 0.1V and 0V to -0.1V for the mobile lube disk and bonded lube disk respectively. This implies that there is a change in electrical potential when the protrusion reduces the spacing between the slider and disk. In addition, the AE method requires very close contact with the disk whereas the Harmonic method requires intermittent contact. During this near contact region in the AE method, other short range forces besides electrostatic forces such as intermolecular force may come into play. With the additional forces involve in the AE measurement, the measured electrical potential may not representing the actual value. These may account for the measurement difference between the AE method and the Harmonics method. The AE method measures the electrical potential during the maximum thermal protrusion. Due to the oscillating electrostatic force needed in the measurement, the Harmonics method requires a few nanometer of flying height variation and hence it can only measure the electrical potential at a level where the slider is in fully flying condition. Therefore, using the Harmonics method at near contact condition is nearly impossible where the flying height variation would cause head-disk contact and distort the measurement results.

7.4 Summary

In this chapter, a proposed thermal protrusion induced periodic touch down method was used to measure the electrical potential between a bonded and mobile lubricated disk case. The results indicate a 0.3V difference in electrical potential between the lubricants. These results were compared with a modified Kelvin force method or harmonics method. It shows that the proposed AE method is more suitable for near contact electrical potential measurement compared with the harmonic method.

CHAPTER 8

EXPLORATION OF NEW ENERGY ASSISTED MAGNETIC RECORDING BY COMBINED FIELD EMISSION AND MODERATE IONIZATION IN AIR

The effectiveness of magnetic recording process in ultra-high density lies on the working principles of the head-disk system. This chapter will address this head-disk system issues for future magnetic recording process especially in energy assisted magnetic recording. In this chapter, the magnetic writing process in an energy assisted magnetic recording experiment is enhanced by a combined field emission and moderate ionization between the write pole and magnetic media. When appropriate bias voltages are applied across the head-media gap, field emission from the write pole results in a sustainable moderate ionization without catastrophic air breakdown. The elevated media temperature from electron bombardment leads to reduced media coercivity. Our results show 25% improvement to writing ability on perpendicular magnetic recording media using a modified read/write head.

8.1 Introduction

Reducing grain size of the magnetic media to increase the areal density is limited by the superparamagnetic effect (Lu and Charap, 1995) that causes the grains to be thermally unstable and susceptible to switching of their magnetic polarity, if the grain size is below certain level. To overcome this problem, future recording media must have increased coercivity (H_c) which requires higher writing power to switch the magnetization of the magnetic grains. The magnetic field generated by the magnetic head itself is not strong enough for such future media. Thus different methods have been explored to overcome this obstacle. One of the existing approaches is so called thermal assisted magnetic recording, wherein the medium's temperature is elevated and, thus, the media coercivity reduces. Ruigrok et al. (2000) and others Rottmayer et al. (2006) proposed using laser light as the heating source. However, the practicality of having a laser source mounted on the slider is questionable due to the complication of the head structure. Furthermore, the laser spot size and intensity on the medium is limited by the wavelength and spectral transmittances of the disk substrate. Another possible approach to the thermal assisted magnetic recording is the use of field-emission current for heating (Nakamura et al., 1995; Zhang et al., 2006). Here, most of the efforts to date have been focused on static measurements using the scanning tunneling microscope (STM) tip as the heating source, and these do not reflect the real situation in a hard disk drive. Limited attention has been given to the implementation and dynamic measurements of the field emission assisted recording during read/write operations of an actual recording head flying over a spinning disk medium.

This chapter reports the use of actual read/write heads and medium to generate the field-emission. The dynamic read/write performance of the head is studied using a spinstand. This method uses the writer part of the head as an electron emitter. The electron beam is directed from the electron emitter towards the magnetic recording medium by the electric field in the head-media gap to impinge and heat up the portion to be recorded. A major advantage of our method is that minimum modification on current head structure is required.

8.2 Experiment Results and Discussion

A schematic of the transducer region is given in Figure 8.1. The transducer region includes the writer (write pole and return pole) which is used to write the magnetic bits to the disk media, as well as the reader that is used for readback of the magnetic bits. Both of the slider body and the writer is connected together and grounded. In this head design, external access to the writer is available via modification to the slider suspension. A bias voltage is thus applied to the writer, allowing it to operate as an electron emitter. Connection of the bias voltage to the slider body was removed to prevent the generation of large electrostatic forces that can affect the (8~12nm) flying height, as well as to prevent tunneling from the write pole to other parts on the slider.

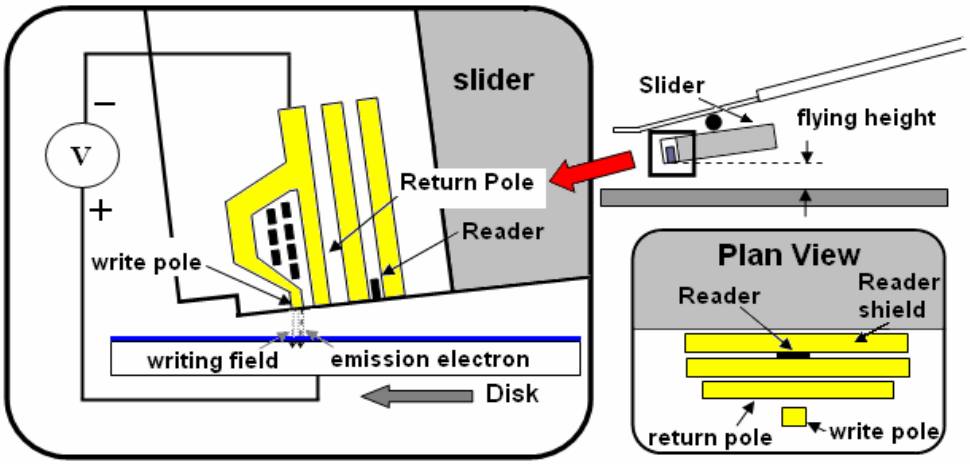

Figure 8.1 The schematic diagram represents the structure of the head for field emission assisted recording.

The ensuing attractive electrostatic force depends on the applied voltage and the other physical parameters of a slider-disk interface (Knigge et al., 2004). The electrostatic force between the head and media is limited by the size of the write pole. The relationship between the electrostatic force (Knigge et al., 2004) and the applied voltage is shown in Figure 8.2. The calculated electrostatic force at the write pole was 39 μN with 4V applied voltage and 10 nm flying height. This is much smaller than the simulated average air-bearing force between the slider and the medium of 3.8 mN. Thus, the bias voltage used on the write pole has minimum effect on the flying height of the slider.

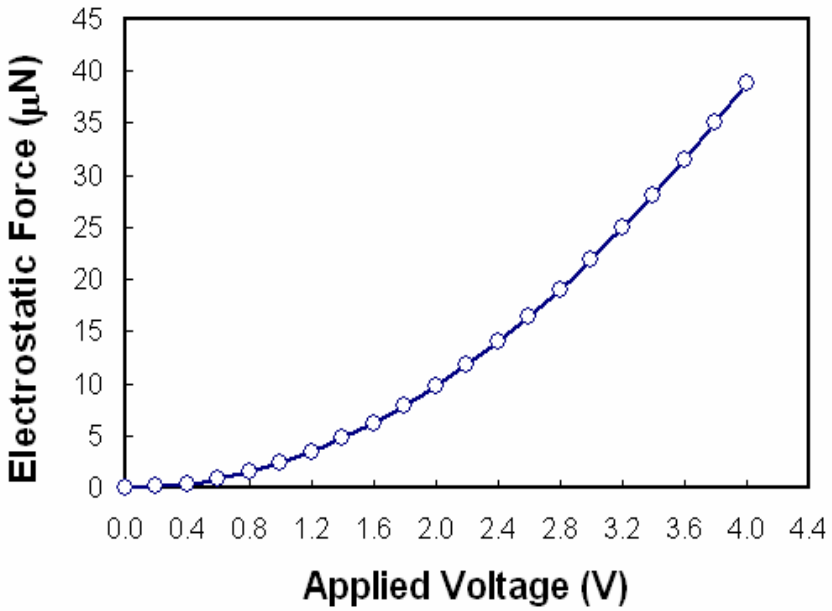

Figure 8.2 The results show the relationship between the calculated electrostatics force and the applied bias voltage.

Magnetic read/write operations were performed both with/without write pole bias. In this experiment, the medium was tested with the modified head on a read/write spinstand. The typical magnetic characteristics of the media measured at room temperature were: Hc: 5.2 kOe and Ms: 250 emu/cc. The medium was spun at a rate of 25 ms^{-1} in relation to the flying head, and the read/write operations were performed using a linear density of 60 kfci. The read/write performance was tested by varying the resulting electron current which was controlled by the voltage applied to the write pole. When applying a typical write pole bias of 2V, the measured current across the head and the medium is about 2.1 μA. This corresponds to a power of 4.2 μW applied. The writer consists of a write pole connected to a much larger return pole. Since the dimension of the write pole ($150x200nm^2$) is more favorable in terms of

field enhancement when compared to the large return pole (3500x56000nm^2), the former contributes largely to the field emission process.

Given that the head-media spacing is less than the mean free path of the electron (~500nm in air[12]), Fowler-Nordheim (F-N) field emission (Fowler and Nordheim, 1928) can be easily achieved for our small head-media gap. Figure 8.3 shows the I-V curve measured using a Keithley Sourcemeter 2602.

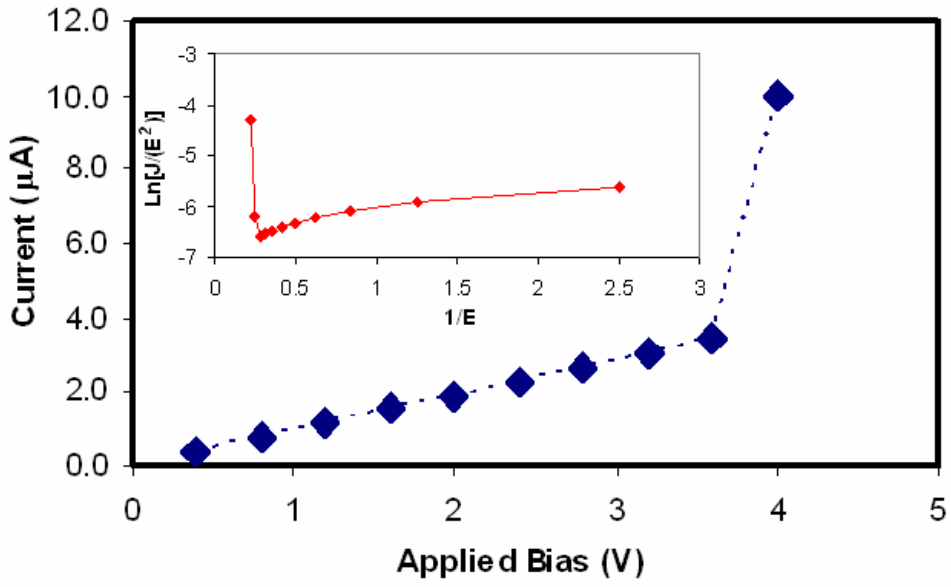

Figure 8.3 I-V curve measured using a Keithley Sourcemeter 2602.

For write pole bias voltages less than 3.6 V, a roughly linear I-V relationship is seen in Fig. 8.3. Similar linear relationship was presented by others (L. Zhang et al., 2004) when using a blunt STM tip (refer to Figure 4 and Figure 5 in L. Zhang et al., 2004) which cross section is in the same length-scale as our write pole (length = 200nm). Beyond 3.6V, the current increases dramatically as shown in Fig. 8.3. When electrons are injected into air, three different behaviors can be present, namely "blow-up", "stable" or "die-off", depending on the gap width and applied voltage. For very small

gaps, field emission can maintain a sufficient electron population and the anode current will be stable (W. Zhang et al., 2004). The obtained I-V curve does not strictly follow the F-N form (Figure 8.3 inset). Its deviation may be due to accompanying ionization discharge effects since it resembles the low current part of a typical discharge I-V curve in ideal gas (Peterson et al., 2005). Experimental results by others (Slade and Taylor, 2002) also show the deviation (reduced breakdown voltages) of Paschen's curve in air (Nasser, 1971) at small gaps for which field emission is suggested as the reason (Peterson et al., 2005). Our field mission-ionization conditions could be sustained without leading to a "blow-up" condition, as is also reported that field emission can help to create a moderate ionization effect without catastrophic air breakdown (Slade and Taylor, 2002). Analysis of the media lubricant and the read/write head showed that no head or media degradation had taken place. Only for gap currents of 4 mA and above, degradation to disk lubricant was detectable. Results for this will be discussed elsewhere. The degradation of lube is probably due the decomposition mechanism of the lubricant from the effect of electrons (Zhao et al., 2001, Wei et al., 1998).

For our recording experiments, the field emission-ionization heating was found to be sufficient to assist the writing and erasing operations, but did not result in data erasure when no magnetic writer field was applied. For our write pole size, the calculated power density is 1.4 $x10^8$ W/cm^2. When a linear spin-speed of 25m/s is considered, an equivalent recording bit area of $150x423nm^2$ (60kfci) takes 16.9ns to pass by, and the corresponding energy density is 2.37 J/cm^2.

Unlike Nakamura's (1995) case using the STM, our recorded data tracks did not show width dependence on increased write pole bias. In fact, the magnetic track width did not increase when field emission was applied, indicating that no recording resolution was lost. The recording density was also found to be limited by the resolution of the magnetic write pole, and is not affected by the wider return pole. This is expected since the write pole is at the trailing edge of the slider, and largely responsible for the field emission. Figure 8.4 shows the read/write performance for different gap currents. For typical writing current of 20mA on perpendicular recording media, 25% Signal to Noise Ratio (SNR) improvement can be achieved with a 3.5μA gap current.

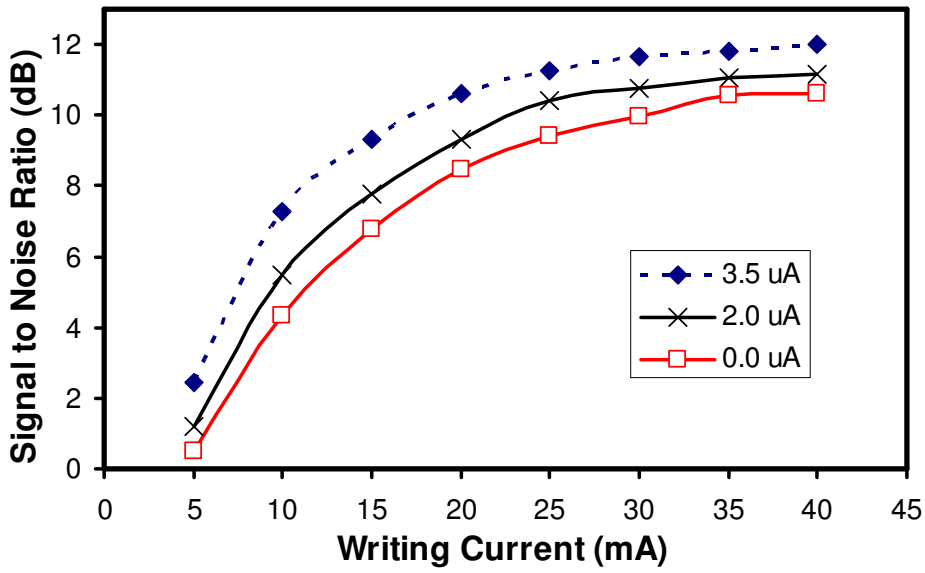

Figure 8.4 The results show the read/write performance for different gap currents.

Figure 8.5 shows the readback signal from tracks that were written with different linear velocities. The results show the differences between signal amplitudes for both with and without a 2 μA gap current. The flying height reduction is merely 2.1% of the average flying height of 10nm compared with a 17.2% linear velocity reduction from 27.9 to 23.1 ms^{-1}. The gap current remains at about 2μA when the linear velocity was reduced. However, a steeper increase in the readback signal of 5.1% was observed when prior recording was performed with supplied gap current. Reduction in the linear velocity corresponds to an increased heating time from 15.2ns to 18.3ns that improves writing performance. The observed heating performance agrees to others (Hwang and Na, 2005; Goldstein and Yakowitz, 1975) that study Scanning Electron Microscope (SEM) irradiation, suggesting that reducing the linear velocity increases the electron density reaching the media.

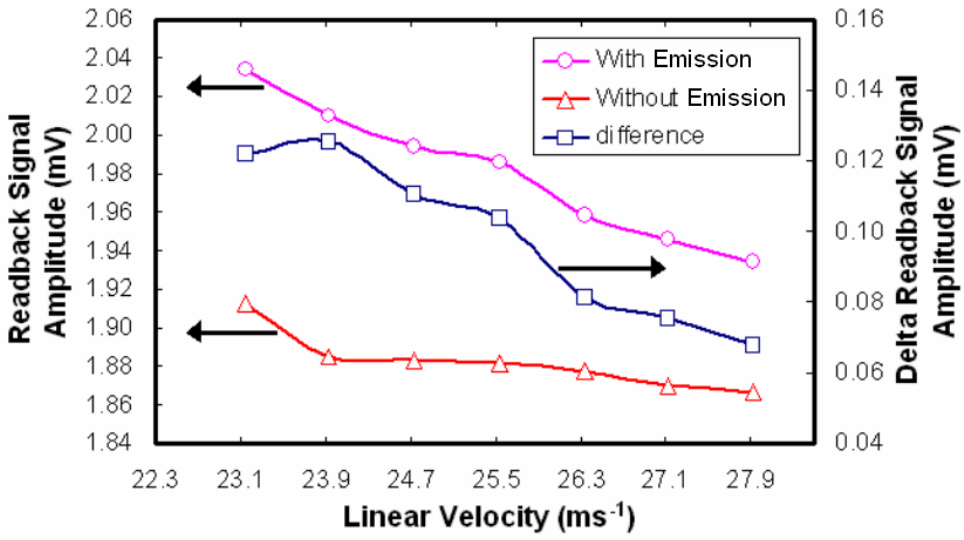

Figure 8.5 The readback signal measurement from tracks that were written with different linear velocities.

8.3 Summary

New approaches of head-disk system and integration are explored in this chapter, aiming at increasing the writing power of conventional writing head over high coercivity (Hc) media. Field emission from the write pole was observed in the testing that results in a sustainable moderate ionization without catastrophic air breakdown when appropriate bias voltages are applied across the head-media gap. The I-V curve does not strictly follow the F-N form, and is attributed to accompanying ionization discharge effects that assist in the writing process, but without damage to media and lubricant. Using a spinstand, dynamic read/write with tunneling currents up to 3.5μA is performed. For typical writing current of 20 mA in perpendicular recording, 25% Signal to Noise Ratio (SNR) improvement can be achieved with 3.5μA field emission from the head. Such performance is promising for energy assisted magnetic recording.

CHAPTER 9

CONCLUSIONS

The research of this thesis is focused on studying the critical issues in the area of head disk system and integration in which they will determine the future increase of areal density to beyond 1 Tb/in^2 for the magnetic recording storage. The research includes the methodology study of the ultra-low spacing, interface dynamics between the read/write head and disk media as well as the system level study of the future head and media configuration.

As the head disk spacing reduces to 3.5 nm, the head disk interface stability has become the key parameter that determines the extension of areal density to beyond 1 Tb/in^2. In order to achieve a reliable read/write process and comply with the 3.5 nm flying height design target, it is necessary to have proper study on the head disk interface issues with accurate and repeatable flying height measurement. As new head disk system technologies such as thermal actuator and energy assisted magnetic recording emerge, new flying height reliability issues will surface, posing fresh engineering challenges for system level integration and potentially degrading the recording performance. This thesis studies and explores potential solutions for some of these critical issues.

9.1 Explore and Characterize the Interface Stability of the Slider in Extremely Low Flying Height

Reducing flying height (FH) or head-media spacing to 3.5 nm and below is one of the major technology challenges in the magnetic recording. Under such a low flying height, the flying height variation due to disk distortion and spindle motor vibration is no longer negligible and must be taken into consideration when tackling flying instability issues. The flying stability of the slider and the flying height variation induced by the disk distortion and the spindle vibration with an extremely low flying height are discussed and reported in Chapter 2 and 3. In chapter 2, the interaction between the disk distortion and the slider was investigated. The measured results reviewed that flying height varies proportionally to the intensity of the disk distortion. These results indicate the relationship between the flying height variation and the air-bearing design. The explanations for these results are done by a theoretical modeling. The simulation results from the models also show that flying height variation induced by the crown sensitivity of the slider and the disk clamping distortion could deteriorate the flying stability of the slider.

The dynamic variation of slider's flying height induced by spindle motor vibration is studied using the *in-situ* testing method and the results are discussed in chapter 3. A pair of (0,1) unbalanced modes with a frequency split was detected in the measured flying height variation when the impact hammer excited the spindle. The measured results revealed that the balanced modes relatively do not have a significant impact on the flying height variation compared to that of the imbalanced modes. Detailed studies show that these imbalanced vibration modes are related to the air-bearing designs. Higher air

bearing roll stiffness will reduce the amount of flying height variation induced by spindle vibration.

The two-dimensional flying height stability issue is discussed in Chapter 4. A novel method is developed to determine the motion of the slider in flying height and off-track direction simultaneously. The proposed method successfully separates the position error and the flying height signals from the readback signals so that accurate measurement of slider's motion (in-plane and out-of-plane) can be determined. This method includes writing a pair of adjacent dual-frequency pattern tracks, followed by appropriate filtering of the readback signals from these tracks for the in-situ motion measurement. The results show the relative movement of the slider in two dimensions, both during thermal actuator controlled contact and full flying condition. This method provides a detailed understanding of the slider two-dimensional slider motion during contact which is important for near-contact magnetic recording.

The improvement on the extremely low flying height measurement using the optical methodology is discussed in chapter 5. A novel optical calibration method is developed. The methodology includes a dual head cartridge setup and a new flying height calibration method to improve the accuracy in the maximum and minimum calibration curves in the light intensity measurement. Better standard deviation can be achieved using the proposed method which provides a higher accuracy and repeatability measurement, especially for low flying height sliders and extremely high negative air-pressure ABS design sliders.

9.2 Interface Characteristics of Thermal Flying Height Controlled (TFC) Slider

Proximity contact and interaction between the slider and the disk utilizing the thermal actuator is another important issue that has been intensively studied in this research. The research in this area includes the studies on the cooling effect of the thermal protrusion and the influence of electrical potential at near contact region.

The cooling effect of the thermal actuator on the flying slider using the developed Harmonics method is presented in chapter 6. The heat transfer from the thermal actuator to the disk and air flow is discussed with disks of different lube thickness. Using the 2^{nd} harmonics signal, the non-linearity associated with the cooling effect was successfully detected with greater sensitivity than the conventional MR measurement method.

A thermal protrusion induced periodic touchdown method to measure the electrical potential is introduced in chapter 7. The results show the electrical potential dependence on head-disk's working functions, especially different lube condition are used. A modified Kelvin force method is compared with our proposed method with the latter showing better measurement results for near contact flying height measurement with thermal protrusion.

9.3 Energy Assisted Magnetic Recording for Terabit Areal Density

Energy assisted magnetic recording is slated to be used in the future when the areal density of the magnetic recording goes beyond 1 Tb/in^2. In chapter 8, a new energy assisted magnetic recording method was proposed to enhance the magnetic recording process by the combined field emission and moderate ionization between the write pole and magnetic media. When appropriate bias voltages are applied across the head-media gap, field emission from the write pole was observed to be able to sustain a moderate ionization without catastrophic air breakdown. The ionization discharge effect assists in the writing process without creating damage to the media or degrading the lubricant. The dynamic read/write was performed in perpendicular magnetic recording and a 25% Signal to Noise Ratio (SNR) improvement can be achieved with 3.5μA field emission from the head. The results show a promising method for energy assisted magnetic recording.

LIST OF PUBLICATIONS

Patents filed:

1. PCT Filed on 12 December 2006, International Application No. PCT/SG2006/000387: Method and Tester for Optical Flying Height Measurement. Inventors: Liu Bo, Yuan Zhimin and Ng Ka Wei.
2. U.S. provisional patent filed on 12 December 2005, application no. 60/749,104, Method of optical measurement. Liu Bo, Yuan Zhimin and Ng Ka Wei.

Publications in Journals:

1. K.W. Ng, C.H. Wong, S.H. Leong, Z. Yuan, B. Liu, and T.C. Chong, A Method to Study the Cooling Effect of the Thermal Actuator, Journal of Applied Physics, vol. 103, 07F532, 2008.
2. K.W. Ng, Z. Yuan, B. Liu, S.H. Leong and T.C. Chong, Method for the In-situ Motion Measurement of Head-slider in Both Flying Height and Off-track Direction, IEEE Trans. on Magnetics, vol. 44, pp 640, 2008.
3. K.W. Ng, B. Liu, S.H. Leong, M. Zhang, Z. Yuan, and T.C. Chong, Study on the Influence of Lubricant to Contact Potential, submitted to Microsystems Technologies.
4. K.W. Ng, Z. Yuan and B. Liu, Spacing Fluctuation Induced by Disk Clamping Distortion, IEEE Transactions on Magnetics**,** vol. 39, no. 5, September 2003.
5. K.W. Ng, Z. Yuan and B. Liu, Flying Height Stability and Spindle Motor Vibration, Journal of Applied Physics, vol. 97, no. 10, May 2005.
6. K.W. Ng, Z. Yuan and B. Liu Disk clamping distortion and slider crown sensitivity induced flying height variation, Journal of Magnetism Magnetic Material, vol. 303, pp 72-75, 2006.
7. K.W. Ng, S.H. Leong, Z. Yuan, B. Liu and Y. Ma, Heat Assisted Magnetic Recording by Combined Field Emission and Ionization in Air, Applied Physics Letter, vol. 91, 172511, 2007.

Publications in Conferences:

1. K.W. Ng, Z. Yuan and B. Liu, Spacing Fluctuation Induced by Disk Clamping Distortion, published in International Magnetics Conference 2003 (Intermag2003), Boston, USA, 2003.
2. K.W. Ng, Z. Yuan and B. Liu, Flying Height Stability and Spindle Motor Vibration, published in 49th Conference on Magnetism and Magnetic Materials (MMM2004), Jacksonville, USA, 2004.
3. K.W. Ng, Z. Yuan and B. Liu, Disk clamping distortion and slider crown sensitivity induced flying height variation, published in 6th International Symposium on Physics of Magnetic Materials (ISPMM005), Singapore, 2005.
4. K.W. Ng, Z-M. Yuan, B. Liu, T.C. Chong, Reduction of Crown Sensitivity and Disk Shape Induced Flying Height Variation through ABS Design, published in International Magnetics Conference 2006 (Intermag2006), San Diego, USA, 2006.
5. K.W. Ng, Liu, B., S.H. Leong, M. Zhang, Z-M. Yuan and T.C. Chong, Study on the Influence of Lubricant to Contact Potential, published in 17th Annual Conference on Information Storage and Processing (ISPS2007), Santa Clara, USA, 2007.
6. K.W. Ng, C.H. Wong, S.H. Leong, Z. Yuan, B. Liu and T.C. Chong, A Method to Study the Cooling Effect of the Thermal Actuator, published in 52th Conference on Magnetism and Magnetic Materials (MMM2007), Tampa, USA, 2007.
7. S.H. Leong, Z-M. Yuan, K.W. Ng, B. Liu, On-spot (n,k) Compensation by CCD for Precision Optical Flying Height Measurement**,** published in International Magnetics Conference 2006 (Intermag2006), San Diego, USA, 2006.
8. Y. J. Chen, S.H. Leong, K.W. Ng, Z.B. Guo, J.Z. Shi, J.M. Zhao, and B. Liu, A Study of FIB Patterned Discrete Track Recording Media by Spinstand Read/Write Testing and Scanning Probe Microscopy, published in 6th International Symposium on Physics of Magnetic Materials (ISPMM005), Singapore, 2005.

REFERENCES

1. M. Kryder and Roy W. Gustafson, High-density perpendicular recording—advances, issues, and extensibility, J. Magn. Magn. Mater., vol. 287, pp. 449–458, 2005.
2. V. Gupta and D. B. Bogy, Dynamics of sub-5 nm air bearing sliders in the presence of electrostatic and intermolecular forces at the head disk interface, IEEE Trans. Magn., vol. 41, no. 2, pp. 610–615, Feb. 2005.
3. Nikkei Electronics, TDK Achieves World's Highest Surface Recording Density of HDD,<http://techon.nikkeibp.co.jp/english/NEWS_EN/20080930/158806/>, Japan, Sept. 2008.
4. Z. Zhang, Y.C. Feng, T.G Badran, N-H. Yeh, G. Tarnopolsky, G. Girt, E. Munteanu, M. Harkness, S. Richter, H. Nolan, T. Ranjan, R. Hwang, S. Rauch, G. Ghaly, M. Larson, D. Singleton, E. Vas'ko, V. Ho, J.F. Stageberg, V.K. Duxstad, K.S Slade, Magnetic Recording Demonstration Over 100 Gb/in^2, IEEE Trans. Magn., vol. 38, pp. 1861-1866, 2002.
5. A. Moser_, C. Bonhote, Q. Dai, H. Do, B. Knigge, Y. Ikeda, Q. Le, B. Lengsfield, S. MacDonald, J. Li, V. Nayak, R. Payne, M. Schabes, N. Smith, K. Takano, C. Tsang, P. van der Heijden, W. Weresin, M. Williams, M. Xiao, Perpendicular magnetic recording technology at 230 Gb/in^2, J. Magn. Magn. Mater., vol. 303, pp. 271–275, 2006.
6. M.A. Dufresne and A.K. Menon, Ultra flying height air bearing designs, IEEE Trans. Magnetics, vol. 36, no. 5, pp. 2733-2735, 2000.
7. D.W. Meyer, P.E. Kupinski, and J.C. Liu, Slider with temperature responsive transducer positioning, U.S. Patent 5991113, Nov. 23, 1999.

8. P. Machtle, R. Berger, A. Dietzel, M. Despont, W. Haberle, R. Stutz, G.K. Binnig, P. Vettiger, Integrated Microheaters For In-Situ Flying-Height Control of Sliders Used in Hard-Disk Drives, IEEE Proc. MEMS Conference, pp. 196-199, 2001.
9. D. A. Thomson and J. S. Best, The future of magnetic data storage technology, IBM J. Res. Develop., vol. 44, no. 3, pp. 313-322, 2000.
10. R. Wood, The Feasibility of Magnetic Recording at 1 Terabit per Square Inch, IEEE Trans. Magn., vol. 36 , No. 1, pp. 36-42, January 2000.
11. M. Mallary, A. Torabi, and M. Benakli, One terabit per square inch perpendicular recording conceptual design, IEEE Trans. Magn., vol. 38, pp. 1719–1724, Sept 2002.
12. K. Gao and N. Bertram, Transition jitter estimates in tilted and conventional perpendicular recording media at 1 Tb/in^2, IEEE Trans. Magn., vol. 39, pp. 704–709, Mar. 2003.
13. A. Li, X. Liu, W. Clegg, D. F. L. Jenkins, and T. Donnelly, Real-Time Method to Measure Head Disk Spacing Variation Under Vibration Conditions, IEEE Trans. Magn., vol. 52, no. 3, pp. 916–920, 2003.
14. G. Wang, Y. F. Li, and H. J. Lee, The effect of air bearing surface roughness on avalanche test, J. Appl. Phys., vol. 87, pp. 6176–6178, 2000.
15. Jia-Yang Juang, Du Chen, and David B. Bogy, Alternate Air Bearing Slider Designs for Areal Density of 1 Tb/in^2, IEEE Trans. on Magnetics, IEEE Trans. Magn., vol. 42, no. 2, pp. 241-246, 2006.
16. B. Liu and Z.-M. Yuan, In-situ characterization of head disk clearance, Proc. ASME/Tribology Symp. on Interface Tribology Toward 100 Gb/in^2 and Beyond, Seattle, WA, pp. 51–58, 2001.

17. Z.-M. Yuan, B. Liu, W. Zhang, and S. Hu, Engineering study of triple harmonic method for *in-situ* characterization of head-disk spacing, J. Magn. Magn. Mater., vol. 239, pp. 367–370, 2002.
18. R. L.Wallace, Jr., The reproduction of magnetically recorded signals, Bell Syst. Tech. J., vol. 30, pp. 1145–1173, 1951.
19. C. Denis Mee and Eric D. Daniel, Magnetic recording technology, McGraw-Hill, 1990.
20. K. B. Klaassen and J. van Peppen, Method and circuitry for in-situ measurement of transducer/recording media clearance and transducer magnetic stability, US patent 5,130,866, 1990.
21. W. Shi, L. Zhu, D. Bogy, Use of readback signal modulation to measure head/disk spacing variations in magnetic disk files, IEEE Trans. On Magn., vol. 23, pp. 233-240, 1987.
22. B. R. Brown, H. L. Hu, K. B. Klaassen, J. J. Lum, J. van Peppen, W. E. Weresin, Method and apparatus for in-situ measurement of head/recording medium clearance, US patent 4,777,544, 1986.
23. G. L. Best, Comparison of Optical and Capacitive Measurements of Slider Dynamics, IEEE Trans. On Magn., vol. 23, No. 5, pp. 3453~3455, 1987.
24. Y. Li, Flying Height Measurement Metrology for Ultra-Low Spacing in Rigid Magnetic Recording, IEEE Trans. On Magn., vol. 32, pp. 129-134, 1996.
25. P.W. Smith and S.K. Ganapathi, Measurement of Head-Disk Spacing Using Laser Heterodyne Interferometry-Part II: Simulation and Experiments, IEEE Trans. On Magn., vol. 29, pp. 3912-3914, 1993.
26. L-Y. Zhu, K.F. Hallamasek, and D.B. Bogy, Measurement of Head/Disk

Spacing With a Laser Interferometer, IEEE Trans. On Magn., vol. 24, No. 6, pp. 2739-2741, 1988.

27. C. Lacey, R. Shelor, A. J. Cornier, Interferometric Measurement of Disk/Slider Spacing: the Effect of Phase Shift on Reflection", IEEE Trans. On Magn., vol. 29, pp. 3906-3908, 1993.
28. Born, M. and Wolf, E., Principle of Optics, Pergamon Press, Oxford, 1989.
29. M. Kurita, T. Yamazaki, H. Kohira, M. Matsumoto, R. Tsuchiyama, J. Xu, T. Harada, Y. Inoue, L. Su, K. Kato, An Active-Head Slider with a Piezoelectric Actuator for Controlling Flying Height, IEEE Trans. On Magn., vol. 38**,** No. 5, pp. 2102-2104, 2002.
30. W. Qian, H. Tang, D. Kuo, and J. Gui, Disk shape and its effect on flyability, in IEEE Trans. Magn., vol. 39, Mar. 2003, pp. 735–739.
31. B. H. Thornton and D. B. Bogy, Numerical flying height modulation due to disk clamping distortion and flutter, Computer Mechanics Lab., Dept. Mech. Eng., Univ. California, Berkeley, 2001.
32. CML Air Bearing Design Program Interface (CMLAir32, Version 6.12), Computer Mechanics Lab., Dept. Mech. Eng., Univ. California, Berkeley, 2000.
33. Q. H. Zeng, B. H. Thornton, D. B. Bogy, and C. S. Bhatia, Flyability and flying height modulation measurement of sliders with sub-10 nm flying heights, IEEE Trans. Magn., vol. 37, pp. 894–899, Mar. 2001.
34. L. Guo and Y. Chen, Disk flutter and its impact on HDD servo performance, IEEE Trans. Magn., vol. 37, pp. 866–870, Mar. 2001.
35. J. S. McAllister, Characterization of disk vibrations on aluminum and. alternate substrates, IEEE Trans. Magn., vol. 33, pp. 968–973, Jan. 1997.

36. S. Lee and A. A. Polycarpou, Presented at TISD-2003, Monterey, Paper No. O46, 2003.
37. Ono, K., and Takahashi, K., Analysis of Bouncing Vibrations of a 2-DOF Tripad Contact Slider Model With Air Bearing Pads Over a Harmonic Wavy Disk Surface, ASME 98-TRIB-58, pp. 1–10, 1998.
38. K. Iida, K. Ono, and, M. Yamane, Dynamic Characteristics and Design Consideration of a Tripad Slider in the Near-Contact Regime, ASME J. Tribology vol. 124, pp. 600, 2002.
39. D.B. Bogy, H.M. Stanley, M. Donovan, E. Cha, Some Critical Tribological Issues in Contact and Near-Contact Recording, IEEE Trans. Magn., vol. 29, pp. 230-233, 1993.
40. W. Qian, H. Tang, D. Kuo, and J. Gui, Disk shape and its effect on flyability, IEEE Trans. Magn., vol. 39, pp. 735–739, 2003.
41. B.H. Thornton, D.B. Bogy, C.S. Bhatia, The effects of disk morphology on flying-height modulation: Experiment and. Simulation, IEEE Trans Magn vol. 38, pp. 107–111, 2002.
42. I.Y. Shen and C.-P. Roger Ku, On the rocking motion of a rotating flexible-disk/rigid-shaft system, Advance in Inform. Storage Processing System ASME, vol. 1, pp. 259, 1995.
43. C. Tseng, J. Shen and I.Y. Shen, Vibration of rotating-shaft. HDD spindle motors with flexible stationary parts, IEEE Trans. Magn. vol. 39, pp. 794-799, 2003.
44. CML Air Bearing Design Program Interface (CML Air32, Version 6.12), CML., Dept. Mech. Eng., Univ. California, Berkeley, 2000.
45. J.-G. Tseng and J. A. Wickert, Split Vibration Modes in Acoustically-

Coupled Disk Stacks," ASME Journal of Vibration and Acoustics, 120(1), pp 234-239, 1998.

46. R. Wood, The Feasibility of Magnetic Recording at 1 Terabit per Square Inch, IEEE Trans. On Magnetics, vol. 36, no. 1, pp. 36-42, January 2000.
47. R-H Wang, V. Nayak, F-Y Huang, W. Tang, F. Lee, Head-Disk Dynamics in the Flying, Near Contact, and Contact Regimes, Journal of Tribology, Vol. 123 pg 561-565, 2001.
48. A. A. Mamun, T. H. Lee, G. X. Guo, , W. E. Wong, and W. C. Ye, Measurement of Position Offset in Hard Disk Drive Using Dual Frequency Servo Bursts, IEEE Trans. on Instrumentation and Measurement, Vol. 52, No. 6, pp. 1870-1880, 2003.
49. Louis Joseph Serrano, US patent 6,034,835, 2000.
50. G. J Smith, Dynamic In-situ Measurement of Head-to-Disk Spacing, IEEE Trans .Magn., vol. 35, no. 5, pp. 2346-2351, Sept. 1999.
51. C. Denis Mee and Eric D. Daniel, "Magnetic recording technology", McGraw-Hill, 1990.
52. J. Zhu and B. Liu, In situ flying height analysis at disk drive level, J. Magn. and Mag. Mater., vol. 303, pp. 97-100, 2006.
53. C. Lacey, E.W. Ross, Method and apparatus to calibrate intensity and determine fringe order for interferometric measurement of small spacings, U.S. Patent 5,457,534, 1993.
54. T. Ohkubo and J. Kishigami, Accurate Measurement of Gas-lubricated Slider Bearing Separation Using Visible Laser Interferometry, Journal of Tribology Transaction of the ASME, vol. 110, pp. 148-155, Oct 1987.
55. S.H. Leong, Z. Yuan, K.W. Ng, B. Liu, On-Spot (n,k) Compensation by

CCD for Precision Optical Flying Height Measurement, IEEE Transactions on Magnetics, Vol. 42, 10, pp. 2534- 2536, Oct. 2006.

56. M. Kurita, T. Shiramatsu, K. Miyake, A. Kato, M. Soga, H. Tanaka, S. Saegusa and M. Suk, Active flying-height control slider using MEMS thermal actuator, Microsyst. Technol., vol. 12, pp. 369-375, 2006.
57. Y. Li and G. Wang, In-situ Alumina Recession and protrusion measurement on a magnetic head, IEEE Trans. Magn., vol. 34, pp. 1771-1773, 1998.
58. B.K. Gupta, K. Young, S. Chilamakuri, and A. Menon, Head design considerations for lower thermal pole tip recession and alumina overcoat protrusion, Tribology Int., vol. 33, pp. 309-314, 2000.
59. L. Chen, D.B. Bogy, and B. Strom, Thermal dependence of MR signal on slider flying state, IEEE Trans. Magn., vol. 36, pp. 2486-2489, 2000.
60. J.-Y. Juang and D.B. Bogy, Air-Bearing Effects on Actuated Thermal Pole-Tip Protrusion for Hard Disk Drives, ASME J. Tribology, vol. 129, pp. 570-578, 2007.
61. R.H. Wang, X.Z. Wu, W. Weresin and Y.S. Ju, Head protrusion and its implications on head-disk interface reliability, IEEE Trans. Magn., vol. 37, pp. 1842–1844, 2001.
62. A.V. Kulkarni, S.K. Chilamakuri, B.K. Gupta and A. Menon, Pole Tip Recession (PTR) measurements with high accuracy,precision, and throughput, IEEE Trans. Magn. vol. 36, pp. 2736-2738, 2000.
63. Y. Li, Write-Induced Pole-Tip-Protrusion and Its Effect on Head-Disk Interface Clearance, IEEE Trans. Magn., vol. 40, No.4, pp 3145-3l47, 2004.

64. H. Tian, C.Y. Cheung, and P.K. Wang, Non-Contact Induced Thermal. Distribution of MR Head Signals, IEEE Trans. Magn., Vol.33, No.5, pp 3l30-3l32, 1997.

65. D.W. Abraham, A. P. Praino, M.E. Re, H. K Wickramasinghe, Method and apparatus for detecting asperities on magnetic disks using thermal proximity imaging, U.S. Patent 5527110, 1996.

66. S. Mao, E. Linville, J. Nowak, Z. Zhang, S. Chen, B. Karr, P. Anderson, M. Ostrowski, T. Boonstra, H. Cho, O. Heinonen, M. Kief, S. Xue, J. Price, A. Shukh, N. Amin, P. Kolbo, P.-L. Lu, P. Steiner, Y. C. Feng, N.-H. Yeh, B. Swanson, and P. Ryan, Tunneling Magnetoresistive Heads Beyond 150 Gb/in^2, IEEE Trans. Magn., vol. 40, pp. 307-312, 2004.

67. Y. Peng, X. Lu and J. Luo, Nanoscale Effect on Ultrathin Gas Film Lubrication in Hard Disk Drive, ASME J. Tribology, vol. 126, pp 347-352, 2004.

68. S. Fayeulle; H. Berroug, B. Hamzaoui, D. Treheux and C. Le Gressus, Role of dielectric properties in the tribological behaviour of insulators, Wear, Vol. 162-164, pp. 906-912, 1993.

69. K. Nakayama, Triboemission of charged particles and resistivity of solids. Tribology Letters, vol. 6, pp. 37-40, 1999.

70. K. Nakayama, B. Bou-Said and H. Ikeda, Tribo-electromagnetic phenomena of hydrogenated carbon films-tribo-electrons, -ions, -photons, and –charging, ASME Journal of Tribology, vol. 119, pp. 764-768, 1997.

71. Z. Feng, C. Shih, V. Gubb and F. Poon, A study of tribo-charge/emission at the head-disk interface, Journal of Applied Physics, vol. 85, pp. 5615–5617, 1999.

72. R.J.A. van den Oetelaar, L. Xu, D.F. Ogletree, M. Saleron, H. Tang and J. Gui, Tribocharging phenomena in hard disk amorphous carbon coatings with and without perfluoropolyether lubricants, Journal of Applied Physics, vol. 89, pp. 3993-3998, 2001.

73. J.D. Kiely and Y-T. Hsia, Tribocharging of the magnetic hard disk drive head–disk interface, Journal of Applied Physics, vol. 91, pp. 4631-4636, 2002.

74. K. Bernard; T. Suthar and P. Baumgart, Friction, heat, and slider dynamics during thermal protrusion touchdown, IEEE Trans on Magn, vol. 40, pp. 2510-2512, 2004.

75. D.C. Giancoli, Physics for Scientist and Engineers, 3rd Edition, Prentice Hall, 2000.

76. M. Yasutake, D. Aoki and M. Fujihara, Surface potential measurements using the Kelvin probe force microscope, Thin Solid Films, vol. 273, pp. 279-283, 1996.

77. Z. Zhao, E. R. Karazic, Q. Zhao, M. J. Embree, P. H. Trinh and T. Lam, Lubricant bonding, chemical structure, and additive effects on tribological performances at head–disk interfaces, Microsystem Technologies, vol. 9, 1-2, 2002.

78. P.L. Lu and S.H. Charap, High density magnetic recording media design and identification: susceptibility to thermal decay, IEEE Trans. Magn., vol. 31, pp. 2767-2769, 1995.

79. J.J.M. Ruigrok, R. Coehoorn, S.R. Cumpson, and H.W. Kesteren, Disk recording beyond 100 Gb/in^2 : hybrid recording?, J. Appl. Phys., Vol. 87, pp. 5398-5403, 2000.

80. R.E. Rottmayer, S. Batra, D. Buechel, W.A. Challener, J. Hohlfeld, Y. Kubota, L. Li, B. Lu, C. Mihalcea, K. Mountfield, K. Pelhos, C. Peng, T. Rausch, M.A. Seigler, D. Weller, and X. Yang, Heat-Assisted Magnetic Recording, IEEE Trans. Magn., vol. 42, pp. 2417- 2421, 2006.
81. J. Nakamura, M. Miyamoto, S. Hosaka and H. Koyanagi, High-density thermomagnetic recording method using a scanning tunneling microscope, J. Appl. Phys., Vol. 77, pp. 779-781, 1995.
82. L. Zhang, J.A. Bain, J-G. Zhu, L. Abelmann and T. Onoue, The effect of external magnetic field on mark size in heat-assisted probe recording on CoNi/Pt multilayers, J. Appl. Phys. Vol. 99, pp. 1-5, 2006.
83. B.E. Knigge, C.M. Mate, O. Ruiz, and P.M. Baumgart**,** Influence of contact potential on slider-disk spacing: simulation and experiment, IEEE Trans. Magn., vol. 40, pp. 3165 – 3167, 2004.
84. R.H. Fowler, and L.W. Nordheim, Electron Emission in Intense Electric Fields, Proc. R. Soc. Lond. A, vol. 119, pp. 173-181, 1928.
85. L. Zhang, J.A. Bain, and J-G. Zhu, A model for mark size dependence on field emission voltage in heat-assisted magnetic probe recording on CoNi/Pt multilayers, IEEE Trans. Magn. 40, pp. 2549 – 2551, 2004.
86. W. Zhang, T. Fisher and S.V. Garimella, Simulation of ion generation and breakdown in atmospheric air, J. Appl. Phys., vol. 96, pp. 6066-6072, 2004.
87. M. S. Peterson, W. Zhang, T. Fisher and S.V. Garimella*,* Low-voltage ionization of air with carbon-based materials, Plasma Sources Sci. Technol., Vol. 14, pp. 654-660, 2005.
88. P.G. Slade and E. Taylor, Electrical breakdown in atmospheric air between closely spaced (0.2 /spl mu/m-40 /spl mu/m) electrical contacts, IEEE

Trans. Compon., Packag. Manuf. Technol., Part A, vol. 25, pp. 390- 396, 2002.

89. E. Nasser, Fundamentals of Gaseous Ionization and Plasma Electronics, Wiley-Interscience, New York, 1971.
90. I-H. Hwang and S-K. Na, A study on heat source modeling of scanning electron microscopy modified for material processing, Metallurgical and Materials Trans. B, vol. 36b, pp. 133-139, 2005.
91. J.I. Goldstein and H. Yakowitz: Practical Scanning Electron Microscopy, Plenum Press, New York, NY, pp. 49, 1975.
92. J. Zhang, R. Ji, J.W. Xu, J.K. Ng, B.X. Xu, S.B. Hu, H.X. Yuan, and S.N. Piramanayagam, Lubrication for Heat-Assisted Magnetic Recording Media, IEEE Transactions on Magnetics, vol. 42, 10, pp. 2546-2548, 2006.
93. Y. Ma and B. Liu, A Theoretical Study of Vapor Lubrication for Heat Assisted Magnetic Recording, Tribology Letter, vol. 32, 3, pp. 215-220, 2008.
94. Z. Fan, Z. Zhang and H. Tang, Study of head-disk interaction and spacing based on readback signal, Magnetic Recording Conference APMRC, Asia-Pacific vol. 14-16, pp. 1-2, 2009.
95. X. Zhao, B. Bhushan, Studies on degradation mechanisms of lubricants for magnetic thin-film rigid disks, Proceedings of the Institution of Mechanical Engineers, Part J: Journal of Engineering Tribology, vol. 215, no. 2, pp. 173-188, 2001.
96. J. Wei, W. Fong, D. B. Bogy and C. S. Bhatia, The decomposition mechanisms of a perfluoropolyether at the head/disk interface of hard disk drives, Tribology Letters, vol. 5, no.2, pp. 203-209, 1998.